



LIBRARY
~~RESEARCH FACILITY~~
NAVAL POSTGRADUATE SCHOOL
MONTEREY CALIFORNIA 93943

NAVENVPREDRSCHFAC
CONTRACTOR REPORT
CR 85-05

SHIP-TO-SHIP PROPAGATION: MARITIME DATA ANALYSES

ADA 155484

Joseph L. Manning, James A. Dowling, John R. Hummel

OptiMetrics, Inc.
Ann Arbor, MI 48104

Contract No. N00228-82-C-8171

MARCH 1985

APPROVED FOR PUBLIC RELEASE; DISTRIBUTION IS UNLIMITED



Prepared For:

NAVAL ENVIRONMENTAL PREDICTION RESEARCH FACILITY
MONTEREY, CALIFORNIA 93943-5006

ADA 155484

NAVENVPREDRSCHFAC CR 85-05

QUALIFIED REQUESTORS MAY OBTAIN ADDITIONAL COPIES
FROM THE DEFENSE TECHNICAL INFORMATION CENTER.
ALL OTHERS SHOULD APPLY TO THE NATIONAL TECHNICAL
INFORMATION SERVICE.

AN (1) AD-A155 484
 FG (2) 090300
 FG (2) 200600
 CJ (3) (C)
 CA (5) OPTIMETRICS INC ANN ARBOR MI
 TI (6) Ship-to-Ship Propagation: Maritime Data Analyses.
 TC (8) (U)
 DN (9) Final rept..
 AU (10) Manning, J. L.
 AU (10) Dowling, J. A.
 AU (10) Hummel, J. R.
 RD (11) Mar 1985
 FG (12) 127p
 RS (14) DM1-116
 CT (15) N00228-82-C-8171
 RN (18) NEPRF-CR-85-05
 RC (20) Unclassified report
 DE (23) *OPTICAL RADAR, LIGHT TRANSMISSION, LASER BEAMS, OCEAN
 ENVIRONMENTS, ABSORPTION, AIRBORNE, ATMOSPHERES,
 CHEMICAL LASERS, COMPUTATIONS, DEUTERIUM COMPOUNDS,
 FLUORIDES, IMAGES, LASERS, LENGTH, MEASUREMENT,
 PROFILES, PROPAGATION, PULSED LASERS, RADIOSONDES, SHIP
 TO SHIP, THERMAL BLOOMING, TRANSMITTANCE, WATER VAPOR
 DC (24) (U)
 ID (25) DIAL (Differential Absorption Lidar), WUDN993603,
 PE63754N
 IC (26) (U)
 AB (27) An analysis of two sets of atmospheric optical and
 supporting meteorological data has been performed. The
 first data set was taken by an airborne differential
 absorption lidar (DIAL) system. From this data set,
 vertical water vapor density profiles were extracted
 and used to calculate transmittances for cw and pulsed
 DF lasers. Thermal blooming calculations also were made
 to compare the performance of a laser optimized using a
 standard atmosphere water profile with a laser
 optimized using DIAL-derived profiles. The difference
 was found to be small for the conditions used here. The
 second data set consisted of long-path atmospheric
 transmittance and radiosonde measurements made in
 support of a long focal length imaging demonstration (LFLID).
 Measured transmittances were compared with
 LOWTRAN 6 transmittance calculations. Good agreement
 was obtained in the 3-5 micrometer range. Comparisons
 for the 8-12 micrometer region showed calculated
 transmittances about a factor of 10 lower than measured
 values. Keywords include: DIAL; Atmospheric
 transmission; water vapor profiles; DF laser
 atmospheric propagation; and long focal length imaging.
 AC (28) (U)
 DL (33) 01
 SE (34) F

Page 10

** MAY CONTAIN EXPORT CONTROL DATA **

ADAXXXXXX MICROFICHE ARE HOUSED IN THE GENERAL MICROFORMS RM

CC (35) 395217

#

REPORT DOCUMENTATION PAGE

1a. REPORT SECURITY CLASSIFICATION UNCLASSIFIED			1b. RESTRICTIVE MARKINGS		
2a. SECURITY CLASSIFICATION AUTHORITY			3. DISTRIBUTION / AVAILABILITY OF REPORT Approved for public release; distribution is unlimited		
2b. DECLASSIFICATION / DOWNGRADING SCHEDULE					
4. PERFORMING ORGANIZATION REPORT NUMBER(S) al OMI-116			5. MONITORING ORGANIZATION REPORT NUMBER(S) CR 85-05		
6a. NAME OF PERFORMING ORGANIZATION al OptiMetrics, Inc.		6b. OFFICE SYMBOL (If applicable)	7a. NAME OF MONITORING ORGANIZATION Naval Environmental Prediction Research Facility		
6c. ADDRESS (City, State, and ZIP Code) 2000 Hogback Road, Suite 3 Ann Arbor, MI 48104			7b. ADDRESS (City, State, and ZIP Code) Monterey, CA 93943-5006		
8a. NAME OF FUNDING / SPONSORING ORGANIZATION Naval Air Systems Command		8b. OFFICE SYMBOL (If applicable) (AIR-330)	9. PROCUREMENT INSTRUMENT IDENTIFICATION NUMBER N00228-82-C-8171		
8c. ADDRESS (City, State, and ZIP Code) Department of the Navy Washington, DC 20361			10. SOURCE OF FUNDING NUMBERS		
			PROGRAM ELEMENT NO. 63754N	PROJECT NO. 90182-AA	TASK NO.
11. TITLE (Include Security Classification) Ship-To-Ship Propagation: Maritime Data Analyses					
12. PERSONAL AUTHOR(S) Manning, Joseph L.; Dowling, James A.; Hummel, John R.					
13a. TYPE OF REPORT Final		13b. TIME COVERED FROM TO		14. DATE OF REPORT (Year, Month, Day) 1985, March	
15. PAGE COUNT 130					
16. SUPPLEMENTARY NOTATION					
17. COSATI CODES			18. SUBJECT TERMS (Continue on reverse if necessary and identify by block number) DIAL DF laser atmospheric propagation Atmospheric transmission Long focal length imaging Water vapor profiles		
FIELD	GROUP	SUB-GROUP			
04	01				
04	02				
19. ABSTRACT (Continue on reverse if necessary and identify by block number) An analysis of two sets of atmospheric optical and supporting meteorological data has been performed. The first data set was taken by an airborne differential absorption lidar (DIAL) system. From this data set, vertical water vapor density profiles were extracted and used to calculate transmittances for cw and pulsed DF lasers. Thermal blooming calculations also were made to compare the performance of a laser optimized using a standard atmosphere water vapor profile with a laser optimized using DIAL-derived profiles. The difference was found to be small for the conditions used here. The second data set consisted of long-path atmospheric transmittance and radiosonde measurements made in support of a long focal length imaging demonstration (LFLID). Measured transmittances were compared with LOWTRAN 6 transmittance calculations. Good agreement was obtained in the 3-5 micrometer range. Comparisons for the 8-12 micrometer region showed calculated transmittances about a factor of 10 lower than measured values.					
20. DISTRIBUTION / AVAILABILITY OF ABSTRACT <input checked="" type="checkbox"/> UNCLASSIFIED/UNLIMITED <input type="checkbox"/> SAME AS RPT. <input type="checkbox"/> DTIC USERS			21. ABSTRACT SECURITY CLASSIFICATION UNCLASSIFIED		
22a. NAME OF RESPONSIBLE INDIVIDUAL Haggerty, J.			22b. TELEPHONE (Include Area Code) (408) 646-2805		22c. OFFICE SYMBOL NEPRF WU 6.2-21

TABLE OF CONTENTS

1.	INTRODUCTION	1
1.1.	Background and General Description of this Study.....	1
1.2.	The NASA DIAL System.....	3
2.	DESCRIPTION OF THE DATA SETS.....	4
2.1.	The NASA DIAL Data Set.....	4
2.1.1.	Introduction.....	4
2.1.2.	Meteorological Conditions.....	4
2.1.3.	The NASA DIAL H ₂ O Data.....	9
2.2.	The LFLID Support Data Set.....	9
2.2.1.	Meteorological Conditions Occurring During Collection of the LFLID Support Data.....	23
2.2.2.	The LFLID Support Long-Path Transmittance Data.....	29
3.	REDUCTION AND ANALYSIS OF THE NASA DIAL H ₂ O DATA.....	36
3.1.	Average H ₂ O Profile Over All Flights.....	36
3.2.	Total Column Water Amounts.....	40
3.3.	Fitting the Water Vapor Data.....	52
4.	INFLUENCE OF H ₂ O PROFILES DERIVED FROM THE DIAL DATA ON DF LASER PROPAGATION.....	69
4.1.	Model for Calculation of DF Laser Transmittance.....	69
4.1.1.	Transmittance for a Laser Power Spectrum.....	69
4.1.2.	Transmittance Calculation for the LIDAR Data.....	70

4.2.	Results of Transmittance Calculations.....	74
4.2.1.	CW Laser Transmittance for Individual Profiles.....	75
4.2.2.	Pulsed Laser Transmittances for Individual Profiles.....	85
4.2.3.	Transmittances for Average and Extreme Profiles.....	92
4.2.4.	Transmittance Calculations for a Standard Atmosphere.....	94
4.3.	Description of Thermal Blooming Calculations....	94
4.4.	Results of Thermal Blooming Calculations.....	98
5.	REDUCTION AND ANALYSIS OF THE LFLID SUPPORT AND RADIOSONDE TRANSMITTANCE DATA.....	101
6.	SUMMARY AND CONCLUSIONS.....	114
6.1.	The NASA DIAL Data Base.....	114
6.1.1.	Summary.....	114
6.1.2.	Conclusions and Recommendations.....	114
6.2.	The LFLID Support Data Base.....	116
	REFERENCES.....	119
	ACKNOWLEDGMENTS	121
	DISTRIBUTION	123

INTRODUCTION

1.1 BACKGROUND AND GENERAL DESCRIPTION OF THIS STUDY

A project to measure DF laser transmittance and high-resolution transmittance over pathlengths of several kilometers between two ships was planned by the Navy for 1982. These measurements, along with supporting data such as meteorological measurements, would have generated a data base for analysis and prediction of problems in DF laser propagation, especially at sea. Among the problems which might have been addressed are accuracy of line parameters (both for attenuation calculations and for thermal blooming prediction); aerosol extinction; validation of aerosol models and applicability of existing models for open ocean; HDO/H₂O ratio; and H₂O continuum [1].

The ship-to-ship measurement project did not take place. In this report we present a study based on the analysis of two backup data sets. The first one considered consists of water vapor profiles over open ocean measured with an airborne DIAL system. The second data set consists of slant-path transmittance and radiosonde data measured in conjunction with a Long Focal Length Imaging Demonstration (LFLID). These data, supporting tests conducted by the Naval Air Development Center (NADC), were measured using a 66 km slant-path between the islands of Maui and Lanai in Hawaii. With these data sets it was, of course, not possible to address most of the problems for DF propagation mentioned in the previous paragraph, although this study examines the effects of measured water vapor profiles on the propagation of high-energy DF laser beams, using the LIDAR data set.

The DIAL data were examined for realism and consistency. Transmittances were calculated for pulsed and cw DF lasers for vertical and slant ranges for each profile. The grid over which the data were taken included the boundary of the gulf stream, so the influences of sea surface temperature in general and the gulf stream boundary in particular were examined. Average and extreme water vapor profiles based on the data were generated, and DF laser transmittances for these profiles were compared to transmittances calculated using standard atmosphere water vapor profiles.

Thermal blooming calculations were done to determine whether there would be any real advantage to having a ship-board device to monitor the water vapor profile. The question we set out to answer was this: if a laser system is optimized for atmospheric conditions based on surface measurements and standard atmosphere vertical profiles, how much less effective will it be than if actual vertical measurements were used?

The long-path transmittance data from the Hawaii tests were obtained from the AVCO Corporation which was primarily responsible for carrying the transmittance measurements as part of their support of the LFLID tests. OptiMetrics, Inc. (OMI) participated in the tests by providing and operating a searchlight-blackbody source system on the island of Lanai during the tests. The transmittance data were collected using a 66 km path between Lanai and Mount Haleakala, Maui. The data were compared with predicted transmittances, based on vertical water vapor density profiles obtained from radiosondes. The transmittance predictions were made using the LOWTRAN 6 model [2].

1.2 THE NASA DIAL SYSTEM

The water vapor profiles were measured using an airborne DIAL (differential absorption lidar) system developed by NASA [3]. This system uses two high-conversion-efficiency tunable dye lasers pumped by two frequency-doubled Nd:YAG lasers. One laser operates on an H_2O absorption-line center wavelength while the other is tuned off of the absorption line. The concentration of H_2O at each range is determined from the strengths of the returns for the two wavelengths at that range. The return at the off-line wavelength can also be used for aerosol measurement. The entire system is installed in an Electra aircraft.

Data were taken on 14, 18, and 24 September 1982. Only the data from 24 September were supplied for analysis. Aerosol information was not derived from the data, and the emphasis in our analysis was on water vapor.

DESCRIPTION OF THE DATA SETS

2.1 THE NASA DIAL DATA SET

2.1.1 INTRODUCTION

The DIAL data to be discussed here were taken on 24 September 1982 off the coast of the United States east of Virginia and North Carolina. The flights of the airborne instrument took place between 1126 and 1512 local time. A total of eleven flights took place. Figure 1 displays the area of the flights and shows the flight paths of the various flights. The flights were generally north-south and took place over the Gulf Stream. Table 1 summarizes the flights. The complete data base to be analyzed consists of meteorological data that were collected separately and the NASA DIAL data.

2.1.2 METEOROLOGICAL CONDITIONS

The weather during the flights was generally good. The weather situation was one of clearing and generally warmer weather after a week of rain. Figure 2 displays the surface weather chart for 1800 GMT (1300 local time) for the United States. The test area was under the influence of a high pressure system just to the north of the test site. Table 2 lists the surface observations from Wallops Island, Virginia and ships that were in the vicinity of the test area. Wallops Island reported scattered clouds at the times of their 0000 GMT and 1200 GMT radiosonde launches. The ships reported low clouds with total amounts over 50%. The values reported are consistent with mean values given in the U.S. Navy Marine Climatic Atlas of the World [4].

X

X

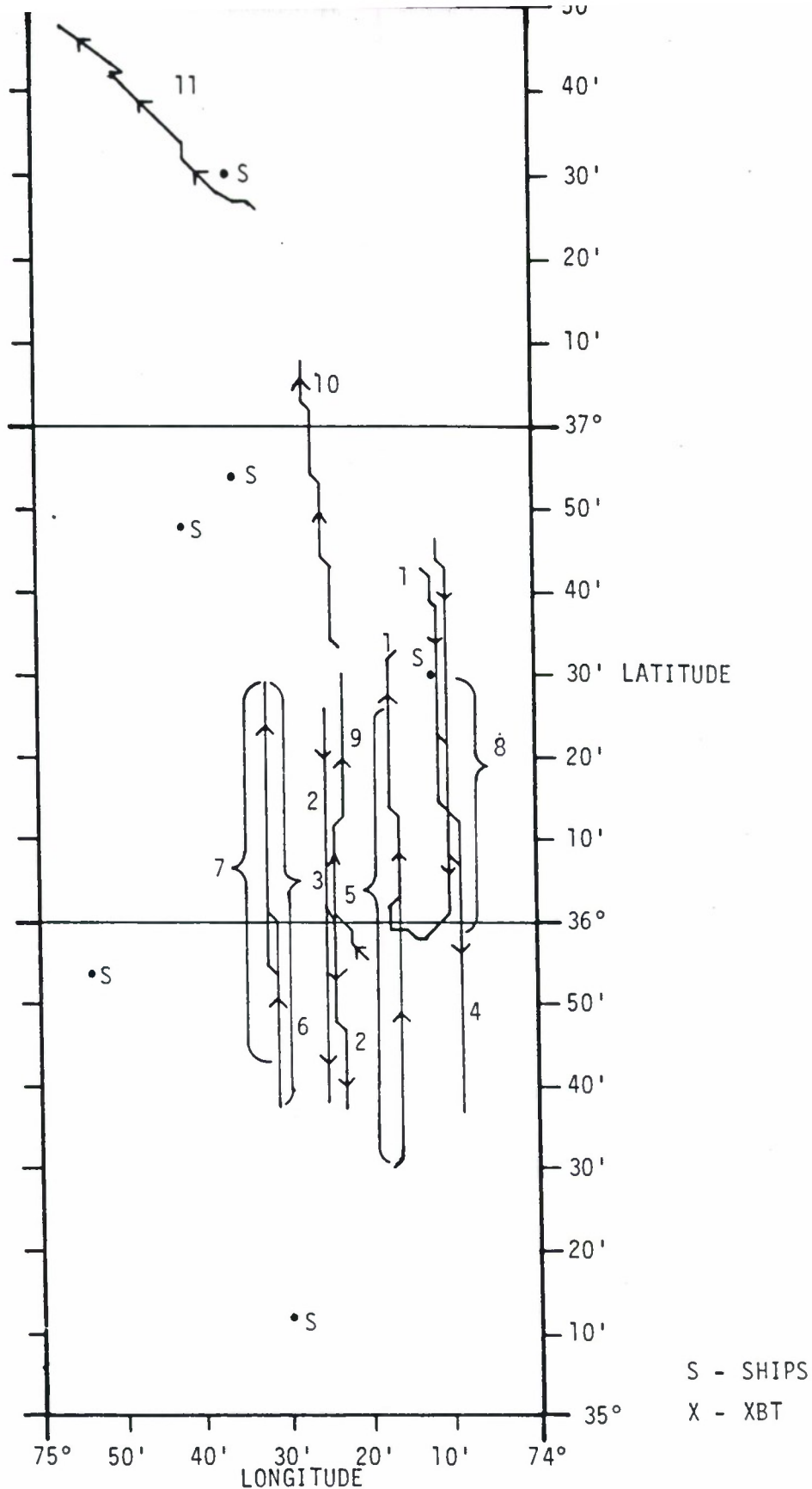


FIGURE 1. FLIGHT PATHS OF THE NASA-LANGLEY AIRCRAFT AND POSITIONS OF EXPENDABLE BATHYTHERMOGRAPHS (XBT) USED TO OBTAIN OCEAN TEMPERATURES AND SHIPS THAT REPORTED METEOROLOGICAL OBSERVATIONS.

TABLE 1. SUMMARY OF FLIGHT PATHS.

FLIGHT	FLIGHT TIME (LOCAL)	LATITUDE COVERAGE (N)
1	11:26:18 - 11:47:19	36°43' - 35°58' - 36°33'
2	12:02:16 - 12:15:36	36°26' - 35°37'
3	12:22:12 - 12:35:10	35°38' - 36°29'
4	12:59:24 - 13:18:01	36°47' - 35°37'
5	13:27:48 - 13:42:28	35°30' - 36°26'
6	13:48:10 - 14:11:55	36°27' - 35°38'
7	14:11:55 - 14:23:38	35°43' - 36°29'
8	14:29:49 - 14:38:09	36°29' - 35°59'
9	14:41:15 - 14:50:08	35°56' - 36°29'
10	14:51:19 - 14:59:59	36°34' - 37° 8'
11	15: 4:41 - 15:12:43	37°26' - 37°48'

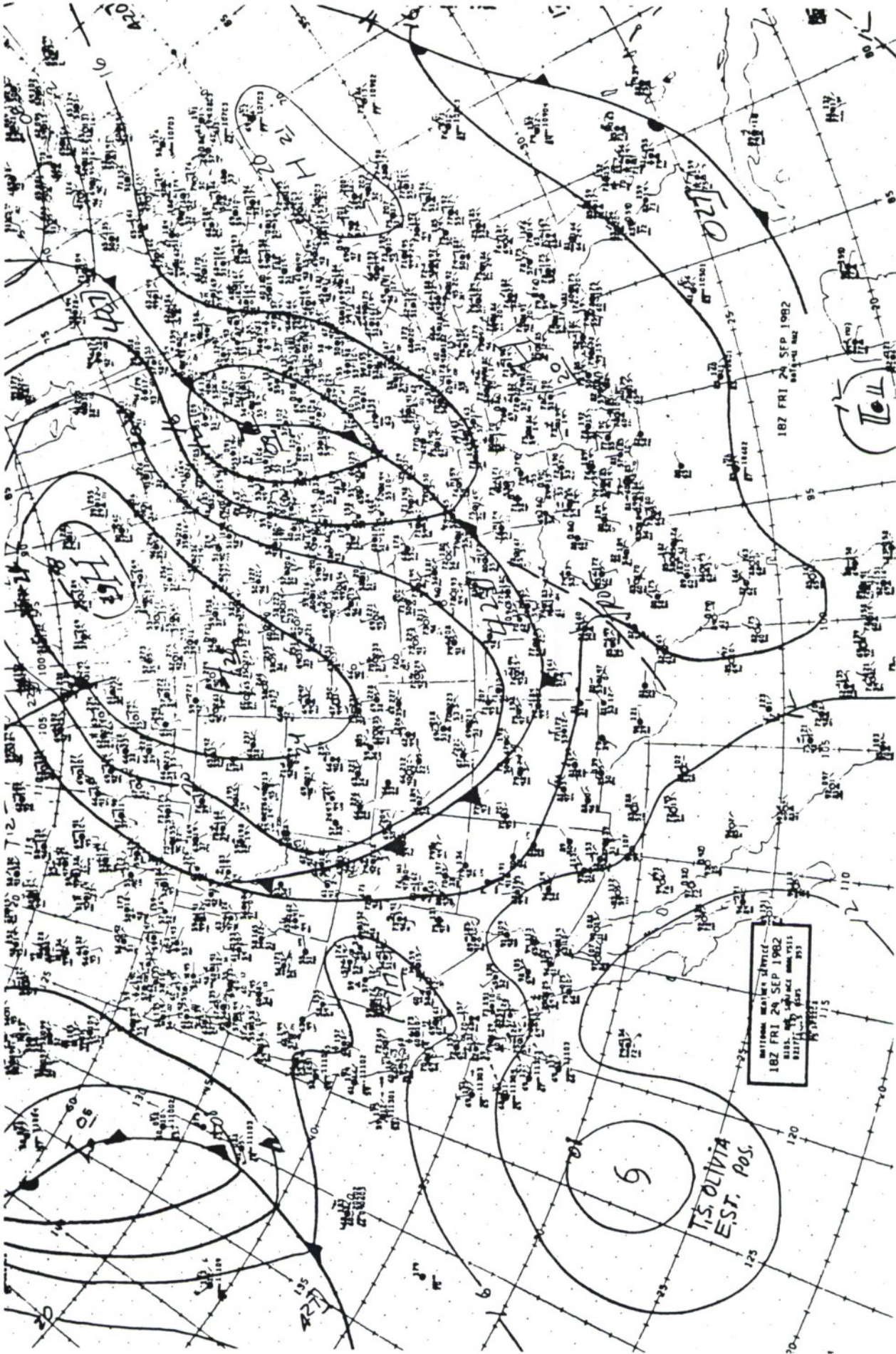


FIGURE 2. SURFACE WEATHER CONDITIONS FOR 1800Z ON 24 SEPTEMBER 1982.

TABLE 2. SURFACE METEOROLOGICAL OBSERVATIONS
FOR 24 SEPTEMBER 1982.

Wallops Island, Virginia (37°51'N, 75°29'W)

TIME (GMT)	SURFACE TEMPERATURE (C)	RELATIVE HUMIDITY (%)	WIND SPEED (KNOTS)	WIND DIRECTION (DEGREES)
1200	10.6	.86	1	350
0000	18.6	63	5	155

Ship Observations

TIME (GMT)	TEMPERATURE AIR OCEAN (C)	RELATIVE HUMIDITY (%)	WIND SPEED (KNOTS)	WIND DIRECTION (DEGREES)
0600 ¹	21.7 24.4	56	9	20
0600 ²	19.9 26.7	52	5	320
1200 ³	18.8 12.7	78	8	350
1800 ⁴	21.1 27.2	62	8	40
1800 ⁵	22.0 ---	67	6	40
1800 ⁶	21.2 21.0	60	9	90

Ship Locations:

- 1 - 36.2°N, 74.5°W
- 2 - 36.9°N, 74.6°W
- 3 - 36.8°N, 74.7°W
- 4 - 35.9°N, 74.9°W
- 5 - 36.5°N, 74.2°W
- 6 - 37.5°N, 74.6°W

Two instrumented buoys were operating in the vicinity of the test area and obtained meteorological data on the days of the flights. Those data are summarized in Table 3. Finally, data were obtained by two ship-dropped expendable bathythermographs (XBT). The XBT's measure water temperature as a function of depth. Those data are given in Table 4.

2.1.3 THE NASA DIAL H₂O DATA

The data obtained by the instrument consisted of water vapor volume mixing ratios as a function of altitude in a vertical column. The data were given at 15 m intervals. The length of the vertical column varied from one location to another but covered the range 131 to 1361 m. The instrument took data about every 20 seconds. Figures 3 through 13 give the average water vapor profile for each of the flights. There is a fair amount of structure in the profile but they generally show decreasing values with altitude. The dramatic changes in the profiles at the top and bottom of the profiles are believed to be indications of the limits of sensitivity of the instrument and not physical. The magnitudes are in general agreement with climatological averages for that latitude [5].

2.2 THE LFID SUPPORT DATA SET

The meteorological conditions occurring during the collection of the long-path transmittance measurements were fairly constant. The most useful long-path measurements were made during the early morning hours on 4 days in July 1984. Although long-path transmittance and radiosonde measurements were collected on several additional days, on these occasions the long-path transmittance measurements were beset by and at least partially contaminated by the

TABLE 3. METEOROLOGICAL DATA OBTAINED FROM INSTRUMENTED BUOYS NEAR THE TEST AREA.

BUOY: 41001 LATITUDE 34° 41' 59"N LONGITUDE 72° 18' 00"W

TIME (GMT)	BOTTOM DEPTH (m)	AIR TEMP (C)	PRESSURE (mb)	WINDSPEED (m/s)	WIND DIRECTION (degrees)	SEA SURFACE TEMP (C)
0 0	4353	22.7	1018.9	5.2	308.0	25.02
1 0	4353	22.7	1019.7	3.8	315.5	24.98
2 0	4353	22.6	1019.8	4.1	322.1	24.93
3 0	4353	22.5	1020.1	3.7	329.8	24.92
4 0	4353	22.2	1020.1	2.3	305.7	24.88
5 0	4353	22.2	1019.9	2.8	306.5	24.84
6 0	4353	22.1	1020.0	3.2	307.0	24.88
7 0	4353	22.0	1019.9	2.6	329.3	24.87
8 0	4353	21.9	1019.6	3.6	324.3	24.87
9 0	4353	22.0	1019.3	3.8	314.7	24.86
10 0	4353	22.0	1019.3	4.7	315.6	24.86
11 0	4353	22.0	1019.6	5.7	348.2	24.85
12 0	4353	22.0	1019.9	6.2	27.0	24.84
13 0	4353	22.0	1020.0	6.8	33.0	24.86
14 0	4353	22.1	1020.3	6.3	49.0	24.88
15 0	4353	22.2	1019.9	7.2	52.2	24.89
16 0	4353	22.5	1019.5	5.2	47.2	24.92
17 0	4353	22.6	1019.3	5.6	50.3	24.94
18 0	4353	22.7	1018.7	5.3	49.2	24.96
19 0	4353	22.8	1017.9	5.0	42.2	24.99
20 0	4353	22.8	1016.9	6.4	37.3	25.00
21 0	4353	22.9	1017.3	7.0	26.7	24.99
22 0	4353	23.0	1017.1	8.5	29.0	24.98
23 0	4353	23.1	1016.7	9.0	32.2	24.96

BUOY: 41002 LATITUDE 32° 18' 00"N LONGITUDE 75° 18' 00"W

TIME (GMT)	BOTTOM DEPTH (m)	AIR TEMP (C)	PRESSURE (mb)	WINDSPEED (m/s)	WIND DIRECTION (degrees)	SEA SURFACE TEMP (C)
0 0	3749	24.6	1018.5	6.2	17.2	28.00
1 0	3749	24.7	1019.0	5.7	46.1	27.97
2 0	3749	24.7	1019.2	6.2	38.3	27.95
3 0	3749	24.6	1019.4	6.2	40.4	27.95
4 0	3749	24.5	1019.5	5.9	47.5	27.95
5 0	3749	24.5	1019.4	5.6	37.6	27.95
6 0	3749	24.4	1019.0	5.4	40.0	27.95
7 0	3749	24.5	1018.3	5.9	44.0	27.92
8 0	3749	24.4	1018.0	6.1	37.5	27.92
9 0	3749	24.5	1017.7	6.8	41.6	27.92
10 0	3749	24.5	1018.2	6.6	40.2	27.90
11 0	3749	24.4	1017.7	7.4	36.4	27.90
12 0	3749	24.4	1018.2	6.8	36.3	27.90
13 0	3749	24.5	1018.3	6.9	43.7	27.90
14 0	3749	24.6	1018.1	7.0	43.2	27.88
15 0	3749	24.7	1018.2	6.8	48.7	27.88
16 0	3749	24.7	1018.0	6.5	51.7	27.88
17 0	3749	24.7	1017.9	6.3	39.5	27.88
18 0	3749	24.7	1017.1	6.4	47.4	27.88
19 0	3749	24.7	1015.8	6.1	45.4	27.88
20 0	3749	24.8	1015.8	5.8	50.4	27.88
21 0	3749	25.0	1015.5	5.5	43.1	27.88
22 0	3749	25.1	1015.1	5.4	60.1	27.90
23 0	3749	25.2	1014.6	5.5	57.5	27.90

TABLE 4. DATA OBTAINED FROM EXPENDABLE BATHYTHERMOGRAPHS.

Time (GMT)	Position		Temperature (C)	Ocean Depth (m)
	Latitude	Longitude		
1:20	37°26'N	75°32'W	21.63	0
2:48	37°28'N	75°22'W	21.27	0

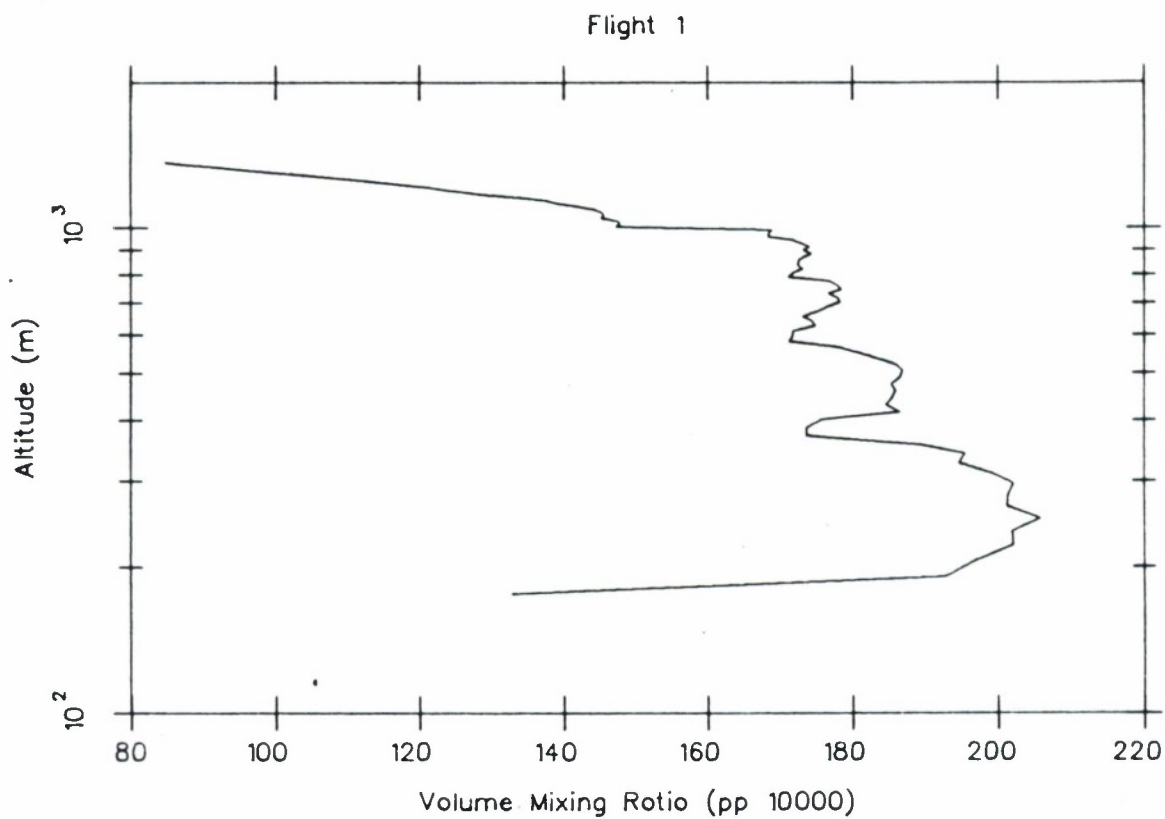


FIGURE 3. AVERAGE WATER VAPOR PROFILE FOR FLIGHT 1.

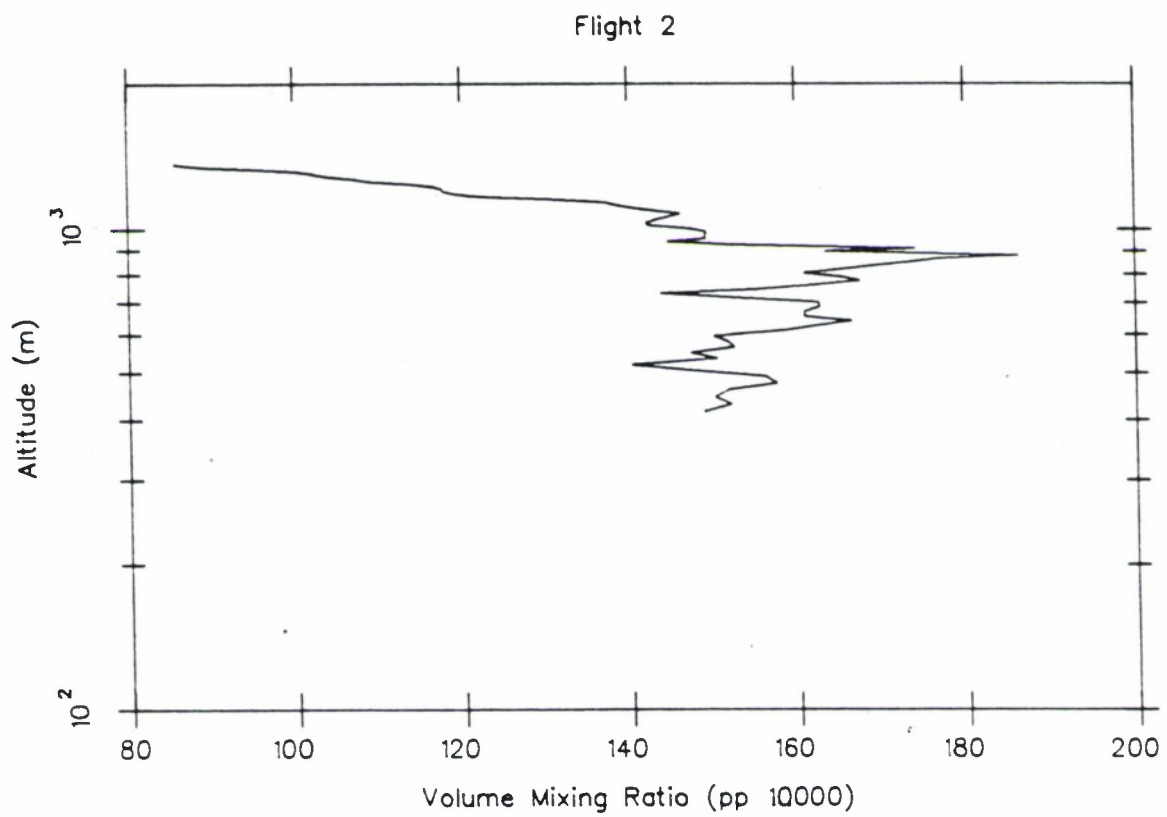


FIGURE 4. AVERAGE WATER VAPOR PROFILE FOR FLIGHT 2.

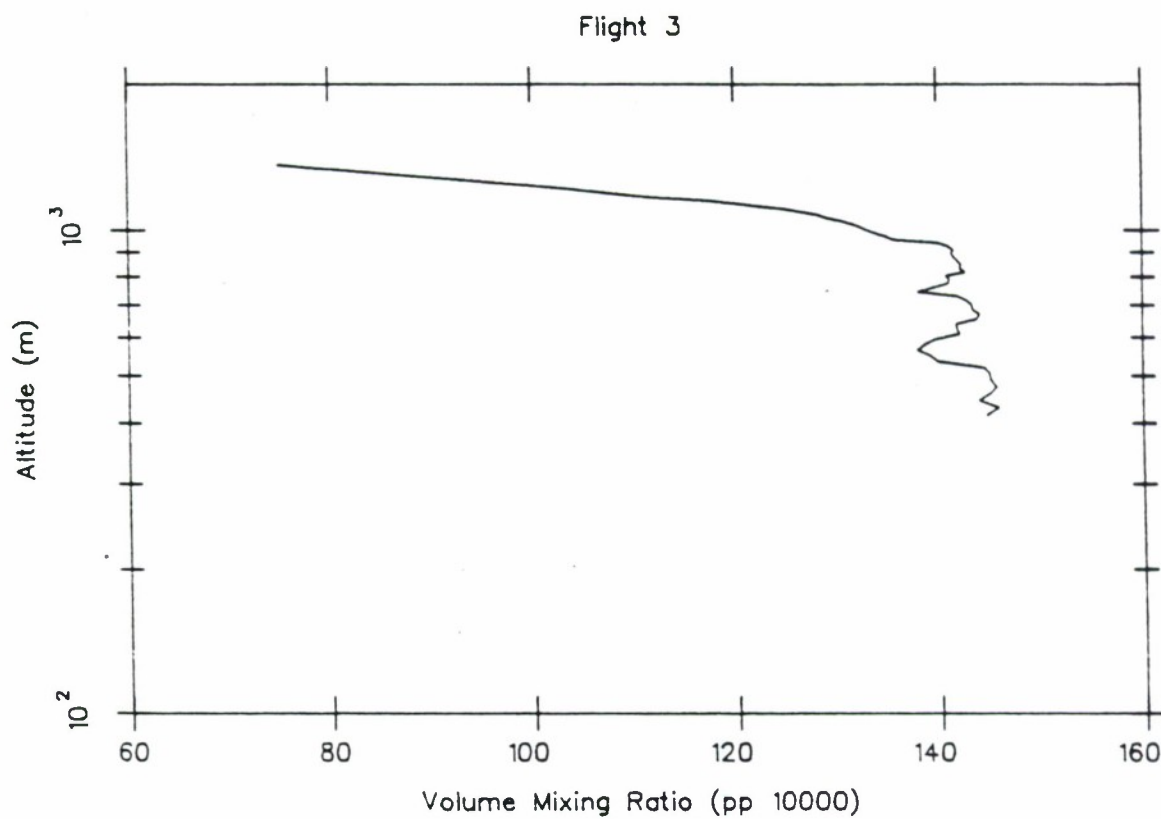


FIGURE 5: AVERAGE WATER VAPOR PROFILE FOR FLIGHT 3.

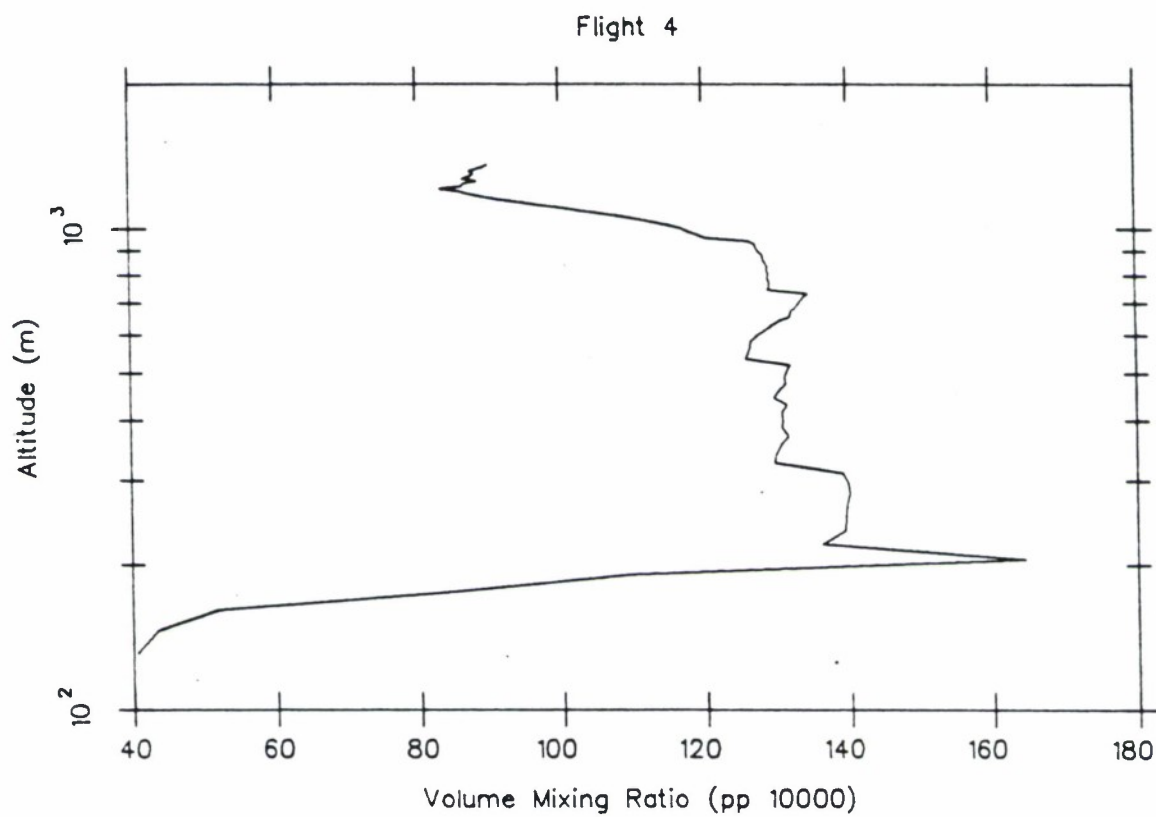


FIGURE 6. AVERAGE WATER VAPOR PROFILE FOR FLIGHT 4.

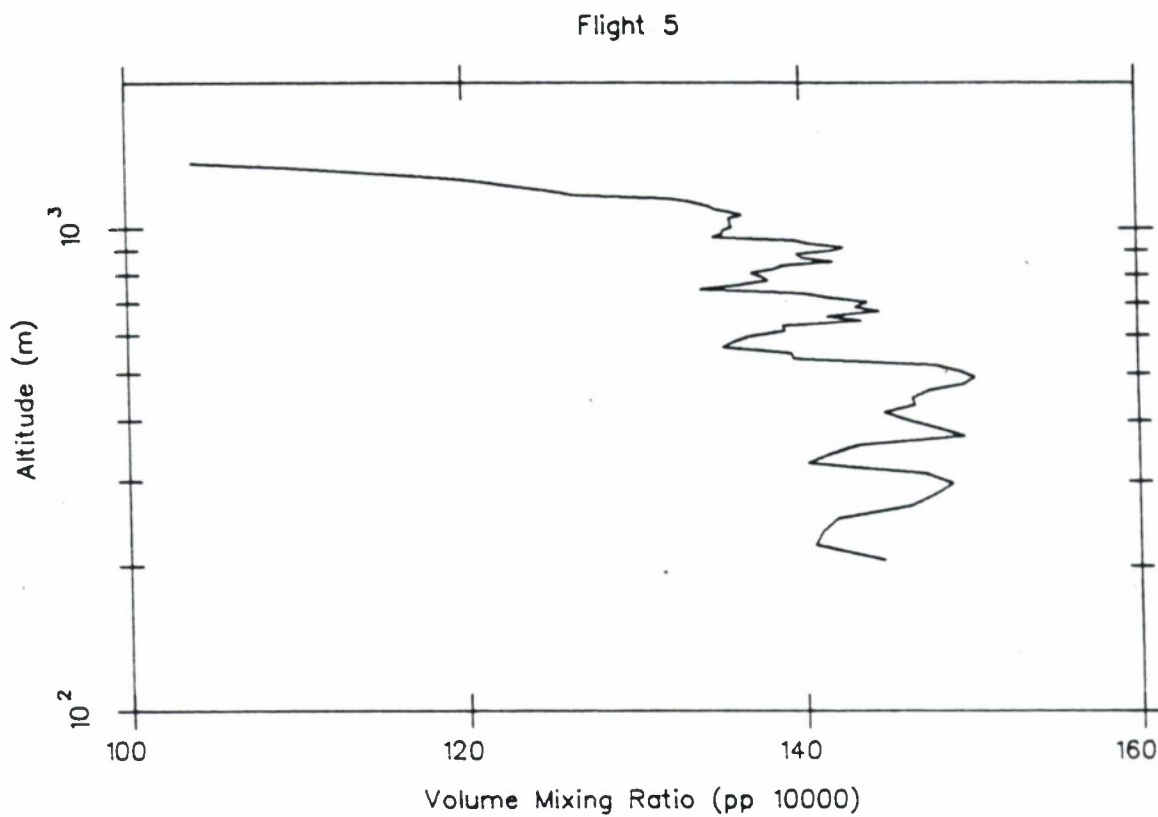


FIGURE 7. AVERAGE WATER VAPOR PROFILE FOR FLIGHT 5.

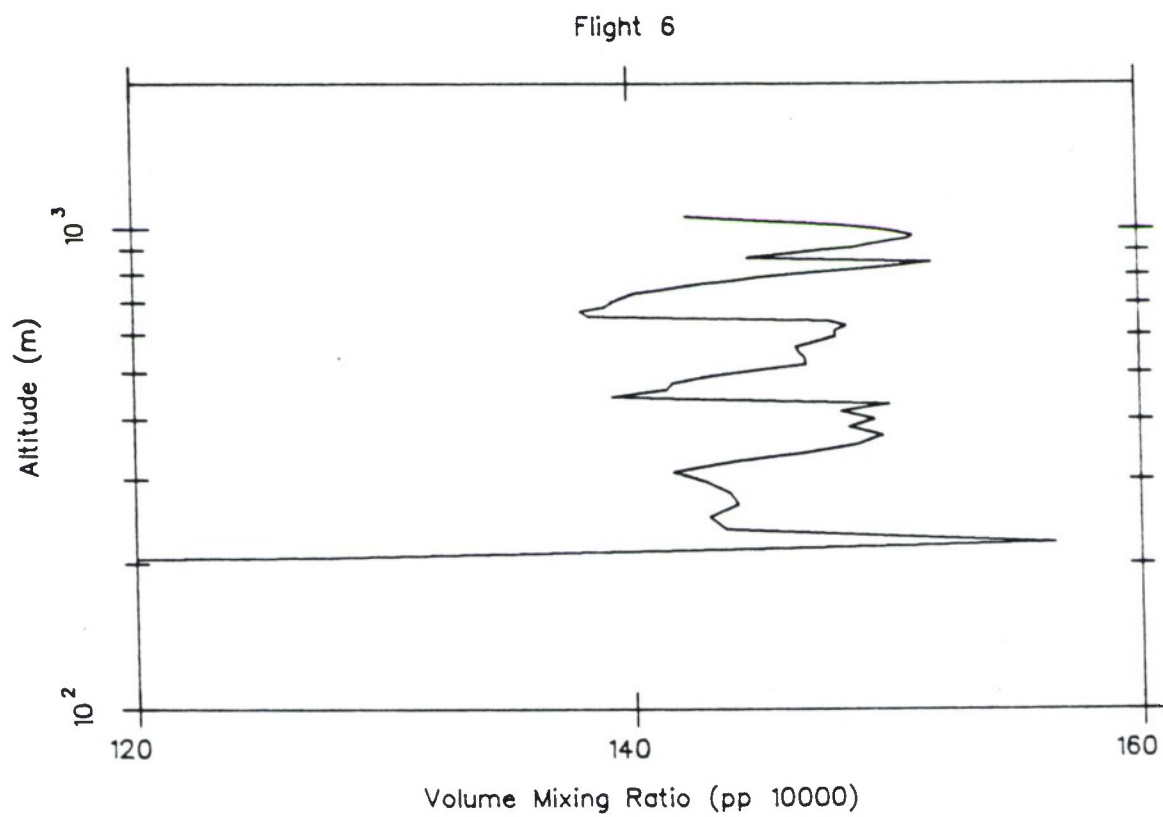


FIGURE 8. AVERAGE WATER VAPOR PROFILE FOR FLIGHT 6.

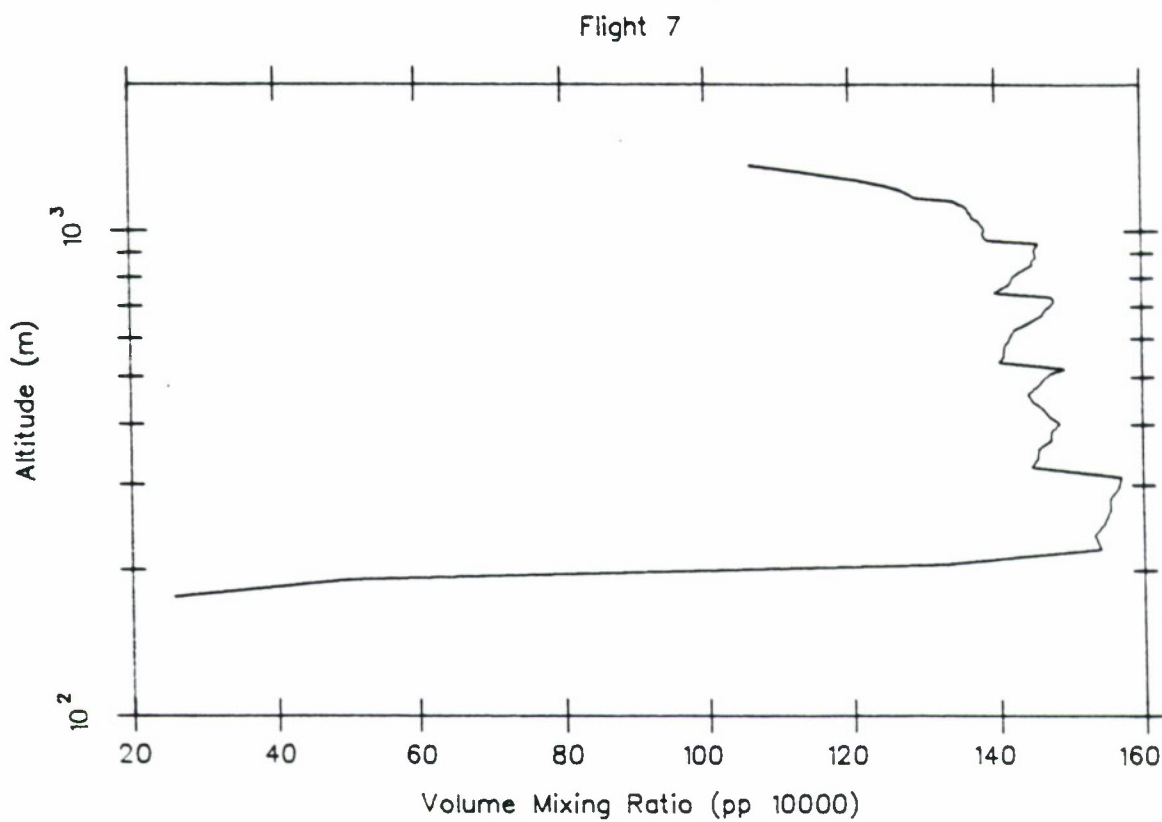


FIGURE 9. AVERAGE WATER VAPOR PROFILE FOR FLIGHT 7.

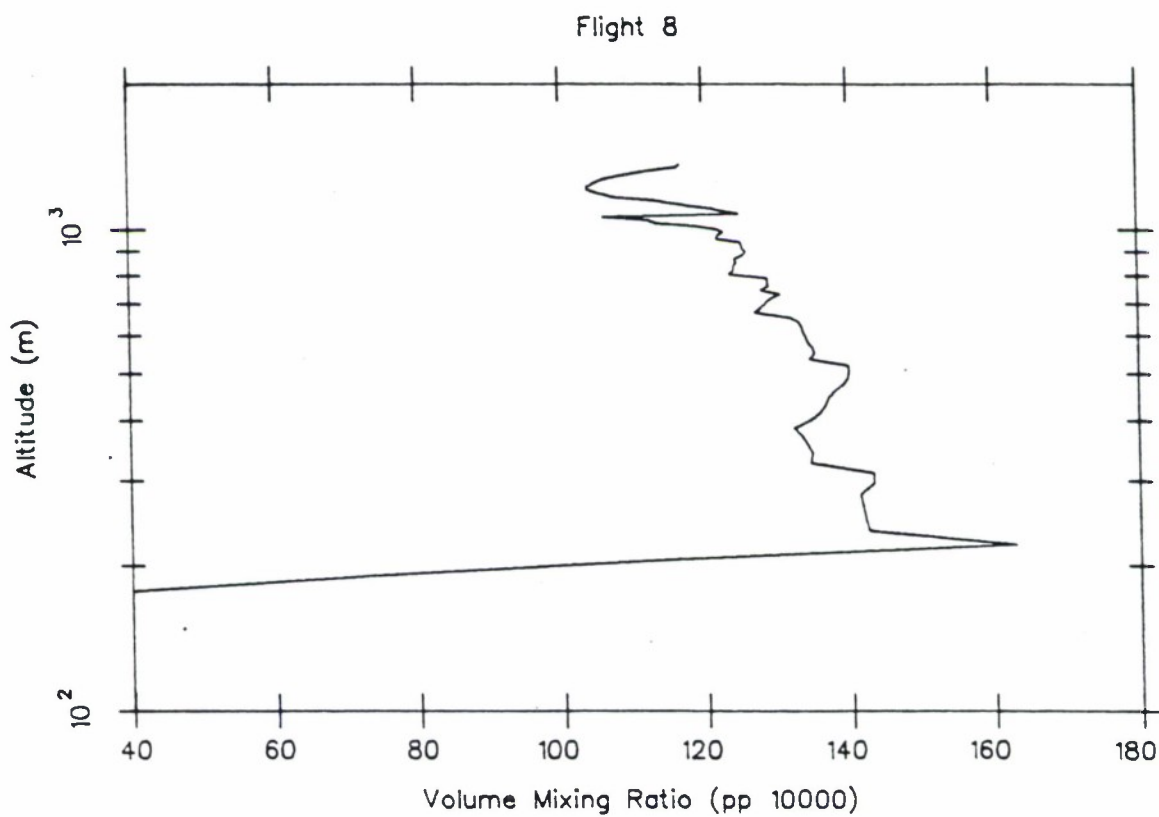


FIGURE 10. AVERAGE WATER VAPOR PROFILE FOR FLIGHT 8.

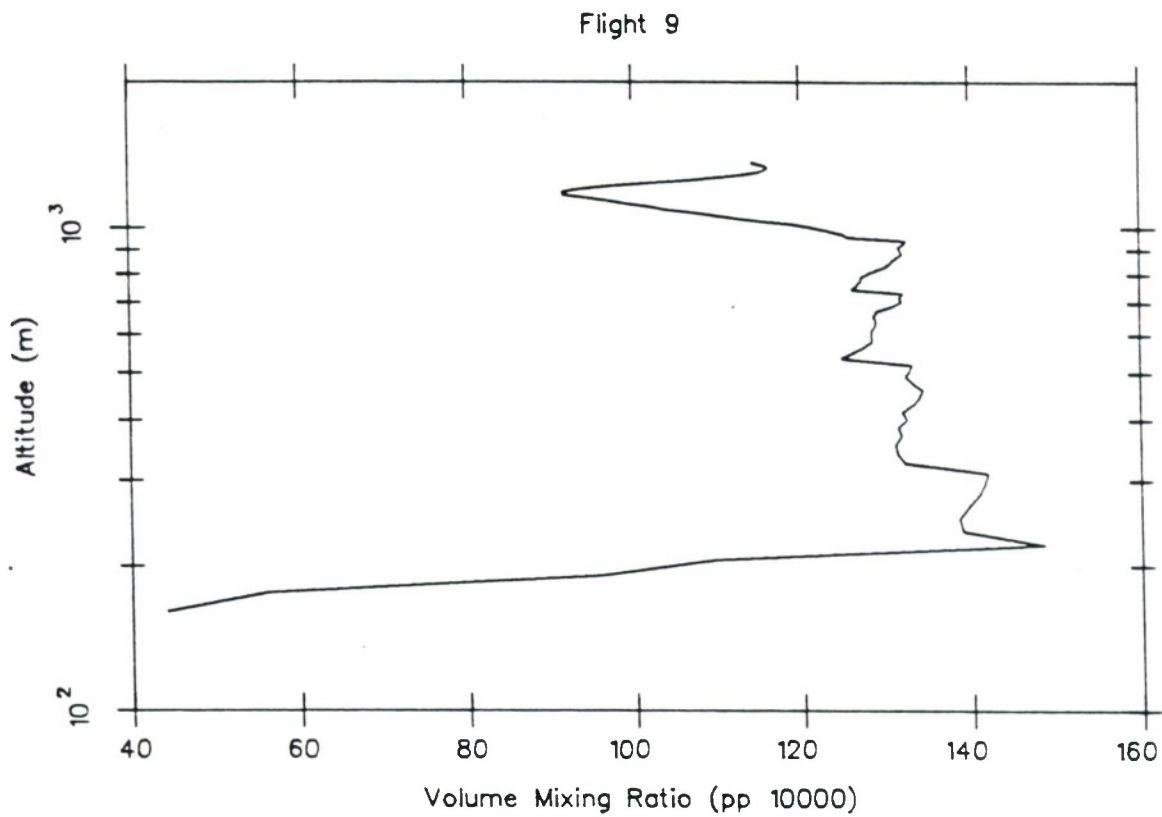


FIGURE 11. AVERAGE WATER VAPOR PROFILE FOR FLIGHT 9.

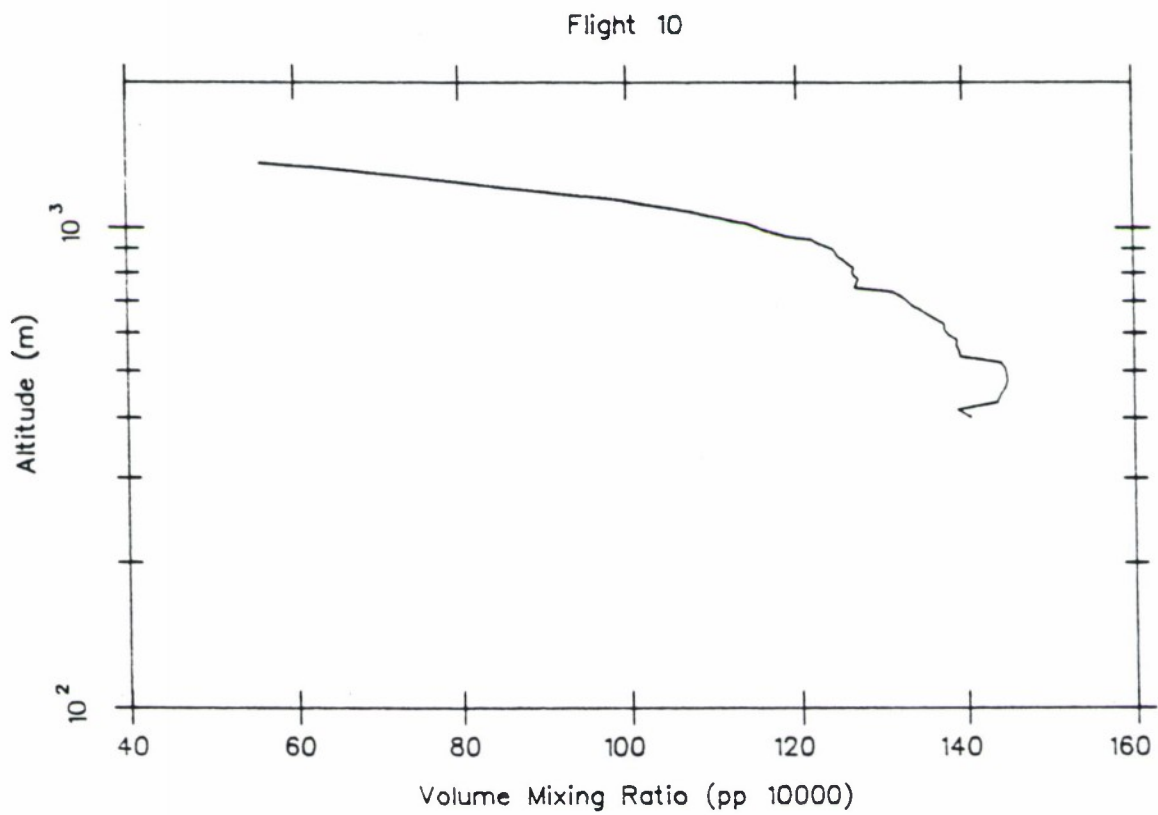


FIGURE 12. AVERAGE WATER VAPOR PROFILE FOR FLIGHT 10.

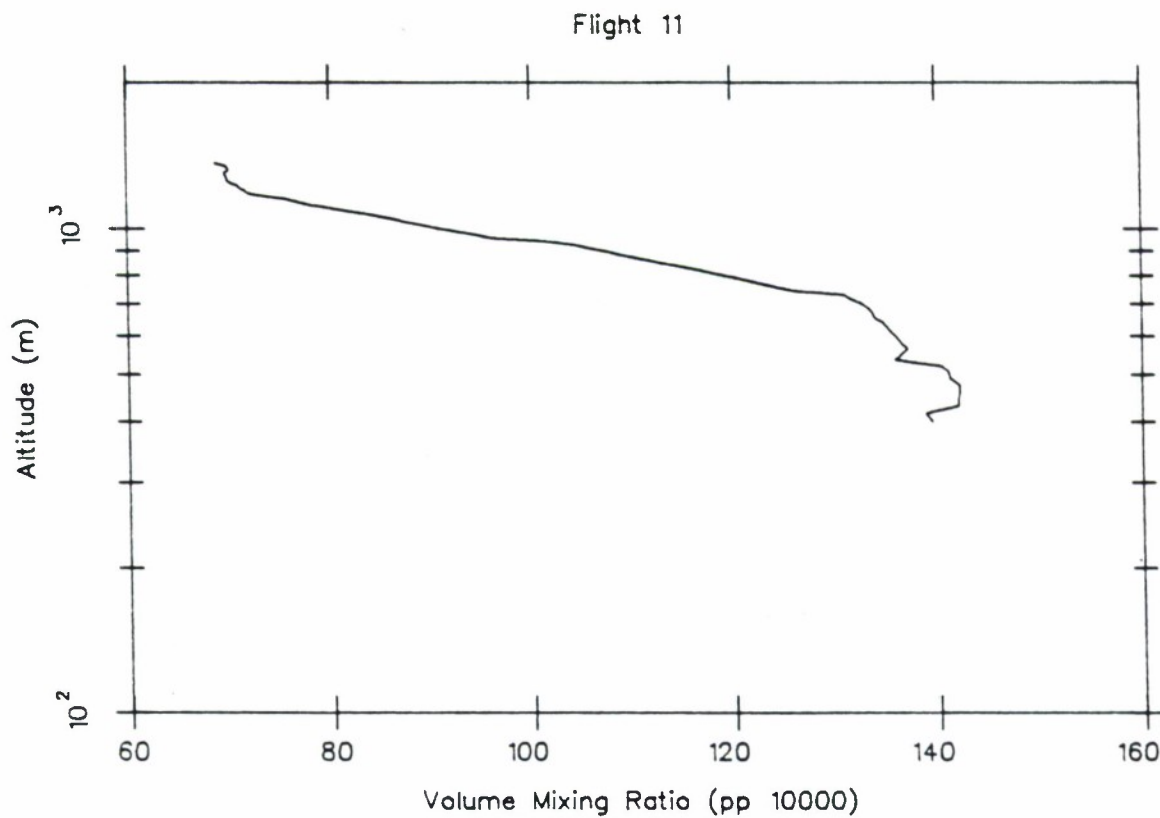


FIGURE 13. AVERAGE WATER VAPOR PROFILE FOR FLIGHT 11.

presence of some degree of cloud cover along the measurement line-of-sight. The four days during which the most reliable transmittance data were collected were July 6, July 12, July 23, and July 25, 1984. Table 5 lists the dates and times for which the transmittance and corresponding radiosonde data discussed in this report were collected. Also listed in Table 5 are the designations of the individual measured spectra. (See the note accompanying the Table for an explanation of these designations which are used to identify the measured spectra in the plots of the data presented in Section 2.2.2).

2.2.1. METEOROLOGICAL CONDITIONS OCCURRING DURING COLLECTION OF THE LFLID SUPPORT DATA

Meteorological conditions were monitored during the LFLID support tests by radiosondes launched from a sea-level location in Kihei, Maui. This site is located approximately 21 km from the Air Force Maui Optical Station (AMOS) site at the top of Mt. Haleakala on Maui. The receiving telescopes used in collecting the long-path transmittance data were located at the AMOS observatory. Figure 14 shows the location of the various sites used in the transmittance and radiosonde measurements. The transmittance-measurement receiver telescopes were located at an altitude of 3.05 km at the AMOS observatory indicated by the symbol R in the Figure. The sources used in the measurement were located approximately 40 m above sea level near Maneli Bay on the island of Lanai (indicated by the symbol S in the Figure). The slant-path range between the source and receiver was 66.2 km.

A preliminary set of measurements was made in January 1984 with the source located at the position S' in the foothills of the West Maui mountains, using a 35 km path.

TABLE 5. TRANSMITTANCE AND RADIOSONDE MEASUREMENT TIMES.

TRANSMITTANCE MEASUREMENT DATE		RADIOSONDE MEASUREMENT DATE		TRANSMITTANCE SPECTRUM DESIGNATION
GMT	HST*	GMT	HST	
<u>7-6-84</u>		<u>7-6-84</u>		
1012	0012	1044	0044	S06R1**
1052	0052	1044	0044	L06R2
1242	0242	1044	0044	S06R5
<u>7-12-84</u>		<u>7-12-84</u>		
1208	0208	1311	0311	S12R1
<u>7-23-84</u>		<u>7-23-84</u>		
1209	0209	1130	0130	S23R1
1246	0246	1130	0130	L23R2
1324	0324	1130	0130	S23R3
1402	0402	1130	0130	L23R4
<u>7-25-84</u>		<u>7-24/25-84</u>		
1051	0051	0836	2236 (7/24)	S25R1
1226	0226	0836	2236 (7/24)	L25R3
1303	0303	0836	2236 (7/24)	S25R4
1343	0343	0836	2236 (7/24)	L25R5
1419	0419	0836	2236 (7/24)	S25R6

* = HST (Hawaiian Standard Time)

** = A code identifying a particular measured transmittance spectrum. The initial S[L] indicates the short wavelength (3-5 μm) or [long] wavelength (8-12 μm) spectral band. The next two digits indicate the date in July 1984 when the spectrum was measured and the last two digits indicate the sequential position of the particular data file recorded on that date; e.g. S23R3 indicates a short wavelength spectrum recorded on July 23 in the third sequential file for that date.

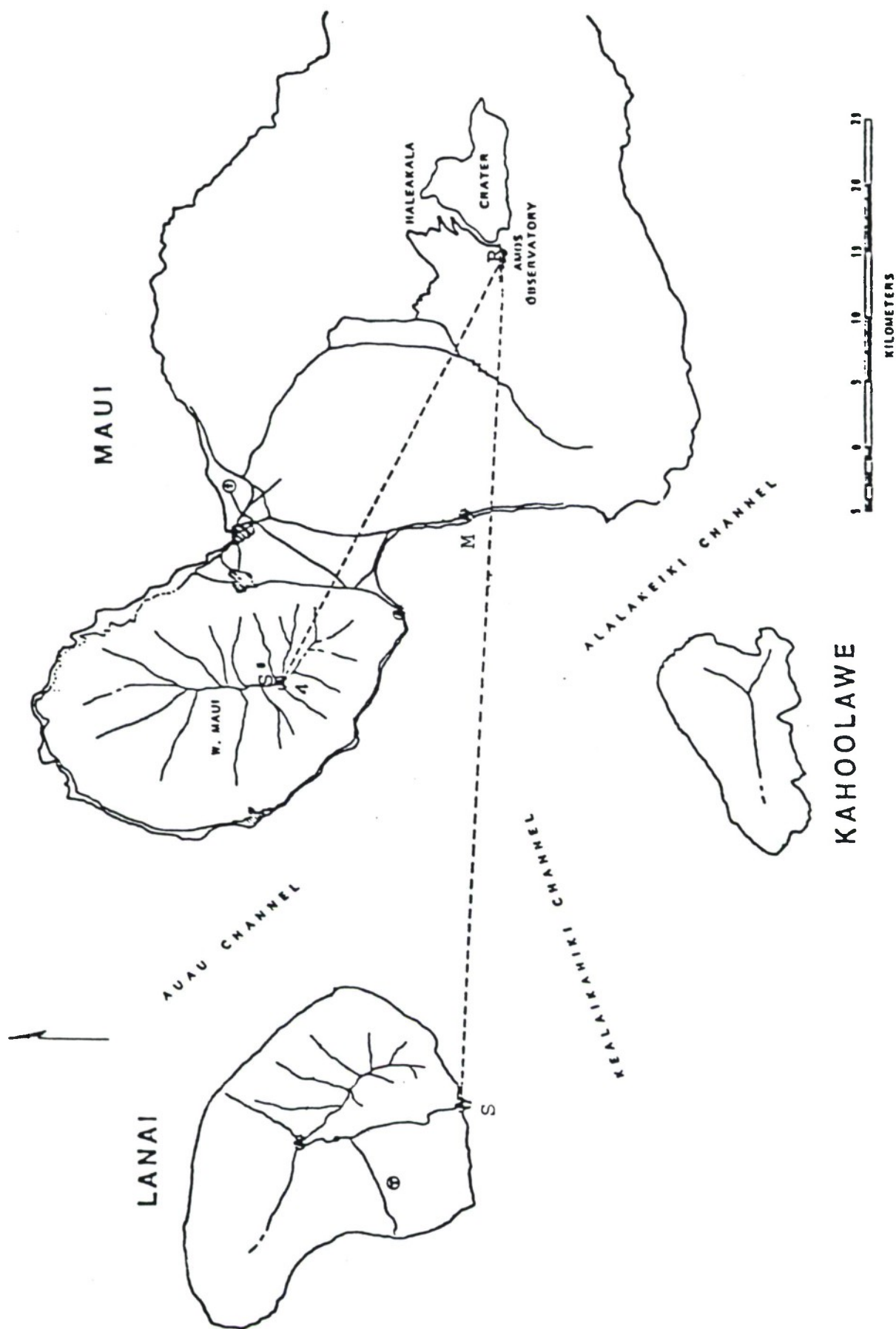


FIGURE 14. SITES USED IN LFLID SUPPORT MEASUREMENTS.

The data from the earlier tests are not considered here, however. The site in Kihei used for the radiosonde launches is shown by the symbol M in Figure 14.

Figures 15 and 16 show the measured temperature and derived water vapor density profiles, respectively, for the radiosonde data which accompanied the selected long-path transmittance spectra discussed in this report.

The temperature data shown in Figure 15 show the presence of temperature inversions occurring at altitudes between 1.5 and 2.1 km in three of the four measurement periods. Only the data for 6 July show a consistent lapse of temperature with increasing altitude.

The four water vapor density profiles corresponding to the transmittance measurements are shown in Figure 16. They were derived from radiosonde-measured temperature and relative humidity profiles. They show a rather consistent decrease in water vapor density (ρ_{H_2O}) with a relatively small variation at each altitude ($\sim \pm 1.3 \text{ g/m}^3$ from the average value at a given altitude) for altitudes below 2.1 km. Above this level a larger spread in the values is observed ranging from 0.2 g/m^3 to 5.8 g/m^3 at an altitude of 3 km. (The AMOS observatory is located at an altitude of 3.05 km.)

The source (S in Figure 14) was located sufficiently far from the ocean shore that locally high aerosol scattering, related to heavy surf conditions, would not contribute to the measured transmittances. Sugar cane fires, generating a large amount of smoke, are present during the sugar cane harvest and normally occur during daytime and early evening. The long-path transmittance measurements were carried out during the hours between midnight and dawn, well after smoke from the burning cane fields had been ventilated

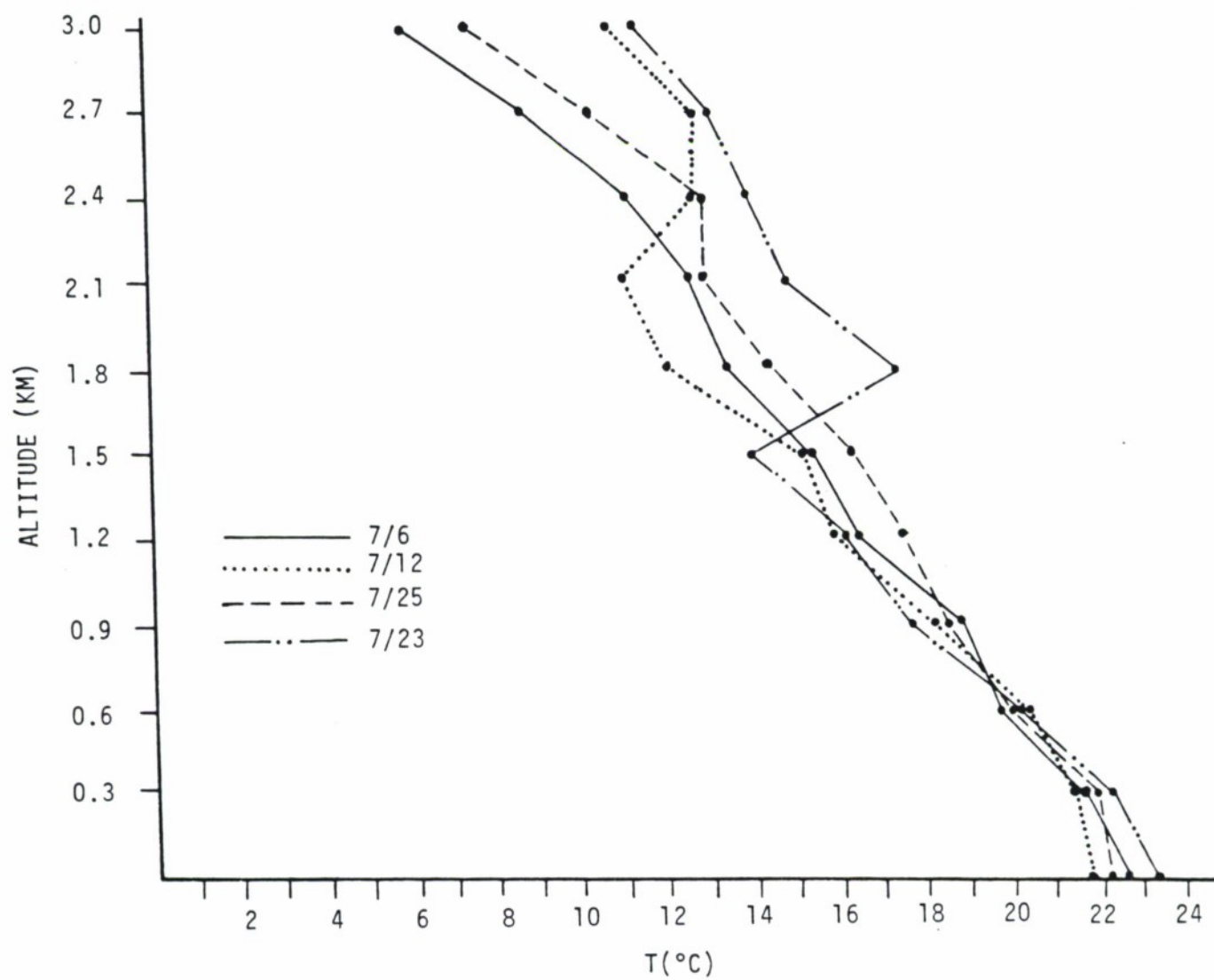


FIGURE 15. VERTICAL TEMPERATURE PROFILES MEASURED WITH A RADIOSONDE.

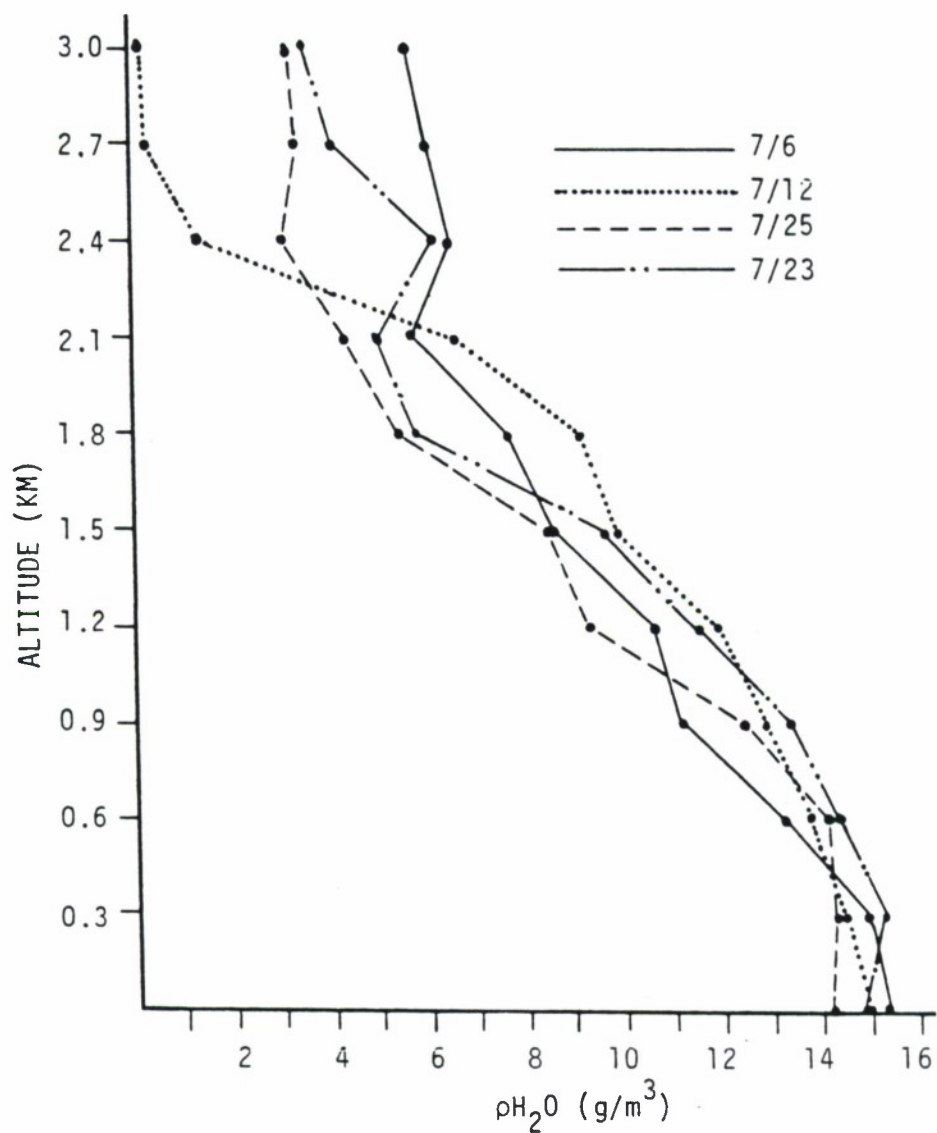


FIGURE 16. VERTICAL WATER VAPOR DENSITY PROFILES DERIVED FROM RADIOSONDE MEASUREMENTS.

away from the path used for the transmittance measurements. Trade winds, a dominant feature of the normal weather patterns of the Hawaiian islands, typically persist from a northeasterly direction at speeds varying between 4 and 10 m/s, and would clear the transmittance-measurement path of island-generated aerosols during the few hours after the cane fields had been burned.

2.2.2 THE LFLID SUPPORT LONG-PATH TRANSMITTANCE DATA

2.2.2.1 Measurement Configurations and Instrumentation

The instrumentation used in the LFLID support transmittance measurements included a 1200 K blackbody source, used alternately with two optical projection systems for two separate measurement configurations. Two large-aperture receiver telescopes were also used in the measurements. One measurement configuration served as the basis for providing an absolute transmittance calibration for the long-path measurements. In this configuration the radiant output from the blackbody source was projected through the optical system of an eight-inch aperture, f/6 Newtonian telescope.

For the absolute-transmittance-measurement configuration the AMOS Advanced Multicolor Tracker or AMOS (AMTA) sensor package [6], mounted on the AMOS 1.2 m aperture, B29 telescope, served as the receiver system. The AMTA package consists of a 25 element infrared sensor array, a dual channel contrast-mode photometer and a boresight TV camera.

A second measurement configuration was used to obtain moderate-resolution (nominally two-percent of the base wavelength) spectral data. In this configuration the blackbody source was used with a 60-inch aperture optical projection system built into a modified World War II anti-aircraft searchlight.

Figure 17 shows a construction diagram for the modified 60" searchlight which is used both as a source and receiver optical system in long-path atmospheric transmittance measurements. The major modification consists in the use of a two-sided secondary mirror to provide a Cassegrainian optical system when used with the original searchlight reflector (a 60" diameter, $f/0.4$, electro-formed parabolic mirror). The incoming radiation blocked by the 15" diameter secondary mirror is collected at a second focal point formed by a parabolic surface incorporated into the back of the secondary mirror.

Figure 18 contains optical diagrams showing the geometry and calculated performance of the modified searchlight optical system when used with a one-inch diameter blackbody source as was the case in the LFLID support measurements.

The searchlight transceiver optical system was provided for the LFLID support tests by the U.S. Army Atmospheric Sciences Laboratory (ASL) at White Sands Missile Range, New Mexico. It was operated during the tests by OMI under contract to ASL.

The design and construction of the modified optical system was originated by Richard Horton of the AVCO Corporation, while formerly with the Naval Research Laboratory (NRL) Washington, D.C. This system was provided to ASL by NRL for use in long-path atmospheric transmittance measurements.

The receiver optical system used when the 60-inch optical projection system was in use was the AMOS 1.6 m aperture telescope, coupled to the AMOS Long Wavelength Infrared (LWIR) Spectral Radiometer [6]. The LWIR sensor package incorporates a two-element Si:As detector cooled to 11 K, providing a spectral coverage from 2 to 24 μm . A

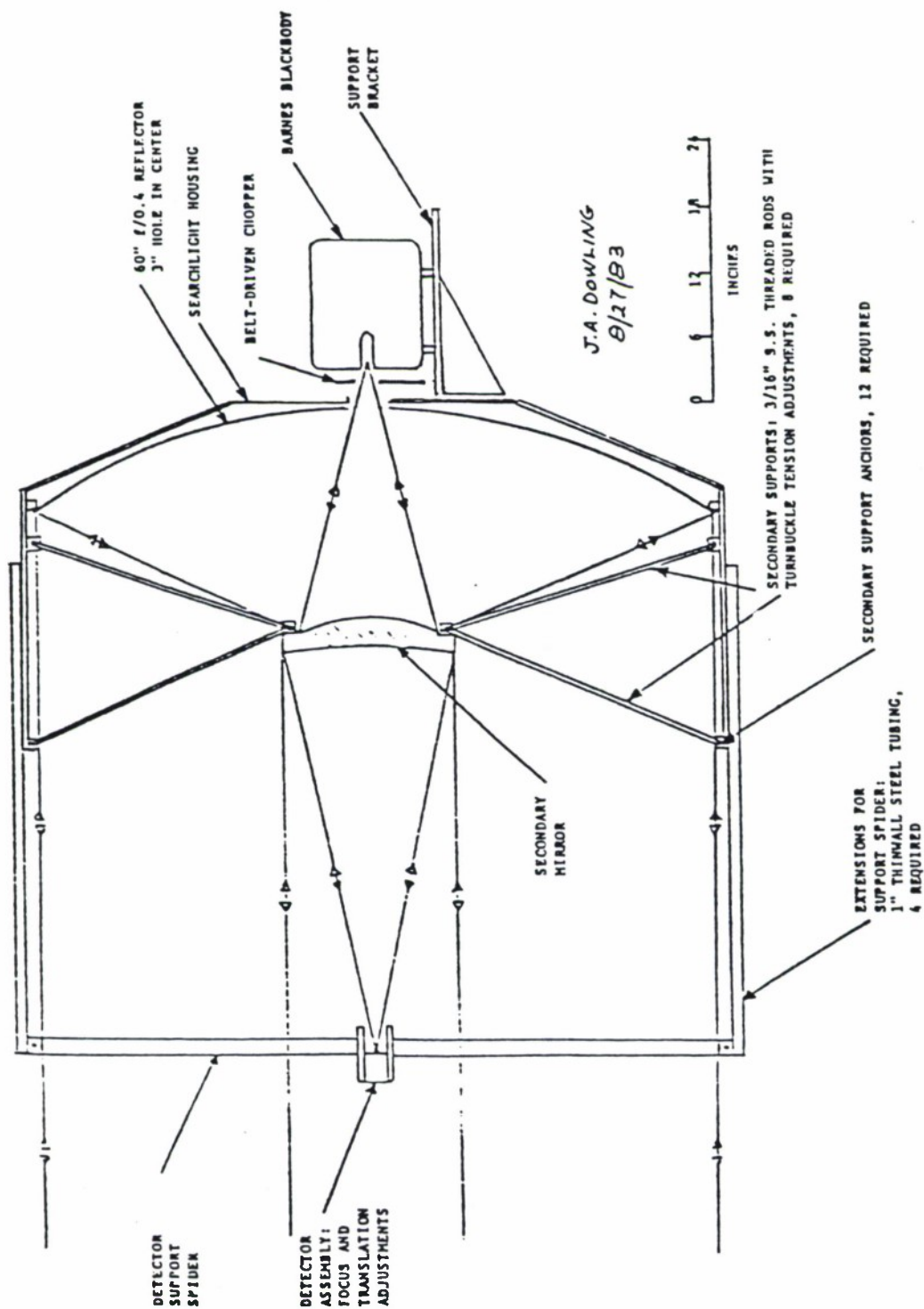


FIGURE 17. 60" SEARCHLIGHT SOURCE CONSTRUCTION DIAGRAM.

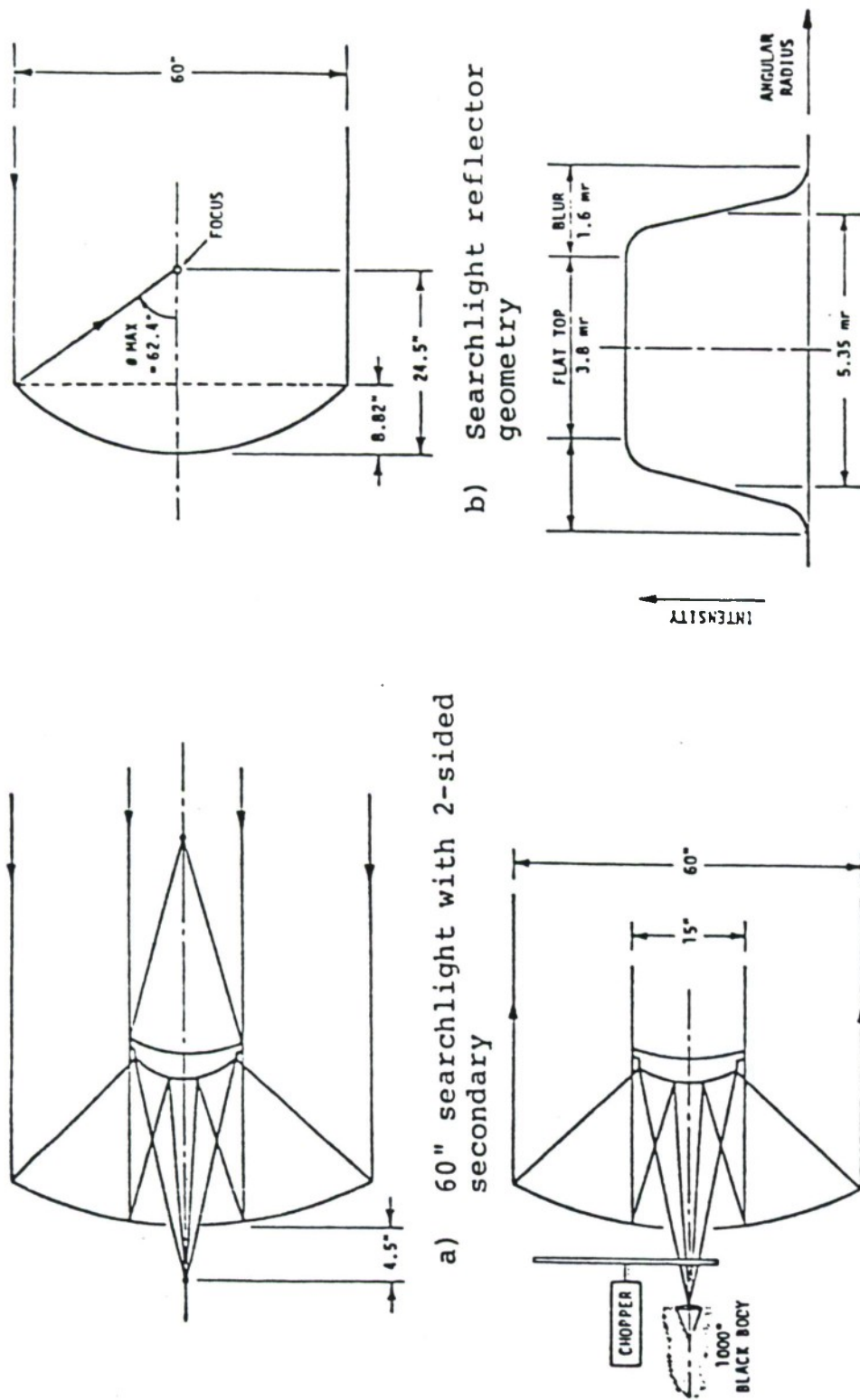


FIGURE 18. MODIFIED 60" SEARCHLIGHT OPTICAL SYSTEM PERFORMANCE.

spectral resolution of 2% of the base wavelength in two bands (3.2 to 5.5 μm and 7.8 to 14.0 μm) is provided by the use of two circular variable filters (CVF). The instantaneous field-of-view of the LWIR spectral radiometer is 10x20 arcseconds.

The transmittance signal from the cooled preamplifier in the LWIR package was processed with a Princeton Applied Research (PAR) model HR-8 lock-in amplifier (LIA). The lock-in amplifier was supplied with a reference signal obtained from a chopper mounted at the source. The chopper-reference was transmitted to the AMOS observatory using a radio link. A 155 MHz single-side-band (SSB) FM transmitter and receiver were operated between the two ends of the transmittance measurement path for this purpose. Voice communications were available when the reference signal was not required.

The analog output signal from the LIA was sent to an ALI 12 bit A/D digitizer, and sampled on program command using a Commodore 64 computer. The analog output from the CVF passband wavelength encoder was digitized using another channel of the digitizer for simultaneous sampling by the data sampling program.

The CVF controller was operated in a step and hold mode, with 101 equal-wavelength steps covering each of the two wavelength bands. Optimally, the transmittance could be sampled at 1% wavelength intervals, requiring 67 samplings and a varying wavelength interval. It was more straightforward to sample the data using a larger number of equal wavelength intervals. The data sampling algorithm allows a settling time, approximately equal to the lock-in-amplifier time constant, between samples to allow low level microphonics produced by the CVF stepper motor to decay. The

measured spectrum can be observed on a slowly-sweeping signal analyzer.

The algorithm used for data collection was optimized to allow data collection under differing noise conditions and for different correlation times for the fluctuations in the transmittance signal.

2.2.2.2 Calibration of the Long-Path Transmittance Data

Two types of calibration measurements were performed to provide an absolute-transmittance calibration of the long-path spectra obtained with the LWIR Spectral Radiometer. The radiometric response of the AMTA sensor package was calibrated using a "Jones Calibration" at the aperture of the 1.2 m telescope. In this measurement the AMTA detector element is overfilled by the blackbody radiant output collected by the 1.2 m telescope and imaged at the AMTA detector. No collimating optics are used with the source in this configuration.

A second radiometric calibration was performed using the blackbody source together with the eight-inch Newtonian telescope collimating optics. In this case two "short-path" measurement geometries were used. One path was approximately 100 m in length. In this case the source and source optics were located near the AMOS observatory on the top of Mt. Haleakala. The second location used for the source and its collimating optics was about 4 km distant from the AMOS observatory at a site near the observatory access road which could be viewed by the two AMOS telescopes.

The two latter measurements provided a calibration of the overall measurement system efficiency including the source and receiver optical systems.

The long-path spectra obtained with the 60" search-light-blackbody source and 1.6 m telescope - LWIR sensor receiver were normalized for absolute transmittance by means of the independent measurements made using the same IR source projected through the 8" Newtonian telescope and received by the 1.2 m telescope - AMTA sensor combination. Convolution integrals of the AMTA filter functions with the measured LWIR relative transmission spectra were performed for each measured spectrum and the results were equated with the measured transmittance for that particular AMTA filter band. The resulting multiplicative scale factors thus obtained were used to provide the absolute normalization of the LWIR Spectral Radiometer spectra. The estimated uncertainties in the absolute calibration of the resulting spectra are approximately $\pm 30\%$.

Prior to the absolute transmittance normalization described above, instrumental, wavelength-dependent effects were removed from the LWIR Spectral Radiometer data by ratioing each long-path spectrum to a "zero-path" spectrum. The latter were obtained using the blackbody source and 60" projection optics with the 1.6 m telescope and LWIR Spectral Radiometer operating over the 100 m path near the AMOS observatory.

REDUCTION AND ANALYSIS OF THE NASA DIAL H₂O DATA3.1 AVERAGE H₂O PROFILE OVER ALL FLIGHTS

An average water vapor profile was obtained from the DIAL data by averaging all of the data from flights 1 through 10 for each altitude. The resulting profile is shown in Figure 19. There were only a few soundings with data below 250 m altitude, and this is why the average profile is somewhat erratic at the lowest altitudes. At most of the other altitudes several hundred values were used in the average.

Standard deviations of the H₂O data were also calculated for each altitude. Water vapor profiles representing the average value plus one standard deviation and the average minus one standard deviation for each altitude are also shown in Figure 19.

The water vapor concentrations are represented in Figure 19 in parts per 10,000. Table 6 gives the equivalent of 100 parts per 10,000 in other units which are commonly used for water vapor.

For purposes of comparison, the water vapor profile for the midlatitude summer standard atmosphere [2] is plotted in the same units in Figure 20. Above about 600 m the standard atmosphere and the average profile from the data are roughly equivalent. Below 600 m, the average profile is somewhat drier than the standard atmosphere. Also shown in Figure 20 is the midlatitude summer profile shifted to result in 100% relative humidity at the surface. The entire profile was shifted by the amount of water vapor (parts per 10,000) required to give saturation at the surface. This did not

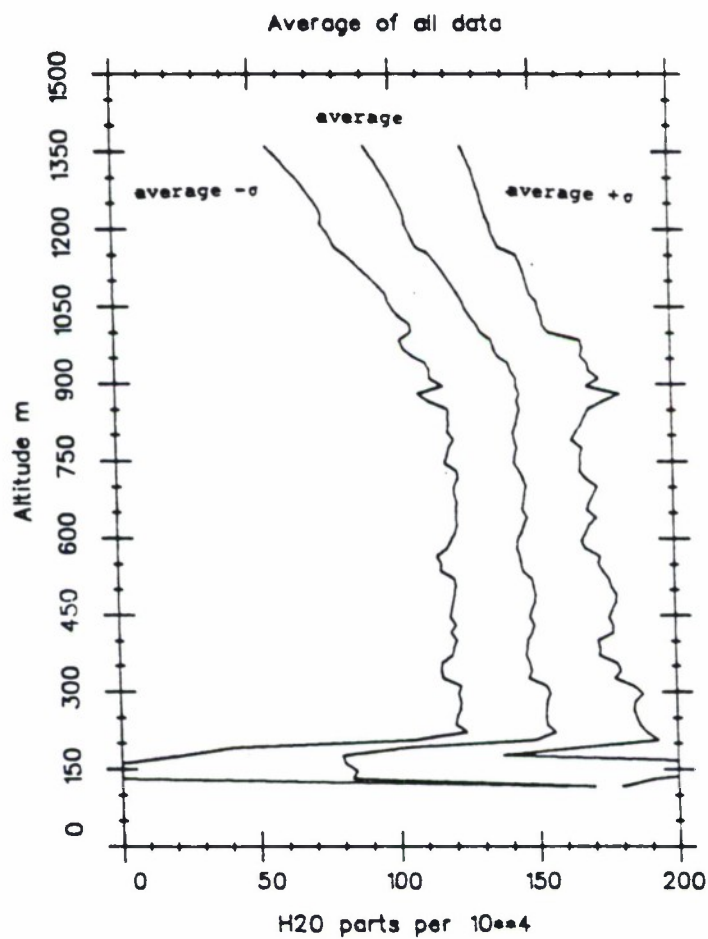


FIGURE 19. WATER VAPOR PROFILE OBTAINED FROM AVERAGING ALL DATA IN FLIGHTS 1 THROUGH 10, AND PROFILES RESULTING FROM ADDING AND SUBTRACTING THE STANDARD DEVIATION OF THE DATA AT EACH ALTITUDE.

TABLE 6. CONVERSION FACTORS FOR WATER VAPOR UNITS.

	PARTS PER 10,000	g/m^3	TORR
Sea Level	100	7.56	7.60
1 km Altitude	100	6.73	6.77

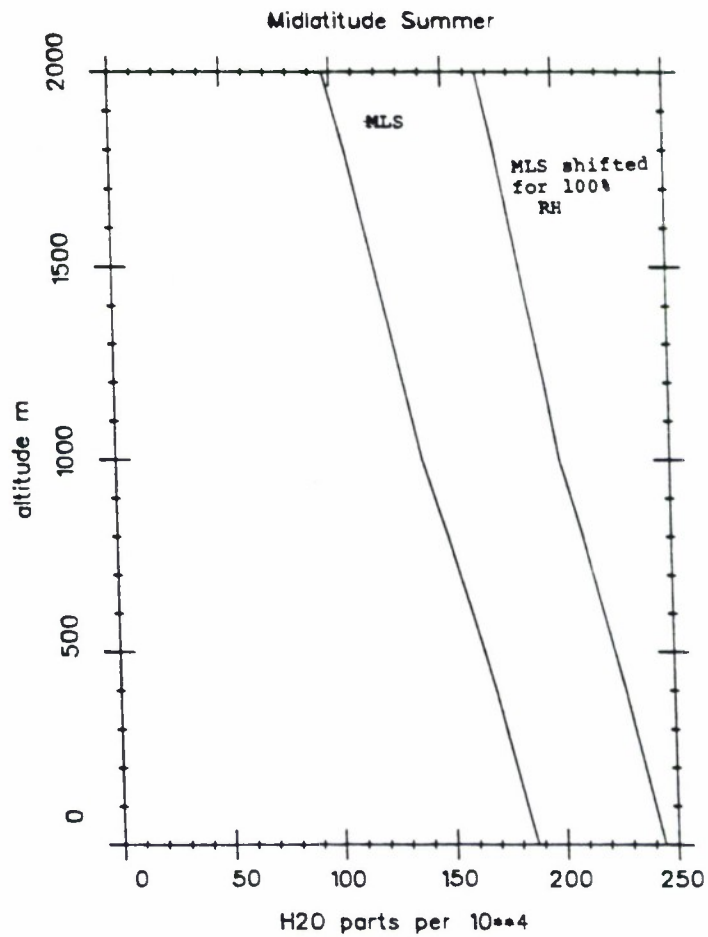


FIGURE 20. MIDLATITUDE SUMMER STANDARD ATMOSPHERE WATER VAPOR PROFILE (MLS) AND THE MIDLATITUDE SUMMER PROFILE SHIFTED TO GIVE 100% RELATIVE HUMIDITY AT THE SURFACE.

result in saturation at any of the higher altitudes. although relative humidity is high at all altitudes. The standard atmosphere profile for 100% humidity at the surface contains considerably more water vapor than the average-plus-one-standard-deviation profile obtained from the data.

3.2 TOTAL COLUMN WATER AMOUNTS

The total amount of water in each of the vertical columns sampled, the precipitable water, can be calculated from the mixing ratio profiles. The precipitable water, h in cm, in a column of water is given as

$$h = \frac{P_0}{g \rho_{H_2O} H} \int_{z_1}^{z_2} q_v(z) e^{\frac{-z}{H}} dz \quad (1)$$

where P_0 is the surface pressure, H is the pressure scale height g is the acceleration of gravity $q_v(z)$ is the volume mixing ratio at the height z and ρ_{H_2O} is the density of liquid water. Figures 21 to 31 display the precipitable water values calculated using (1) for each of the flights. Flight 1 had a separate downward and upward leg and the results from the legs have been plotted separately. Also results from Flight 11 have not been included. The reason is that Flight 11, apparently, corresponds to the flight back to NASA-Langley and is not in the area sampled during the other flights. In evaluating the results in Figures 21 to 31 one must remember that the vertical columns sampled varied from one location to another. Therefore, the variation seen in the figures is not entirely a measure of changes in the atmospheric content of water vapor but instead represents the variation in the depth of the atmosphere sampled.

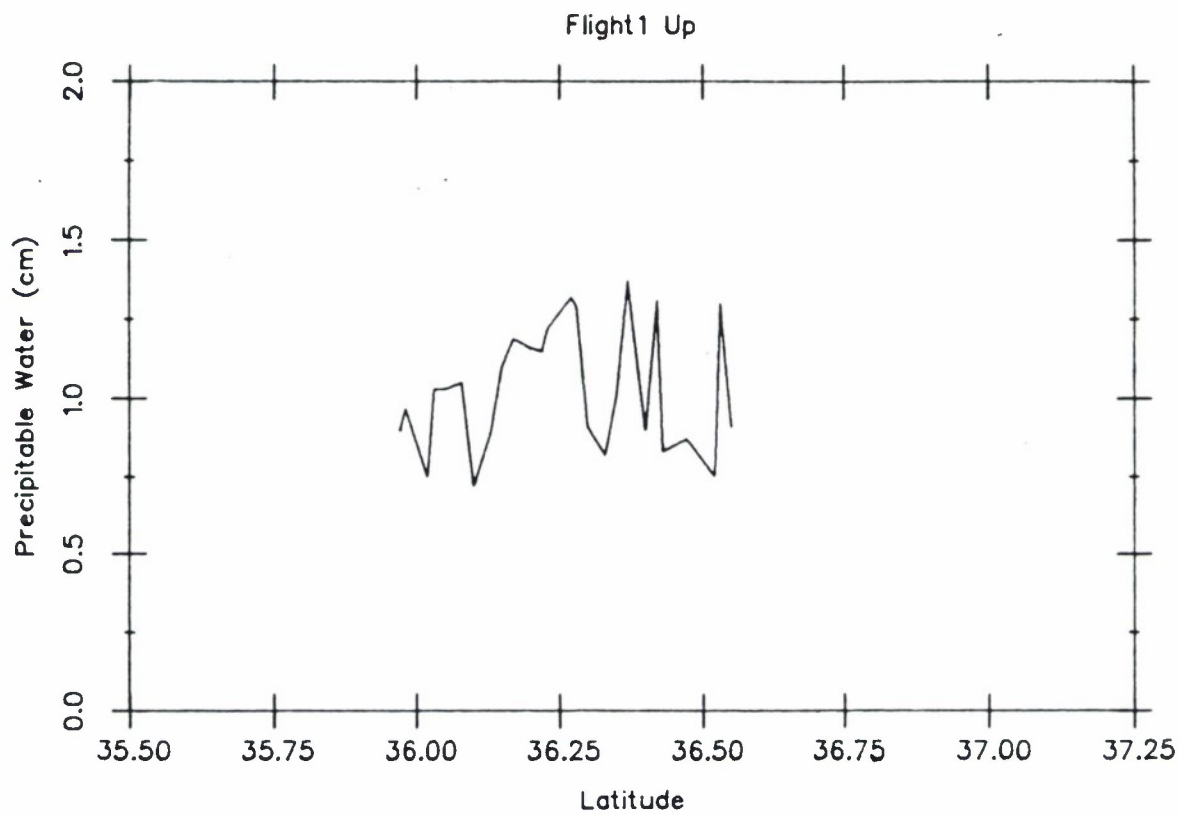


FIGURE 21. PRECIPITABLE WATER AMOUNTS IN THE VERTICAL AIR COLUMNS SAMPLED BY THE NASA-DIAL INSTRUMENT.

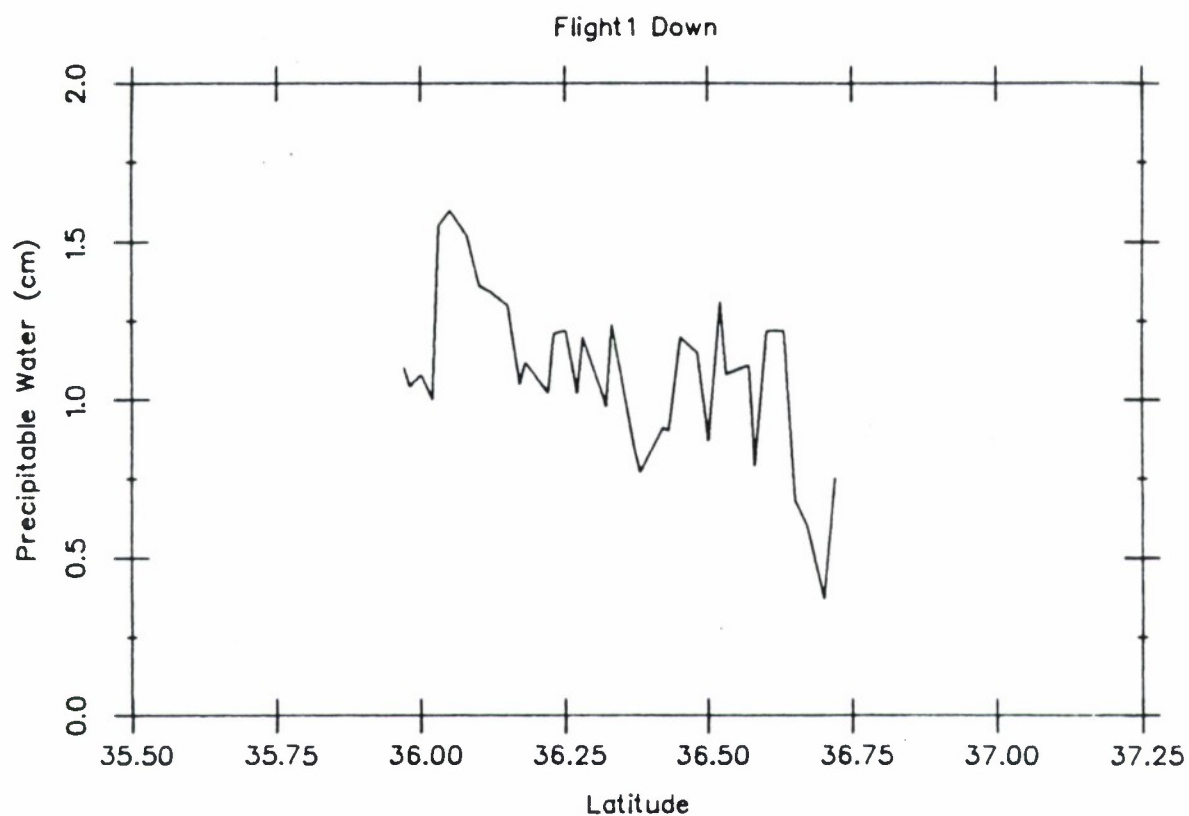


FIGURE 22. PRECIPITABLE WATER AMOUNTS IN THE VERTICAL AIR COLUMNS SAMPLED BY THE NASA-DIAL INSTRUMENT.

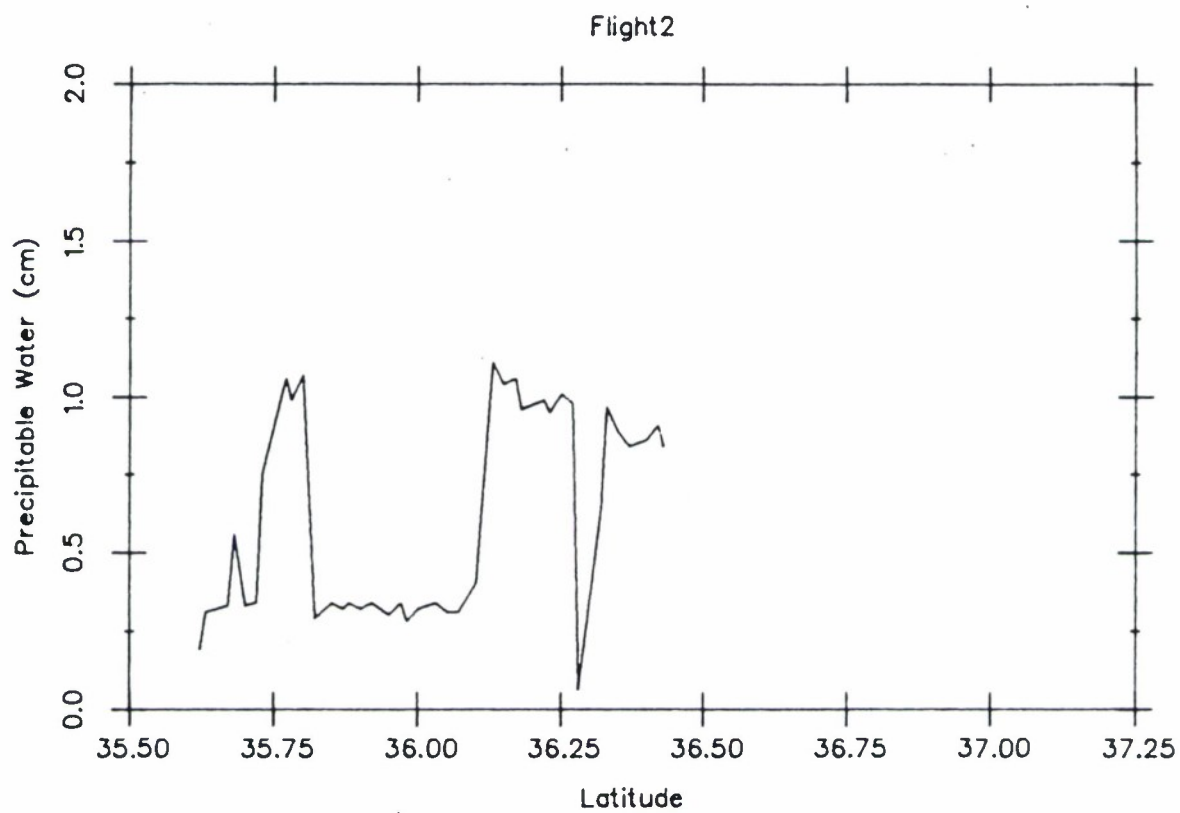


FIGURE 23. PRECIPITABLE WATER AMOUNTS IN THE VERTICAL AIR COLUMNS SAMPLED BY THE NASA-DIAL INSTRUMENT.

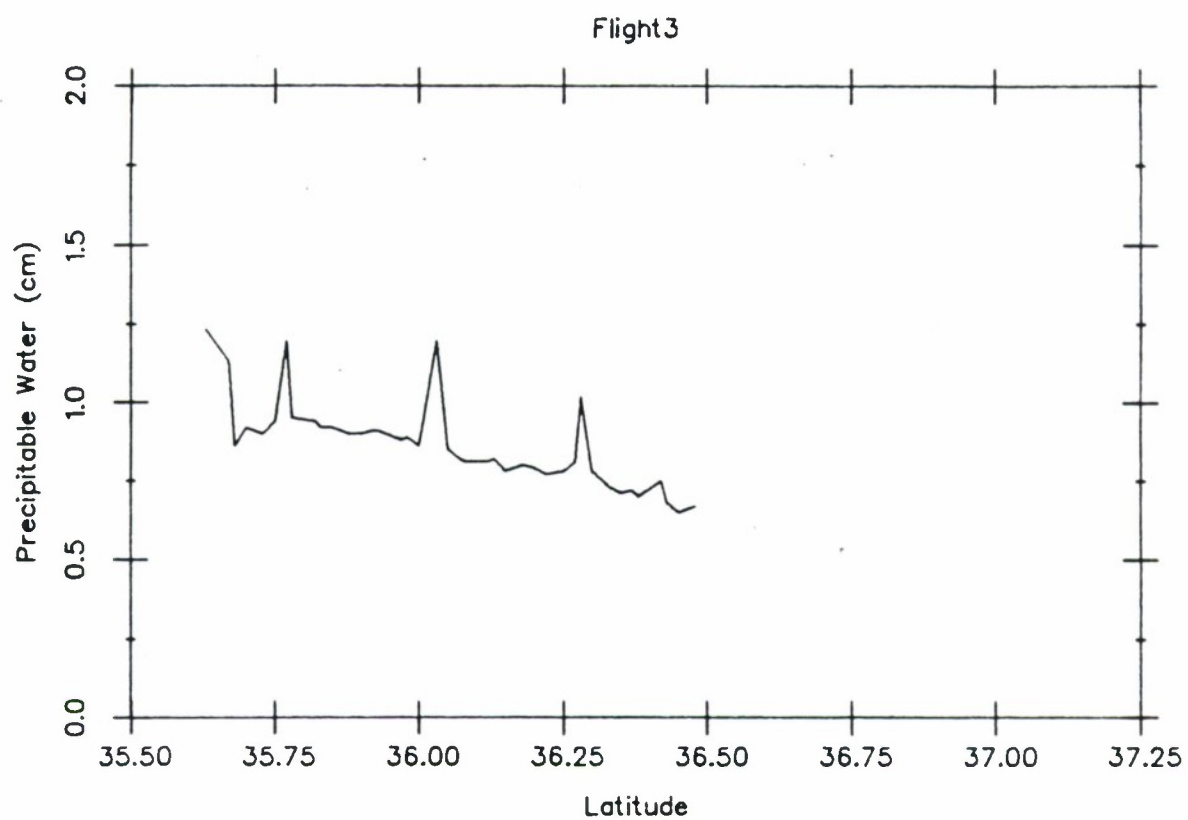


FIGURE 24. PRECIPITABLE WATER AMOUNTS IN THE VERTICAL AIR COLUMNS SAMPLED BY THE NASA-DIAL INSTRUMENT.

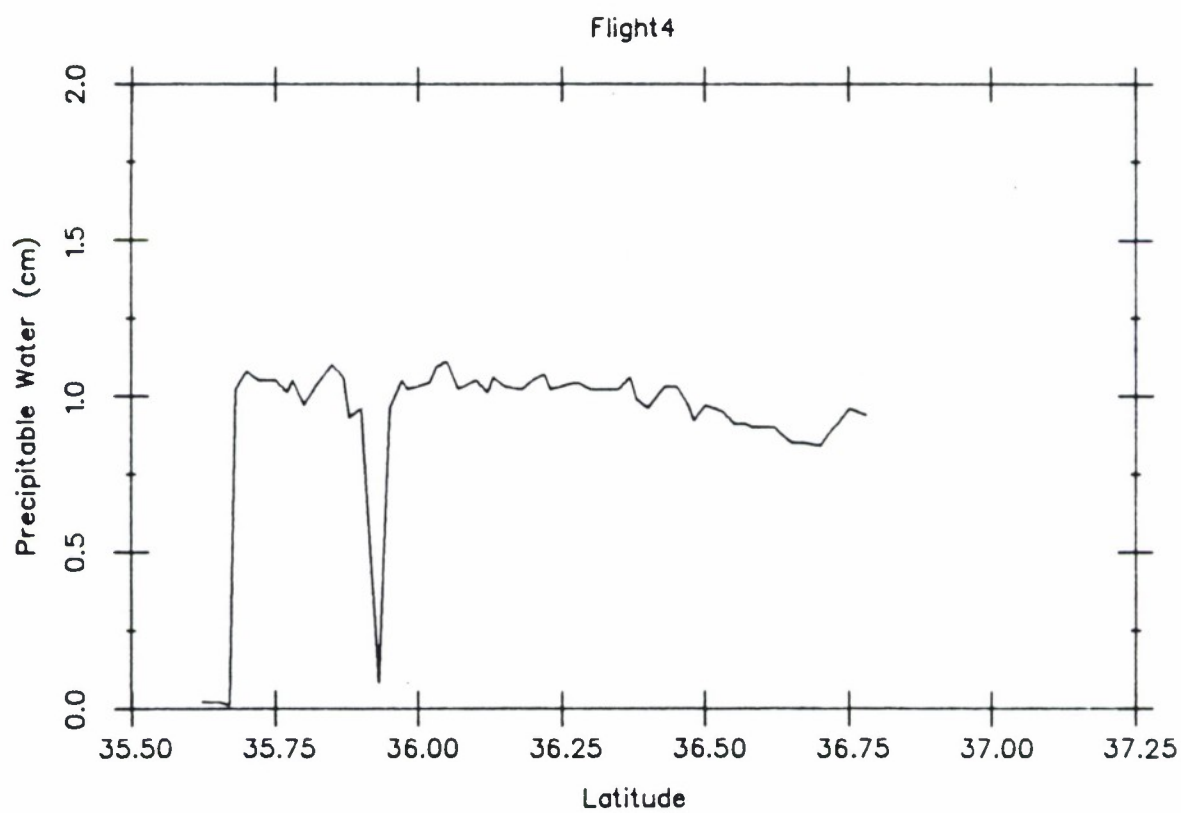


FIGURE 25. PRECIPITABLE WATER AMOUNTS IN THE VERTICAL AIR COLUMNS SAMPLED BY THE NASA-DIAL INSTRUMENT.

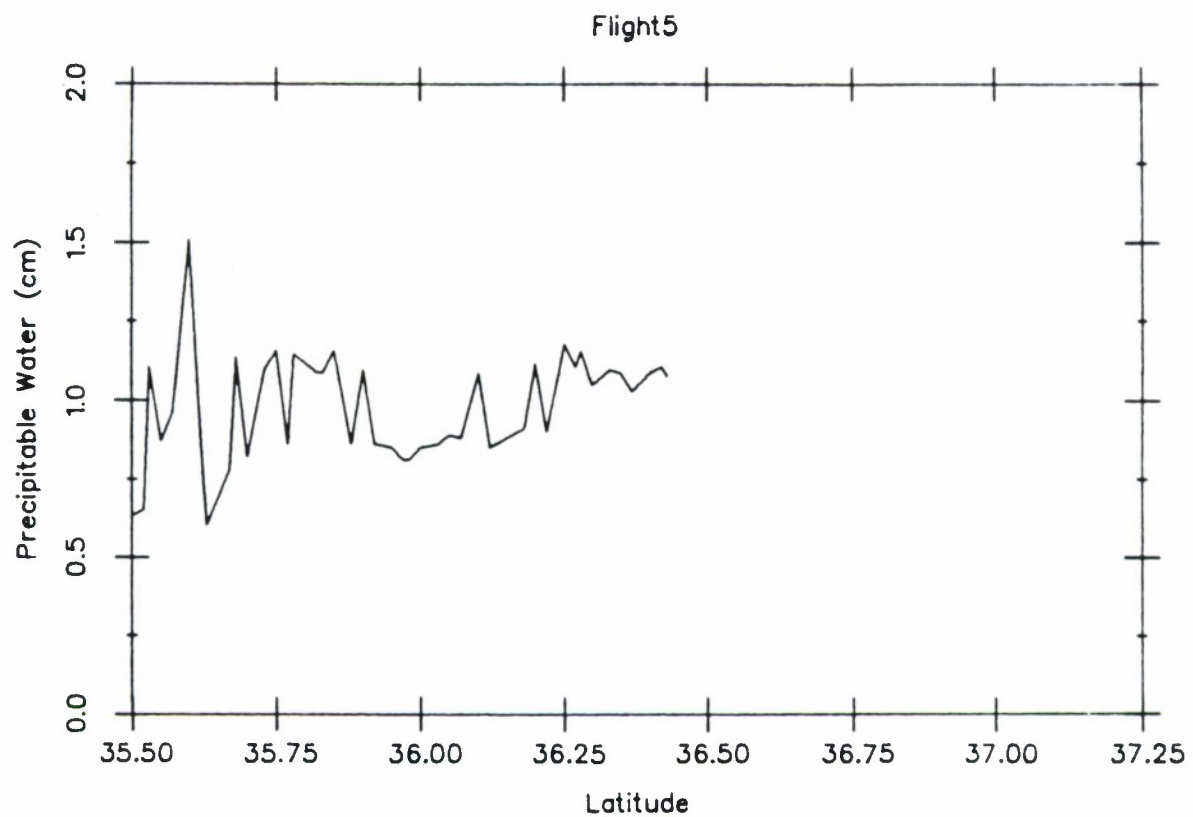


FIGURE 26. PRECIPITABLE WATER AMOUNTS IN THE VERTICAL AIR COLUMNS SAMPLED BY THE NASA-DIAL INSTRUMENT.

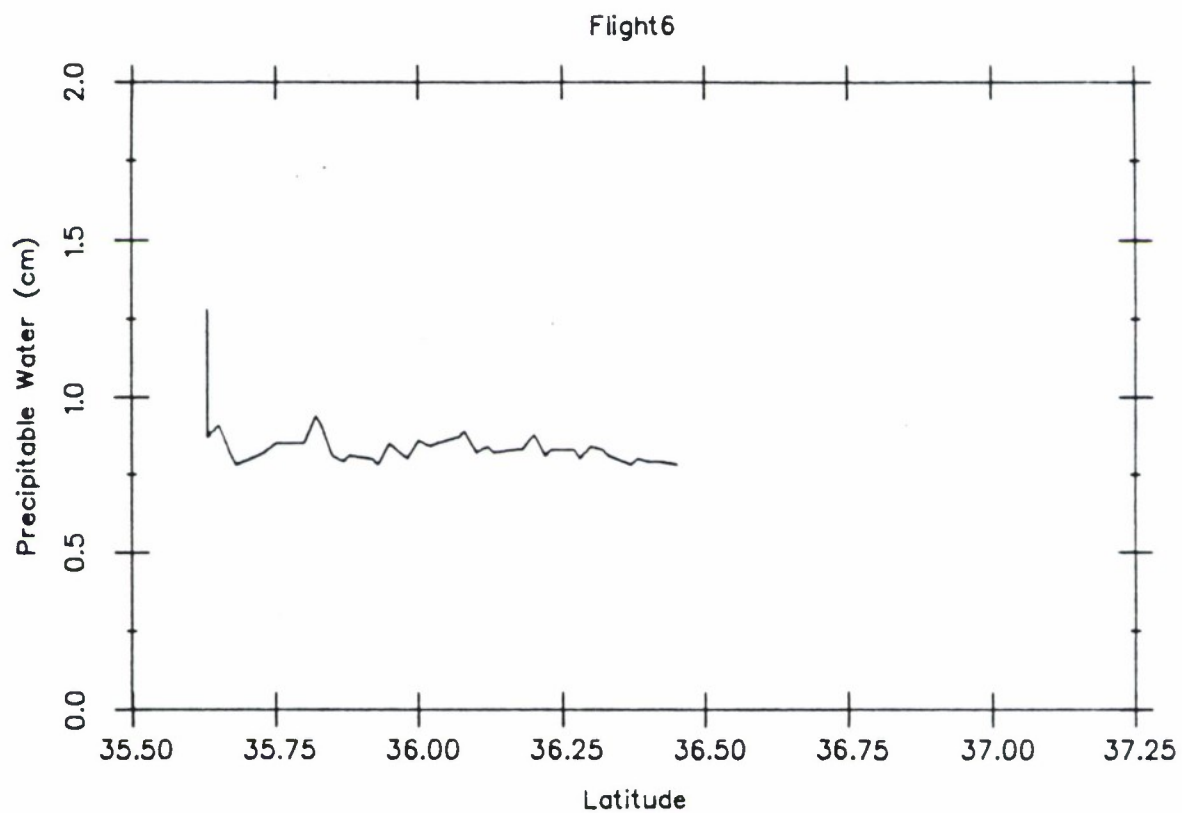


FIGURE 27. PRECIPITABLE WATER AMOUNTS IN THE VERTICAL AIR COLUMNS SAMPLED BY THE NASA-DIAL INSTRUMENT.

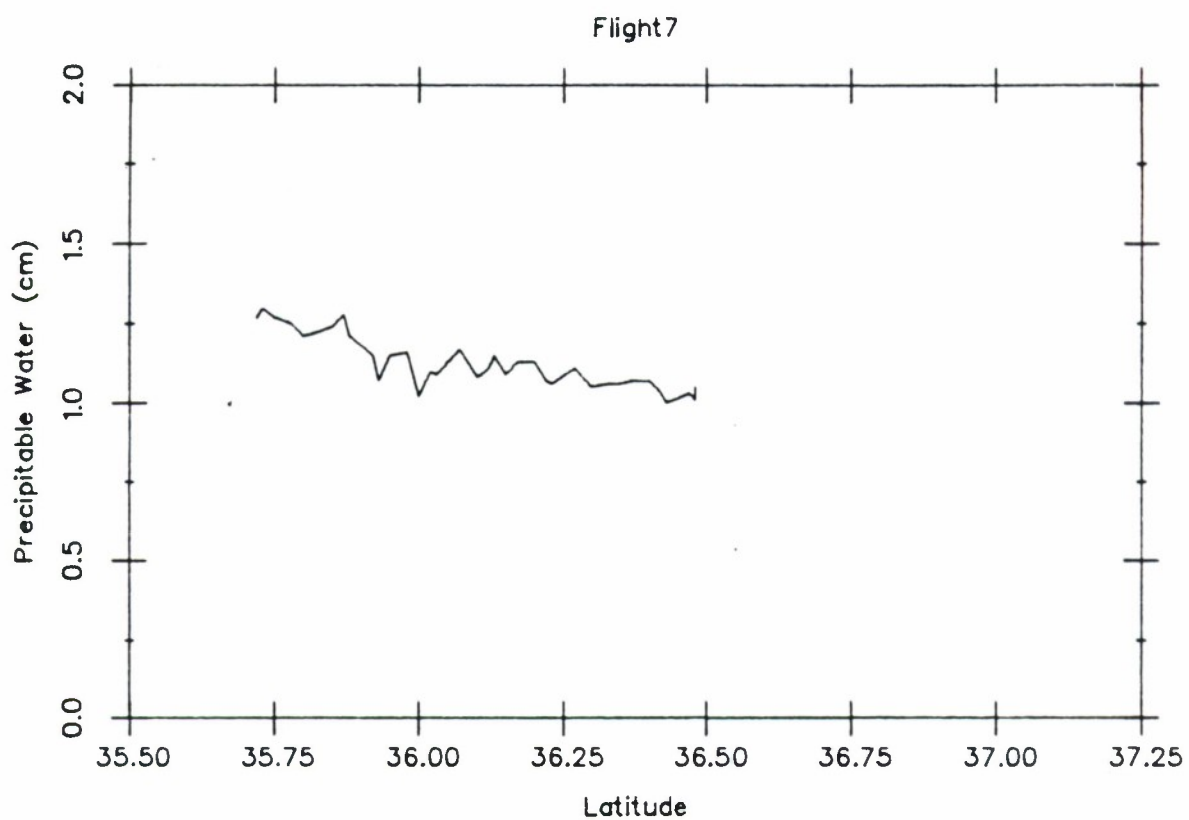


FIGURE 28. PRECIPITABLE WATER AMOUNTS IN THE VERTICAL AIR COLUMNS SAMPLED IN THE NASA-DIAL INSTRUMENT.

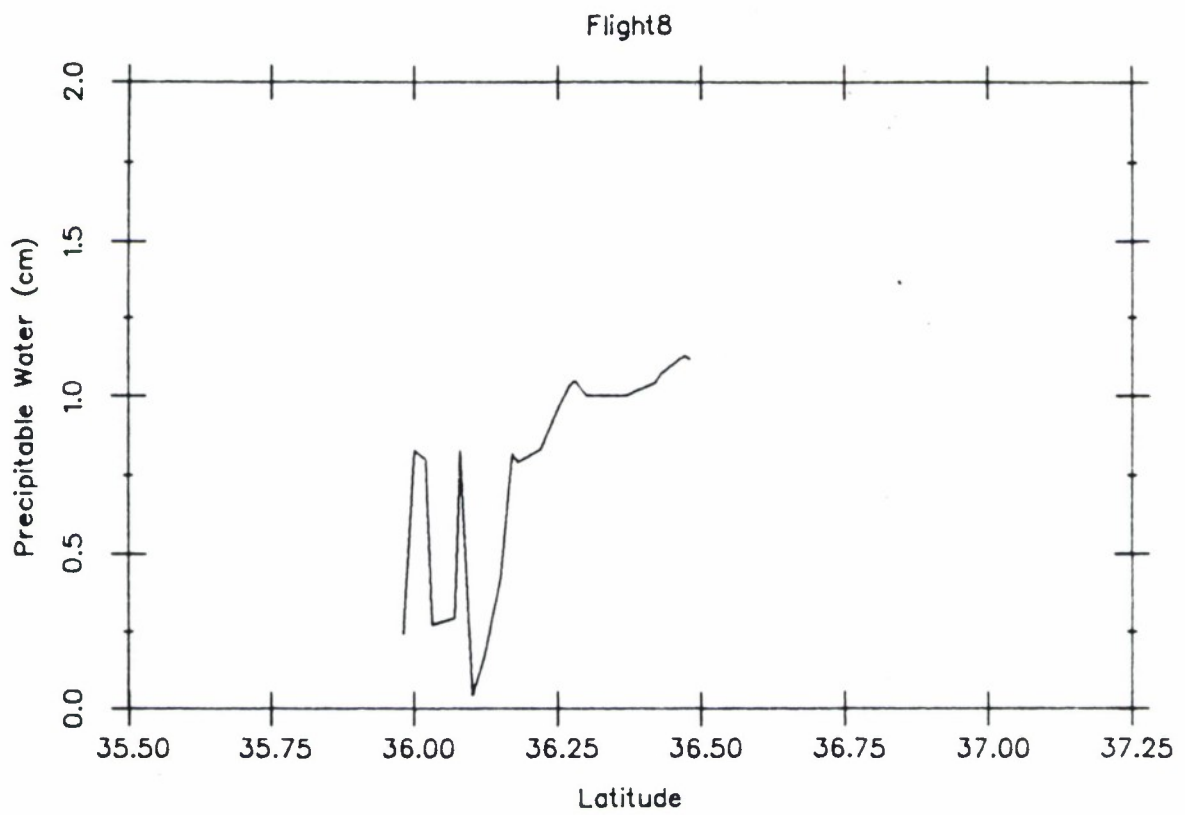


FIGURE 29. PRECIPITABLE WATER AMOUNTS IN THE VERTICAL AIR COLUMNS SAMPLED IN THE NASA-DIAL INSTRUMENT.

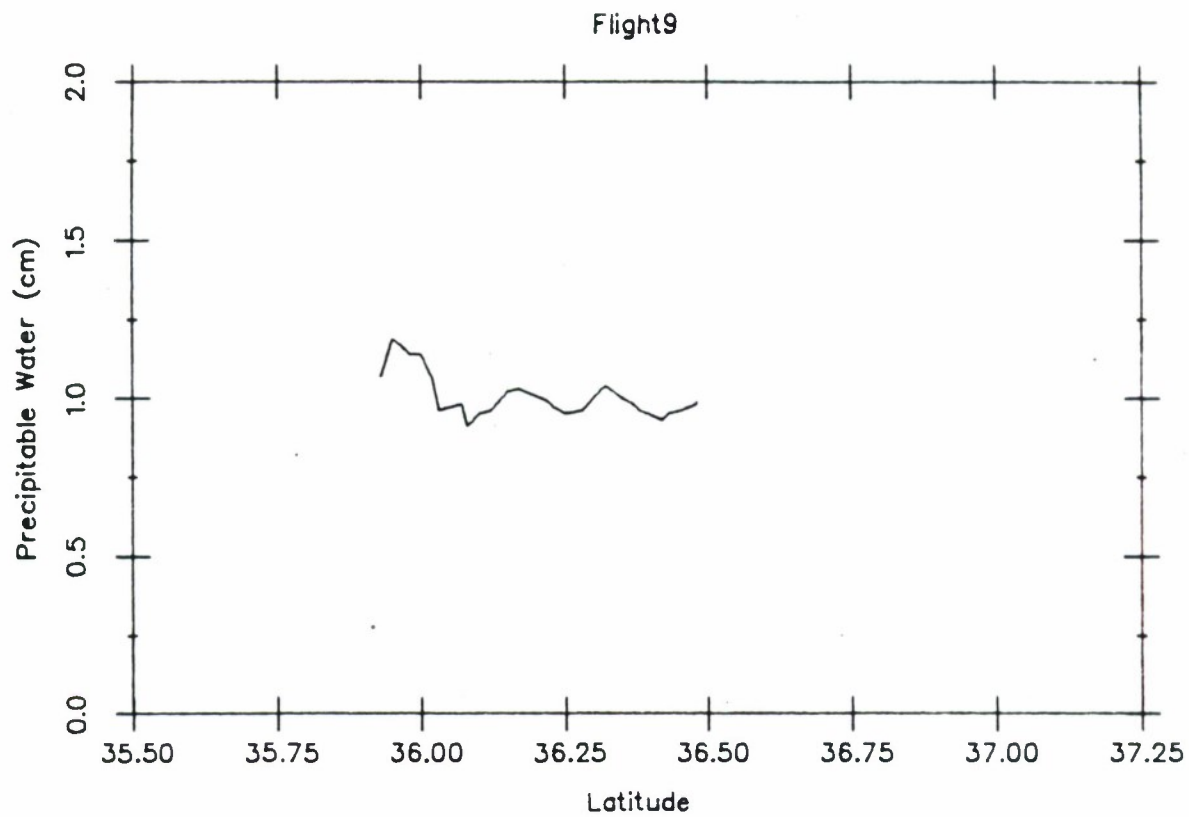


FIGURE 30. PRECIPITABLE WATER AMOUNTS IN THE VERTICAL AIR COLUMNS SAMPLED IN THE NASA-DIAL INSTRUMENT.

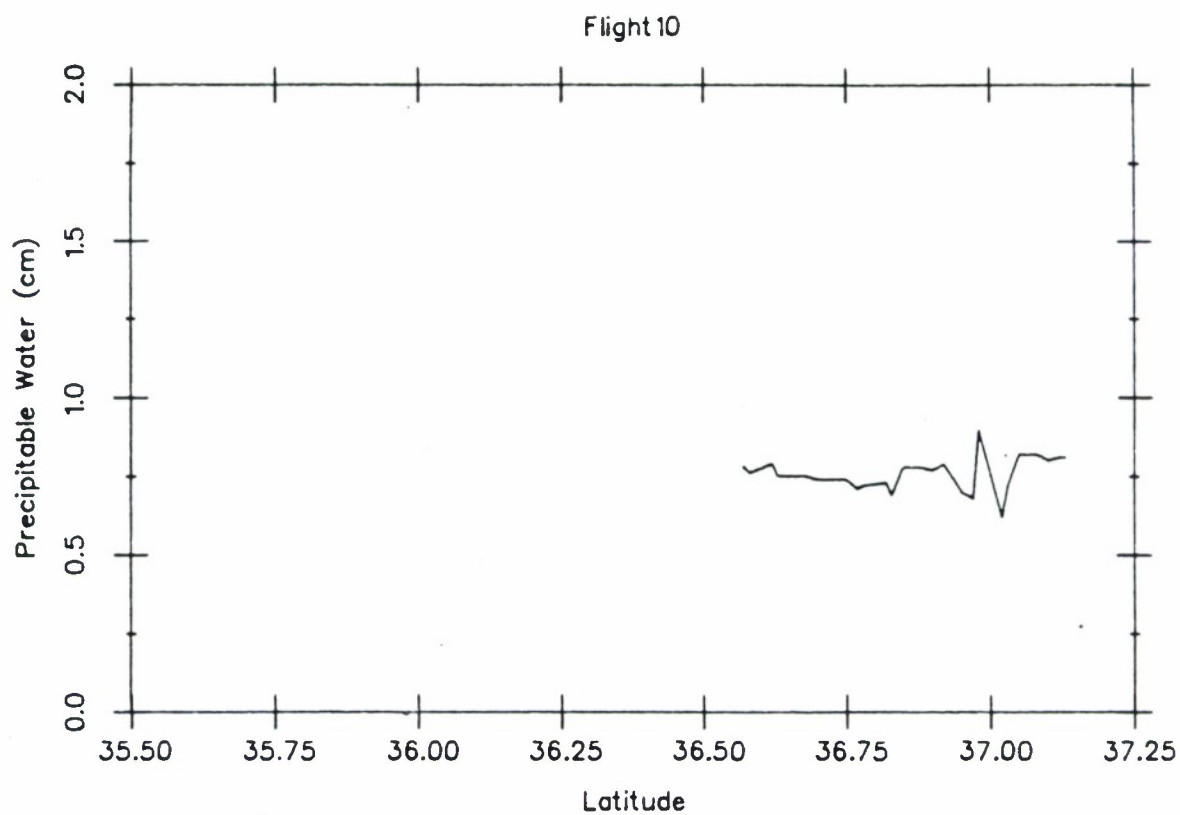


FIGURE 31. PRECIPITABLE WATER AMOUNTS IN THE VERTICAL AIR COLUMNS SAMPLED IN THE NASA-DIAL INSTRUMENT.

One can now ask the question if these results can be used to infer information about the atmosphere that can be used in atmospheric propagation calculations.

3.3 FITTING THE WATER VAPOR DATA

Even though the water vapor profiles in Figures 3 to 13 show a fair amount of structure they can be fit reasonably well with a relationship of the form

$$q_v(z) = q_0 + m \log_{10} z \quad (2)$$

Table 7 gives the calculated values of m and q_0 for the flights. Flights 2 and 6 were excluded from this analysis due to the dramatic structure (see Figures 4 and 8). The average value of -31.005 is similar to the value of -29.8 from Starr et al [5] for annually and latitudinally averaged conditions for 35° N during the IGY. With the average value of m one can solve for the surface values of the volume mixing ratio, q_{v0} , required to reproduce the average profiles given in Figures 3 to 13. Then, with the surface value known one can solve for the surface temperature required to give the calculated q_{v0} . These surface temperatures can then be compared against the data given in Tables 2 to 4.

The surface value of q_{v0} is given, using the Claussius-Clapeyron equation, as

$$q_{v0} = r_0 \frac{6.11}{P_0} \exp \left[5412 \left(\frac{1}{273} - \frac{1}{T_0} \right) \right] \quad (3)$$

where r_0 is the surface value of the relative humidity, P_0 is the surface pressure and T_0 is the surface temperature. Solving for T_0 gives

TABLE 7. CALCULATED SLOPE, M, AND INTERCEPTS, QO, TO THE EMPIRICAL FITS TO THE AVERAGED WATER VAPOR PROFILES.

FLIGHT	SLOPE M	INTERCEPTS (PP 10,000)
1	-43.185	299
3	-19.932	198
4	-23.253	192
5	-13.288	178
7	-23.253	209
8	-43.185	250
9	-33.219	223
10	-43.185	256
11	-36.541	237
All Flights	-31.005	227

$$T_o = \frac{5412}{\ln \left[\frac{6.11 r_o}{P_o q_{vo}} \exp \left(\frac{5412}{273} \right) \right]} \quad (4)$$

The values of q_{vo} and T_o calculated from (3) and (4) for the flights are given in Table 8. In the calculations the surface relative humidity is assumed to be 63%, based on the results in Table 2. The calculated surface temperatures agree well with those measured (see Tables 2 to 4). Using (3) and (4) one could use the DIAL data to infer the surface temperature at the base of the vertical columns sampled.

Using the empirical relationship (2) and the average slope and intercept over all the flights the surface temperatures required to produce the precipitable water in the sampled columns of air were iteratively solved for using the secant method [7]. Then, with the surface temperature known, the precipitable water in a vertical column extending from the surface to 1361 m was calculated as well as the average surface temperature for each flight. The results are given in Tables 9 to 18. The surface temperatures inverted from this method are a bit higher than those in Tables 2 to 4 but are in reasonable agreement. The precipitable water values are also consistent with climatological values for that latitude and temperature [5]. This tends to indicate that the data obtained by the NASA DIAL instrument were similar to climatological conditions. To test this the inversion of surface temperatures was redone using a climatological expression for the relative humidity suggested by Manabe and Wetherald [8],

TABLE 8. CALCULATED VALUES OF THE SURFACE WATER VAPOR
VOLUME MIXING RATIO AND SURFACE TEMPERATURE
FROM THE FLIGHT AVERAGED DATA.

FLIGHT	q_{vo} (pp 10,000)	T (K)
1	299	304
3	198	298
4	192	297
5	178	296
7	209	298
8	250	301
9	223	300
10	256	302
11	237	301
All Flights	227	300

TABLE 9. INVERTED TEMPERATURES AND CALCULATED TOTAL COLUMN PRECIPITABLE WATER AMOUNTS FOR FLIGHT 1.

Down Leg

Time	Latitude	Longitude	Zmin (m)	Zmax (m)	Precipitable Water (cm)	Surface Temperature (K)	Column (cm)
11:26:18	36 43	74 13	476	1361	0.75	298.73	2.04
11:26:38	36 42	74 12	836	1361	0.37	297.50	1.78
11:26:58	36 40	74 12	641	1361	0.60	298.77	2.05
11:27:18	36 39	74 12	611	1361	0.68	299.53	2.22
11:27:38	36 38	74 11	176	1361	1.22	300.20	2.38
11:27:58	36 36	74 11	131	1361	1.22	299.73	2.27
11:28:18	36 35	74 11	446	1361	0.79	298.86	2.07
11:28:38	36 34	74 11	176	1361	1.11	299.24	2.16
11:28:58	36 32	74 11	176	1361	1.08	298.98	2.10
11:29:19	36 31	74 11	131	1361	1.31	300.47	2.44
11:29:39	36 30	74 11	386	1361	0.87	299.10	2.12
11:29:59	36 29	74 11	176	1361	1.15	299.60	2.24
11:30:19	36 27	74 11	176	1361	1.20	300.03	2.34
11:30:39	36 26	74 11	386	1361	0.90	299.42	2.20
11:30:59	36 25	74 11	386	1361	0.91	299.53	2.22
11:31:19	36 23	74 11	491	1361	0.77	299.16	2.14
11:31:39	36 22	74 11	416	1361	0.85	299.21	2.15
11:31:59	36 20	74 11	131	1361	1.24	299.90	2.31
11:32:19	36 19	74 11	341	1361	0.98	299.75	2.27
11:32:39	36 17	74 11	176	1361	1.20	300.03	2.34
11:32:59	36 16	74 11	296	1361	1.02	299.66	2.25
11:33:19	36 15	74 11	176	1361	1.22	300.20	2.38
11:33:39	36 14	74 10	176	1361	1.21	300.11	2.36
11:33:59	36 13	74 10	386	1361	1.02	300.68	2.49
11:34:19	36 11	74 10	326	1361	1.12	300.95	2.56
11:34:39	36 10	74 10	416	1361	1.05	301.35	2.66
11:34:59	36 9	74 10	176	1361	1.30	300.86	2.54
11:35:19	36 7	74 10	176	1361	1.34	301.18	2.62
11:35:39	36 6	74 10	176	1361	1.36	301.34	2.66
11:35:59	36 5	74 10	176	1361	1.52	302.56	2.97
11:36:19	36 3	74 10	131	1361	1.60	302.64	3.00
11:36:39	36 2	74 10	131	1361	1.55	302.28	2.90
11:36:59	36 1	74 10	176	986	1.00	301.69	2.74
11:37:19	36 0	74 11	161	986	1.08	302.31	2.91
11:37:39	35 59	74 12	161	986	1.04	301.89	2.80
11:37:59	35 58	74 13	116	986	1.10	301.84	2.78

THE AVERAGE SURFACE TEMPERATURE IS 300.26 K.

TABLE 9. (continued)

Up Leg

Time	Latitude	Longitude	Zmin (m)	Zmax (m)	Precipitable Water (cm)	Surface Temperature (K)	Column (cm)
11:38:19	35 58	74 14	131	986	0.90	299.88	2.30
11:38:39	35 59	74 15	116	986	0.97	300.46	2.44
11:38:59	35 59	74 17	146	986	0.97	300.90	2.55
11:39:19	36 1	74 17	281	986	0.75	300.27	2.39
11:39:39	36 2	74 17	161	986	1.03	301.79	2.77
11:39:59	36 3	74 16	161	986	1.03	301.79	2.77
11:40:19	36 5	74 16	176	986	1.05	302.23	2.89
11:40:39	36 6	74 16	401	986	0.72	302.01	2.83
11:40:59	36 8	74 16	296	986	0.89	302.38	2.92
11:41:19	36 9	74 16	176	986	1.10	302.76	3.03
11:41:39	36 10	74 16	176	986	1.19	303.68	3.29
11:41:59	36 12	74 16	176	986	1.16	303.38	3.20
11:42:19	36 13	74 16	176	986	1.15	303.28	3.17
11:42:39	36 14	74 17	176	986	1.22	303.97	3.37
11:42:59	36 16	74 17	176	986	1.32	304.92	3.66
11:43:19	36 17	74 17	176	986	1.29	304.64	3.57
11:43:39	36 18	74 17	386	986	0.91	304.38	3.49
11:43:59	36 20	74 17	416	986	0.82	303.80	3.32
11:44:19	36 21	74 17	296	986	1.01	303.83	3.33
11:44:39	36 22	74 17	176	986	1.37	305.38	3.80
11:44:59	36 24	74 17	416	986	0.90	304.90	3.65
11:45:19	36 25	74 17	176	986	1.31	304.83	3.63
11:45:39	36 26	74 17	416	986	0.83	303.94	3.36
11:45:59	36 28	74 17	416	986	0.87	304.50	3.53
11:46:19	36 29	74 17	416	986	0.85	304.22	3.44
11:46:39	36 31	74 17	416	986	0.75	302.78	3.03
11:46:59	36 32	74 17	176	986	1.30	304.74	3.60
11:47:19	36 33	74 16	416	986	0.91	305.03	3.69

THE AVERAGE SURFACE TEMPERATURE IS 303.24 K.

TABLE 10. INVERTED TEMPERATURES AND CALCULATED TOTAL COLUMN PRECIPITABLE WATER AMOUNTS FOR FLIGHT 2.

Time	Latitude	Longitude	Zmin (m)	Zmax (m)	Precipitable Water (cm)	Surface Temperature (K)	Column (cm)
12: 2:16	36 26	74 25	416	1361	0.84	299.10	2.12
12: 2:36	36 25	74 25	386	1361	0.91	299.53	2.22
12: 2:56	36 24	74 25	386	1361	0.86	298.98	2.10
12: 3:16	36 22	74 25	416	1361	0.84	299.10	2.12
12: 3:36	36 21	74 25	416	1361	0.89	299.66	2.25
12: 3:56	36 20	74 25	416	1361	0.97	300.52	2.45
12: 4:16	36 19	74 25	386	1361	0.64	296.36	1.56
12: 4:36	36 17	74 25	836	1361	0.06	288.30	0.33
12: 4:56	36 16	74 25	416	1361	0.98	300.63	2.48
12: 5:16	36 15	74 25	416	1361	1.01	300.94	2.56
12: 5:36	36 14	74 25	416	1361	0.95	300.31	2.40
12: 5:56	36 13	74 25	416	1361	0.99	300.73	2.50
12: 6:16	36 11	74 25	416	1361	0.96	300.42	2.43
12: 6:36	36 10	74 25	416	1361	1.06	301.45	2.68
12: 6:56	36 9	74 25	416	1361	1.04	301.25	2.63
12: 7:16	36 8	74 25	416	1361	1.11	301.94	2.81
12: 7:36	36 6	74 25	386	746	0.40	300.58	2.47
12: 7:56	36 5	74 25	416	746	0.34	299.84	2.29
12: 8:16	36 4	74 25	416	746	0.31	298.91	2.08
12: 8:36	36 3	74 25	416	746	0.31	298.91	2.08
12: 8:56	36 2	74 25	281	746	0.34	296.34	1.56
12: 9:16	36 0	74 24	416	746	0.32	299.23	2.15
12: 9:36	35 59	74 24	416	746	0.28	297.93	1.87
12: 9:56	35 58	74 24	416	746	0.34	299.84	2.29
12: 10:16	35 57	74 24	416	746	0.30	298.59	2.01
12: 10:36	35 55	74 24	416	746	0.34	299.84	2.29
12: 10:56	35 54	74 24	416	746	0.32	299.23	2.15
12: 11:16	35 53	74 24	416	746	0.34	299.84	2.29
12: 11:36	35 52	74 24	416	746	0.32	299.23	2.15
12: 11:56	35 51	74 24	416	746	0.34	299.84	2.29
12: 12:16	35 49	74 24	416	746	0.29	298.27	1.94
12: 12:36	35 48	74 24	386	1361	1.07	301.18	2.61
12: 12:56	35 47	74 23	416	1361	0.99	300.73	2.50
12: 13:16	35 46	74 23	416	1361	1.06	301.45	2.68
12: 13:36	35 44	74 23	416	1361	1.06	298.04	1.90
12: 13:56	35 43	74 23	416	746	0.34	299.84	2.29
12: 14:16	35 42	74 23	416	746	0.33	299.54	2.22
12: 14:36	35 41	74 23	176	746	0.56	298.92	2.09
12: 14:56	35 40	74 23	416	746	0.33	299.54	2.22
12: 15:16	35 38	74 23	416	746	0.31	298.91	2.08
12: 15:36	35 37	74 23	491	746	0.19	296.86	1.66

THE AVERAGE SURFACE TEMPERATURE IS 299.28 K.

TABLE 11. INVERTED TEMPERATURES AND CALCULATED TOTAL COLUMN PRECIPITABLE WATER AMOUNTS FOR FLIGHT 3.

Time	Latitude	Longitude	Zmin (m)	Zmax (m)	Precipitable Water (cm)	Surface Temperature (K)	Column (cm)
12:22:12	35 38	74 31	131	1361	1.23	299.82	2.29
12:22:32	35 40	74 31	131	1361	1.13	298.97	2.10
12:22:52	35 41	74 31	416	1361	0.86	299.33	2.18
12:23:12	35 42	74 31	416	1361	0.92	299.99	2.33
12:23:32	35 44	74 31	416	1361	0.90	299.77	2.28
12:23:53	35 45	74 31	416	1361	0.94	300.20	2.38
12:24:13	35 46	74 31	176	1361	1.20	300.03	2.34
12:24:33	35 47	74 31	416	1361	0.95	300.31	2.40
12:24:53	35 49	74 31	416	1361	0.94	300.20	2.38
12:25:13	35 50	74 31	416	1361	0.92	299.99	2.33
12:25:33	35 51	74 31	416	1361	0.92	299.99	2.33
12:25:53	35 53	74 31	416	1361	0.90	299.77	2.28
12:26:13	35 54	74 31	416	1361	0.90	299.77	2.28
12:26:33	35 55	74 31	416	1361	0.91	299.88	2.30
12:26:53	35 56	74 31	416	1361	0.91	299.88	2.30
12:27:13	35 58	74 31	416	1361	0.88	299.55	2.23
12:27:33	35 59	74 31	416	1361	0.89	299.66	2.25
12:27:53	36 0	74 31	416	1361	0.86	299.33	2.18
12:28:13	36 2	74 32	191	1361	1.20	300.18	2.37
12:28:33	36 3	74 32	416	1361	0.85	299.21	2.15
12:28:53	36 4	74 32	416	1361	0.82	298.87	2.07
12:29:13	36 5	74 32	401	1361	0.81	298.59	2.01
12:29:33	36 7	74 32	416	1361	0.81	298.75	2.05
12:29:53	36 8	74 32	416	1361	0.82	298.87	2.07
12:30:13	36 9	74 32	416	1361	0.78	298.40	1.97
12:30:33	36 11	74 32	416	1361	0.80	298.64	2.02
12:30:53	36 12	74 32	416	1361	0.79	298.52	2.00
12:31:13	36 13	74 32	416	1361	0.77	298.28	1.95
12:31:33	36 15	74 32	416	1361	0.78	298.40	1.97
12:31:53	36 16	74 32	416	1361	0.81	298.75	2.05
12:32:13	36 17	74 32	206	1361	1.02	298.72	2.04
12:32:33	36 18	74 32	401	1361	0.78	298.24	1.94
12:32:53	36 20	74 32	416	1361	0.73	297.80	1.85
12:33:13	36 21	74 32	416	1361	0.71	297.55	1.80
12:33:33	36 22	74 32	416	1361	0.72	297.68	1.82
12:33:53	36 23	74 32	416	1361	0.70	297.43	1.77
12:34:13	36 25	74 32	416	1361	0.75	298.04	1.90
12:34:33	36 26	74 32	416	1361	0.68	297.18	1.72
12:34:53	36 27	74 32	416	1361	0.65	296.79	1.64
12:35:10	36 29	74 32	416	1361	0.67	297.05	1.69

THE AVERAGE SURFACE TEMPERATURE IS 298.96 K.

TABLE 12. INVERTED TEMPERATURES AND CALCULATED TOTAL COLUMN PRECIPITABLE WATER AMOUNTS FOR FLIGHT 4.

Time	Latitude	Longitude	Zmin (m)	Zmax (m)	Precipitable Water (cm)	Surface Temperature (K)	Column (cm)
12:58:24	36 47	74 11	131	1361	0.84	297.24	1.73
12:59:44	36 45	74 11	131	1361	0.96	297.43	1.77
13:01:04	36 44	74 11	131	1361	0.91	296.85	1.67
13:02:24	36 43	74 10	131	1361	0.89	296.76	1.64
13:03:44	36 42	74 10	131	1361	0.84	296.26	1.54
13:05:04	36 40	74 10	131	1361	0.85	296.36	1.56
13:06:24	36 39	74 10	131	1361	0.85	296.36	1.56
13:07:44	36 38	74 10	131	1361	0.88	296.66	1.62
13:09:04	36 37	74 10	131	1361	0.90	296.85	1.66
13:10:24	36 35	74 10	131	1361	0.90	296.85	1.66
13:11:44	36 34	74 10	131	1361	0.91	296.95	1.67
13:13:04	36 33	74 10	131	1361	0.91	296.95	1.67
13:14:24	36 32	74 10	131	1361	0.95	297.34	1.75
13:15:44	36 30	74 10	131	1361	0.97	297.53	1.79
13:17:04	36 29	74 10	131	1361	0.92	297.05	1.69
13:18:24	36 28	74 10	131	1361	0.97	297.53	1.79
13:19:44	36 27	74 10	131	1361	1.03	298.08	1.90
13:21:04	36 26	74 10	131	1361	1.03	298.08	1.90
13:22:24	36 24	74 10	131	1361	0.96	297.43	1.77
13:23:44	36 23	74 10	131	1361	0.99	297.71	1.83
13:25:04	36 22	74 10	131	1361	1.06	298.35	1.96
13:26:24	36 21	74 10	131	1361	1.02	297.99	1.89
13:27:44	36 19	74 10	131	1361	1.02	297.99	1.89
13:29:04	36 18	74 10	131	1361	1.04	297.99	1.89
13:30:24	36 17	74 10	131	1361	1.04	298.17	1.92
13:31:44	36 16	74 10	131	1361	1.04	298.17	1.92
13:33:04	36 14	74 10	161	1361	1.07	298.28	1.95
13:34:24	36 13	74 10	131	1361	1.07	298.44	1.98
13:35:44	36 12	74 9	131	1361	1.05	298.26	1.94
13:37:04	36 11	74 9	161	1361	1.02	298.26	1.95
13:38:24	36 9	74 9	131	1361	1.03	298.08	1.90
13:39:44	36 8	74 9	176	1361	1.06	298.79	2.06
13:41:04	36 7	74 9	161	1361	1.01	298.19	1.93
13:42:24	36 6	74 9	161	1361	1.05	298.55	2.01
13:43:44	36 4	74 9	176	1361	1.02	298.43	1.98
13:45:04	36 3	74 9	161	1361	1.11	299.09	2.12
13:46:24	36 2	74 9	161	1361	1.09	298.92	2.08
13:47:44	36 1	74 9	161	1361	1.04	298.46	1.99
13:49:04	35 59	74 9	176	1361	1.02	298.43	1.88
13:50:24	35 58	74 9	161	1361	1.05	298.55	2.01
13:51:44	35 57	74 8	176	1361	0.96	297.86	1.86
13:53:04	35 56	74 9	1211	1361	0.08	295.66	1.43
13:54:24	35 54	74 9	176	1361	0.86	297.86	1.86
13:55:44	35 53	74 9	176	1361	0.83	287.57	1.80
13:57:04	35 52	74 9	161	1361	1.06	298.65	2.02
13:58:24	35 51	74 9	176	1361	1.10	299.16	2.14
13:59:44	35 49	74 8	176	1361	1.03	298.52	2.00
14:01:04	35 48	74 9	176	1361	0.97	297.95	1.88
14:02:24	35 47	74 9	176	1361	1.05	298.70	2.04
14:03:44	35 46	74 9	131	1361	1.01	297.90	1.87
14:05:04	35 45	74 9	161	1361	1.05	298.55	2.01
14:06:24	35 44	74 8	176	1361	1.05	298.70	2.04
14:07:44	35 43	74 8	176	1361	1.08	298.88	2.10
14:09:04	35 42	74 8	131	1361	1.02	297.99	1.89
14:10:24	35 41	74 9	131	1361	0.01	290.84	0.66
14:11:44	35 40	74 9	1316	1361	0.01	290.80	0.66
14:13:04	35 39	74 9	1271	1361	0.02	290.80	0.66
14:14:24	35 37	74 9	1271	1361	0.02	290.80	0.66

THE AVERAGE SURFACE TEMPERATURE IS 297.48 K.

TABLE 13. INVERTED TEMPERATURES AND CALCULATED TOTAL COLUMN PRECIPITABLE WATER AMOUNTS FOR FLIGHT 5.

Time	Latitude	Longitude	Zmin (m)	Zmax (m)	Precipitable Water (cm)	Surface Temperature (K)	Column (cm)
13:27:48	35 30	74 17	581	1361	0.63	298.41	1.97
13:28: 8	35 31	74 16	566	1361	0.65	298.51	1.99
13:28:28	35 32	74 16	131	1361	1.11	298.80	2.06
13:28:48	35 33	74 16	416	1361	0.87	299.44	2.20
13:29: 8	35 34	74 16	416	1361	0.96	300.42	2.43
13:29:28	35 36	74 16	131	1361	1.51	301.99	2.82
13:29:48	35 37	74 16	476	1361	0.86	300.05	2.34
13:30: 8	35 38	74 16	566	1361	0.60	297.79	1.84
13:30:28	35 40	74 16	536	1361	0.78	299.85	2.30
13:30:48	35 41	74 16	131	1361	1.14	299.06	2.11
13:31: 8	35 42	74 16	416	1361	0.82	298.87	2.07
13:31:28	35 44	74 16	206	1361	1.10	299.46	2.21
13:31:48	35 45	74 16	206	1361	1.16	299.99	2.33
13:32: 8	35 46	74 16	416	1361	0.86	299.33	2.18
13:32:28	35 47	74 16	131	1361	1.15	299.14	2.13
13:32:48	35 49	74 16	161	1361	1.09	298.92	2.08
13:33: 8	35 50	74 16	191	1361	1.09	299.22	2.15
13:33:28	35 51	74 16	131	1361	1.16	299.23	2.15
13:33:48	35 53	74 16	416	1361	0.86	299.33	2.18
13:34: 8	35 54	74 16	206	1361	1.10	299.46	2.21
13:34:28	35 55	74 16	416	1361	0.86	299.33	2.18
13:34:48	35 57	74 16	416	1361	0.85	299.21	2.15
13:35: 8	35 58	74 16	416	1361	0.81	298.75	2.05
13:35:28	35 59	74 16	416	1361	0.81	298.75	2.05
13:35:48	36 0	74 16	416	1361	0.85	299.21	2.15
13:36: 8	36 2	74 16	401	1361	0.86	299.15	2.14
13:36:28	36 3	74 16	416	1361	0.89	299.66	2.25
13:36:48	36 4	74 16	401	1361	0.88	299.38	2.19
13:37: 8	36 6	74 16	191	1361	1.09	299.22	2.15
13:37:28	36 7	74 16	416	1361	0.85	299.21	2.15
13:37:48	36 8	74 16	401	1361	0.86	299.15	2.14
13:38: 8	36 9	74 16	416	1361	0.88	299.55	2.23
13:38:28	36 11	74 16	401	1361	0.91	299.70	2.26
13:38:48	36 12	74 16	191	1361	1.12	299.49	2.21
13:39: 8	36 13	74 16	416	1361	0.90	299.77	2.28
13:39:28	36 15	74 17	131	1361	1.18	299.40	2.19
13:39:48	36 16	74 17	206	1361	1.11	299.55	2.23
13:40: 8	36 17	74 17	206	1361	1.16	299.99	2.33
13:40:28	36 18	74 17	191	1361	1.05	298.85	2.07
13:40:48	36 20	74 17	206	1361	1.10	299.46	2.21
13:41: 8	36 21	74 17	131	1361	1.09	298.62	2.02
13:41:28	36 22	74 17	191	1361	1.03	298.67	2.03
13:41:48	36 24	74 17	191	1361	1.09	299.22	2.15
13:42: 8	36 25	74 17	191	1361	1.11	299.40	2.19
13:42:28	36 26	74 17	206	1361	1.08	299.28	2.16

THE AVERAGE SURFACE TEMPERATURE IS 299.31 K.

TABLE 14. INVERTED TEMPERATURES AND CALCULATED TOTAL COLUMN PRECIPITABLE WATER AMOUNTS FOR FLIGHT 6.

Time	Latitude	Longitude	Zmin (m)	Zmax (m)	Precipitable Water (cm)	Surface Temperature (K)	Column (cm)
13:48:10	36 27	74 25	206	1061	0.78	298.68	2.03
13:48:30	36 25	74 25	251	1061	0.79	299.42	2.20
13:48:50	36 24	74 25	251	1061	0.79	299.42	2.20
13:49:10	36 23	74 25	251	1061	0.80	299.55	2.23
13:49:30	36 22	74 25	251	1061	0.78	299.30	2.17
13:49:50	36 20	74 25	251	1061	0.81	299.68	2.26
13:50:10	36 19	74 25	251	1061	0.83	299.93	2.31
13:50:30	36 18	74 25	251	1061	0.84	300.05	2.34
13:50:50	36 17	74 25	251	1061	0.80	299.55	2.23
13:51:10	36 16	74 25	251	1061	0.83	299.93	2.31
13:51:30	36 14	74 25	251	1061	0.83	299.93	2.31
13:51:50	36 13	74 25	251	1061	0.81	299.68	2.26
13:52:10	36 12	74 25	236	1061	0.88	300.32	2.40
13:52:30	36 11	74 25	251	1061	0.83	299.93	2.31
13:52:50	36 10	74 25	251	1061	0.83	299.93	2.31
13:53:10	36 8	74 25	251	1061	0.82	299.80	2.28
13:53:30	36 7	74 25	251	1061	0.84	300.05	2.34
13:53:50	36 6	74 25	251	1061	0.82	299.80	2.28
13:54:10	36 5	74 25	176	1061	0.89	299.60	2.24
13:54:30	36 4	74 25	221	1061	0.87	299.98	2.33
13:54:50	36 2	74 25	251	1061	0.85	300.17	2.37
13:55:10	36 1	74 25	191	1061	0.84	299.22	2.15
13:55:30	36 0	74 25	176	1061	0.86	299.25	2.16
13:55:50	35 59	74 25	251	1061	0.80	299.55	2.23
13:56:10	35 57	74 25	251	1061	0.85	300.17	2.37
13:56:30	35 56	74 25	251	1061	0.78	299.30	2.17
13:56:50	35 55	74 25	236	1061	0.80	299.34	2.18
13:57:10	35 53	74 25	251	1061	0.81	299.47	2.21
13:57:30	35 52	74 25	251	1061	0.79	299.42	2.20
13:57:50	35 51	74 25	251	1061	0.81	299.68	2.26
13:58:10	35 50	74 25	221	1061	0.91	300.45	2.44
13:58:30	35 49	74 25	206	1061	0.94	300.58	2.47
13:58:50	35 48	74 25	206	1061	0.85	299.54	2.22
13:59:10	35 46	74 25	206	1061	0.85	299.54	2.22
13:59:30	35 45	74 25	191	1061	0.85	299.34	2.18
13:59:50	35 44	74 25	191	1061	0.82	298.98	2.10
14:00:10	35 43	74 25	191	1061	0.81	298.86	2.07
14:00:30	35 41	74 25	221	1061	0.78	298.88	2.08
14:00:50	35 40	74 25	221	1061	0.82	299.38	2.19
14:01:10	35 39	74 25	206	1061	0.91	300.24	2.39
14:01:30	35 38	74 25	191	1061	0.87	299.57	2.23
14:01:50	35 38	74 25	251	1061	1.28	304.76	3.61

THE AVERAGE SURFACE TEMPERATURE IS 299.76 K.

TABLE 15. INVERTED TEMPERATURES AND CALCULATED TOTAL COLUMN PRECIPITABLE WATER AMOUNTS FOR FLIGHT 7.

Time	Latitude	Longitude	Zmin (m)	Zmax (m)	Precipitable Water (cm)	Surface Temperature (K)	Column (cm)
14:11:55	35 43	74 31	191	1361	1.27	300.77	2.51
14:12:15	35 44	74 31	191	1361	1.30	301.02	2.57
14:12:35	35 45	74 31	176	1361	1.27	300.61	2.48
14:12:55	35 47	74 31	131	1361	1.25	299.98	2.33
14:13:15	35 48	74 31	191	1361	1.21	300.27	2.39
14:13:35	35 49	74 31	176	1361	1.22	300.20	2.38
14:13:55	35 51	74 31	176	1361	1.24	300.36	2.42
14:14:15	35 52	74 31	191	1361	1.28	300.85	2.53
14:14:35	35 53	74 31	191	1361	1.21	300.27	2.39
14:14:55	35 55	74 32	191	1361	1.15	299.75	2.27
14:15:15	35 56	74 32	191	1361	1.07	299.04	2.11
14:15:35	35 57	74 32	191	1361	1.15	299.75	2.27
14:15:55	35 59	74 32	176	1361	1.16	299.68	2.26
14:16:15	36 0	74 32	191	1361	1.02	298.57	2.01
14:16:35	36 1	74 32	206	1361	1.10	299.46	2.21
14:16:55	36 2	74 32	176	1361	1.09	299.07	2.12
14:17:15	36 4	74 32	176	1361	1.17	299.77	2.28
14:17:35	36 6	74 32	191	1361	1.08	299.13	2.13
14:17:55	36 7	74 32	176	1361	1.11	299.24	2.16
14:18:15	36 8	74 32	176	1361	1.15	299.60	2.24
14:18:35	36 9	74 32	191	1361	1.09	299.22	2.15
14:18:55	36 10	74 32	191	1361	1.13	299.57	2.23
14:19:15	36 12	74 32	191	1361	1.13	299.57	2.23
14:19:35	36 13	74 32	191	1361	1.07	299.04	2.11
14:19:55	36 14	74 32	191	1361	1.06	298.94	2.09
14:20:15	36 16	74 32	191	1361	1.11	299.40	2.19
14:20:35	36 17	74 32	191	1361	1.09	299.22	2.15
14:20:55	36 18	74 32	191	1361	1.05	298.85	2.07
14:21:15	36 20	74 32	191	1361	1.06	298.94	2.09
14:21:35	36 21	74 32	176	1361	1.06	298.79	2.06
14:21:55	36 22	74 32	176	1361	1.07	298.89	2.08
14:22:15	36 24	74 32	176	1361	1.07	298.89	2.08
14:22:35	36 25	74 32	176	1361	1.03	298.52	2.00
14:22:55	36 26	74 32	176	1361	1.00	298.24	1.94
14:23:15	36 28	74 32	176	1361	1.03	298.52	2.00
14:23:35	36 29	74 32	176	1361	1.01	298.33	1.96
14:23:38	36 29	74 32	131	1361	1.05	298.26	1.94

THE AVERAGE SURFACE TEMPERATURE IS 299.42 K.

TABLE 16. INVERTED TEMPERATURES AND CALCULATED TOTAL COLUMN PRECIPITABLE WATER AMOUNTS FOR FLIGHT 8.

Time	Latitude	Longitude	Zmin (m)	Zmax (m)	Precipitable Water (cm)	Surface Temperature (K)	Column (cm)
14:29:49	36 29	74 11	161	1361	1.12	299.18	2.14
14:30: 9	36 28	74 11	131	1361	1.13	298.97	2.10
14:30:29	36 27	74 11	191	1361	1.10	299.31	2.17
14:30:49	36 26	74 11	191	1361	1.07	299.04	2.11
14:31: 9	36 25	74 11	191	1361	1.04	298.76	2.05
14:31:29	36 23	74 11	176	1361	1.01	298.33	1.96
14:31:49	36 22	74 10	176	1361	1.00	298.24	1.94
14:32: 9	36 21	74 10	191	1361	1.00	298.39	1.97
14:32:29	36 20	74 10	176	1361	1.00	298.24	1.94
14:32:49	36 18	74 10	176	1361	1.00	298.24	1.94
14:33: 9	36 17	74 10	176	1361	1.05	298.70	2.04
14:33:29	36 16	74 10	176	1361	1.03	298.52	2.00
14:33:49	36 15	74 10	176	1361	0.96	297.86	1.86
14:34: 9	36 13	74 10	176	1061	0.83	298.90	2.08
14:34:29	36 12	74 10	191	1061	0.81	298.86	2.07
14:34:49	36 11	74 10	176	1061	0.79	298.42	1.98
14:35: 9	36 10	74 10	161	1061	0.82	298.58	2.01
14:35:29	36 9	74 10	596	1061	0.42	299.17	2.14
14:35:49	36 7	74 9	671	1061	0.16	293.02	0.98
14:36: 9	36 6	74 9	806	1061	0.04	288.82	0.40
14:36:29	36 5	74 9	191	1061	0.83	299.10	2.12
14:36:49	36 4	74 9	716	1061	0.29	298.63	2.02
14:37: 9	36 2	74 9	701	1061	0.27	297.58	1.80
14:37:29	36 1	74 9	206	1061	0.80	298.93	2.09
14:37:49	36 0	74 9	206	1061	0.83	299.30	2.17
14:38: 9	35 59	74 9	656	1061	0.24	295.58	1.41

THE AVERAGE SURFACE TEMPERATURE IS 297.95 K.

TABLE 17. INVERTED TEMPERATURES AND CALCULATED TOTAL COLUMN PRECIPITABLE WATER AMOUNTS FOR FLIGHT 9.

Time	Latitude	Longitude	Zmin (m)	Zmax (m)	Precipitable Water (cm)	Surface Temperature (K)	Column (cm)
14:41:15	35 56	74 20	131	1361	1.07	298.44	1.98
14:41:35	35 57	74 21	131	1361	1.19	299.48	2.21
14:41:55	35 58	74 22	131	1361	1.16	299.23	2.15
14:42:15	35 59	74 22	131	1361	1.14	299.06	2.11
14:42:35	36 0	74 23	131	1361	1.14	299.06	2.11
14:42:55	36 1	74 24	131	1361	1.06	298.35	1.96
14:43:15	36 2	74 24	176	1361	0.96	297.86	1.86
14:43:35	36 4	74 24	161	1361	0.98	297.91	1.87
14:43:55	36 5	74 24	176	1361	0.91	297.37	1.76
14:44:15	36 6	74 24	176	1361	0.95	297.76	1.84
14:44:35	36 7	74 24	176	1361	0.96	297.86	1.86
14:44:55	36 9	74 24	131	1361	1.02	297.99	1.89
14:45:15	36 10	74 24	176	1361	1.03	298.52	2.00
14:45:35	36 11	74 24	131	1361	1.02	297.99	1.89
14:45:55	36 13	74 23	176	1361	0.99	298.14	1.92
14:46:15	36 14	74 23	176	1361	0.97	297.95	1.88
14:46:35	36 15	74 23	176	1361	0.95	297.76	1.84
14:46:55	36 17	74 23	131	1361	0.96	297.43	1.77
14:47:15	36 18	74 23	161	1361	1.00	298.09	1.91
14:47:35	36 19	74 23	131	1361	1.04	298.17	1.92
14:47:55	36 21	74 23	176	1361	1.00	298.24	1.94
14:48:15	36 22	74 23	161	1361	0.98	297.91	1.87
14:48:35	36 23	74 23	176	1361	0.96	297.86	1.86
14:48:55	36 25	74 23	176	1361	0.93	297.57	1.80
14:49:15	36 26	74 23	191	1361	0.95	297.91	1.87
14:49:35	36 27	74 23	176	1361	0.96	297.86	1.86
14:49:55	36 29	74 23	176	1361	0.98	298.05	1.90
14:50: 8	36 29	74 23	176	1361	0.99	298.14	1.92

THE AVERAGE SURFACE TEMPERATURE IS 298.14 K.

TABLE 18. INVERTED TEMPERATURES AND CALCULATED TOTAL COLUMN PRECIPITABLE WATER AMOUNTS FOR FLIGHT 10.

Time	Latitude	Longitude	Zmin (m)	Zmax (m)	Precipitable Water (cm)	Surface Temperature (K)	Column (cm)
14:53:19	36 42	74 24	401	1361	0.74	297.76	1.84
14:53:39	36 43	74 24	401	1361	0.74	297.76	1.84
14:53:59	36 45	74 25	401	1361	0.74	297.76	1.84
14:54:19	36 46	74 25	401	1361	0.71	297.39	1.76
14:54:39	36 47	74 25	401	1361	0.72	297.52	1.79
14:54:59	36 49	74 25	401	1361	0.73	297.64	1.81
14:55:19	36 50	74 25	431	1361	0.69	297.46	1.78
14:55:39	36 51	74 25	401	1361	0.78	298.24	1.94
14:55:59	36 53	74 25	401	1361	0.78	298.24	1.94
14:56:19	36 54	74 26	431	1361	0.77	298.45	1.98
14:56:39	36 55	74 26	401	1361	0.79	298.35	1.96
14:56:59	36 57	74 26	431	1361	0.70	297.59	1.80
14:57:19	36 58	74 26	401	1361	0.68	297.02	1.69
14:57:39	36 59	74 26	206	1361	0.90	297.56	1.80
14:57:59	37 1	74 26	431	1361	0.62	296.55	1.60
14:58:19	37 2	74 26	431	1361	0.72	297.84	1.85
14:58:39	37 3	74 27	401	1361	0.82	298.70	2.04
14:58:59	37 5	74 27	431	1361	0.82	299.04	2.11
14:59:19	37 6	74 27	431	1361	0.80	298.81	2.06
14:59:39	37 7	74 27	431	1361	0.81	298.93	2.09
14:59:59	37 8	74 27	431	1361	0.81	298.93	2.09

THE AVERAGE SURFACE TEMPERATURE IS 297.98 K.

$$r(z) = r_0 \left(\frac{P(z)}{P_0} - 0.02 \right) / 0.98 \quad (5)$$

where r_0 is the relative humidity at the surface and P_0 is the surface pressure. With (5) the mixing ratio is given by

$$q_v(z) = r(z) \frac{6.11}{P(z)} \exp \left\{ 5412 \left(\frac{1}{273} - \frac{1}{T(z)} \right) \right\} \quad (6)$$

where the temperature $T(z)$ is given by

$$T(z) = T_0 - \Gamma_d z \quad (7)$$

where Γ_d is the dry adiabatic lapse rate. Using the above approach the resultant surface temperatures are quite similar to those obtained using the empirical relationship derived from the NASA DIAL data, the absolute difference being on the order of a degree K or less. The agreement is not unexpected seeing that the Manabe-Wetherald derived water vapor profile is similar to that obtained from the midlatitude summer atmosphere. What this indicates, then, is that one could use the DIAL derived precipitable water amounts and an assumed profile shape to invert surface temperatures. Conversely, if one only has the surface temperature and surface relative humidity one could calculate the precipitable water amount reasonably well by using a climatologically derived water vapor profile shape.

The inverted absolute temperatures are clearly dependent upon the assumptions made concerning the humidity distribution. The temperature differences, however, are less so and are probably more useful in that they can be used to locate sea surface temperature variations, such as might be

associated with the Gulf Stream. The temperatures given in Tables 9 to 18 show temperature variations on both spatial and temporal scales that can be interpreted as relating to water temperature variations.

The flight pattern used during the tests was such that the plane flew the same flight path at different times of the day. For example, the downward leg of flight 1 and flights 4 and 8 covered, essentially, the same flight paths. The inverted temperatures from the overlapping portions show a variation from one time to another on the order of several degrees. The temperatures inverted from flight 1 are higher than those from the later flights. Likewise the temperatures inverted from the upward leg of flight 1 are higher than those from the overlapping portion of flight 5. An oceanographic analysis provided by the National Weather Service and National Earth Satellite Service indicated that the Gulf Stream was observed to be in the vicinity of the test area and the variations in the inverted surface temperature could be the result of Gulf Stream meanderings.

The surface temperature inversion method presented here is much simpler than that of Rosenberg and Hogan [9]. Their approach involved using a three frequency DIAL to invert the temperature and humidity profiles. In their feasibility study they used H_2O lines and considered both horizontal and vertical viewing angles. Their study indicated that one can invert the temperature and humidity profiles although the error in temperature and humidity increases with increasing horizontal and vertical range. The simple approach presented here assumed knowledge about the shape of both the temperature and humidity profiles. An extensive analysis of the sensitivity of the inversion method to the model assumptions has not been performed at this time.

INFLUENCE OF H₂O PROFILES DERIVED FROM THE DIAL DATA ON DF LASER PROPAGATION

4.1 MODEL FOR CALCULATION OF DF LASER TRANSMITTANCE

4.1.1 TRANSMITTANCE FOR A LASER POWER SPECTRUM

An average transmittance over a laser power spectrum can be defined in terms of the transmittances at the individual laser frequencies. The transmittance at some range r is the ratio of the total beam power P at that range to the beam power P_s at the source:

$$T = P/P_s$$

The total beam power at range r is the sum of the source powers in the individual lines times the transmittances for the individual lines:

$$T = \frac{\sum_i f_i P_s T_i}{P_s}$$

where the f_i define the power spectrum of the laser and T_i is the transmittance for the i th line. The laser transmittance is therefore the sum of the individual transmittances weighted by the power spectrum:

$$T = \sum_i f_i T_i$$

4.1.2 TRANSMITTANCE CALCULATION FOR THE LIDAR DATA

The lidar data consist of water vapor amounts in parts per ten-thousand at each of various altitudes. Typically, there were data for 60 layers between 200 m and 1400 m altitude. Transmittances were calculated for these water vapor profiles, assuming midlatitude summer standard atmosphere conditions for everything except water vapor.

The transmittance calculations were done both for a cw and for a pulsed DF laser. For the cw laser calculations the power spectrum of the MIRACL laser was used, and it is assumed that this is representative of high-powered cw DF lasers. This power spectrum is given in Table 19 [10]. For the pulsed laser calculations, the power spectrum listed in Table 20 was used. This is not a power spectrum for an actual device, but has the general characteristics (more power at higher v and J levels) of high-power pulsed DF lasers. In the pulsed power spectrum, it is assumed that the lines which occur in the region of the $4.3\text{ }\mu\text{m}$ CO_2 band are removed, but that lines at longer wavelengths are still present. This is important, because these longer-wavelength lines suffer some absorption by H_2O . This is not an issue for cw lasers, since they operate on the shorter-wavelength transitions and transmit almost no energy in the region of the CO_2 band and beyond.

A computer code named TRANS was written to perform DF laser transmittance calculations. TRANS was used to calculate transmittance at each laser frequency for each layer, and these results were combined to produce transmittances for 2-km paths oriented vertically and at 30-degree and 60-degree zenith angles. The data for the lowest layer were also used to estimate horizontal transmittance at the surface for a 2-km range.

TABLE 19. CW DF LASER POWER SPECTRUM USED IN TRANSMITTANCE CALCULATIONS.

LINE	POWER SPECTRUM
P ₁ (8)	0.07
P ₁ (9)	0.31
P ₁ (10)	0.16
P ₁ (11)	0.04
P ₂ (8)	0.11
P ₂ (9)	0.08
P ₂ (10)	0.07
P ₂ (11)	0.01
P ₂ (12)	0.01
P ₃ (7)	0.03
P ₃ (8)	0.04
P ₃ (9)	0.06
P ₃ (10)	0.01

TABLE 20. PULSED DF LASER POWER SPECTRUM
USED IN TRANSMITTANCE CALCULATIONS.

LINE	POWER SPECTRUM
P ₁ (8)	0.033
P ₁ (9)	0.041
P ₁ (10)	0.033
P ₂ (6)	0.033
P ₂ (8)	0.066
P ₂ (9)	0.049
P ₂ (10)	0.033
P ₃ (6)	0.041
P ₃ (7)	0.074
P ₃ (8)	0.082
P ₃ (9)	0.074
P ₄ (6)	0.049
P ₄ (7)	0.066
P ₄ (8)	0.049
P ₄ (9)	0.033
P ₅ (6)	0.041
P ₅ (7)	0.057
P ₈ (6)	0.049
P ₈ (7)	0.025
P ₉ (5)	0.016
P ₉ (6)	0.041
P ₉ (7)	0.016

Each calculation by TRANS of transmittance at a laser frequency in a layer of atmosphere consisted of four parts:

- line absorption by H_2O ;
- line absorption by atmospheric species other than H_2O ;
- H_2O continuum; and
- N_2O continuum.

Each of these is discussed below.

4.1.2.1 Line Absorption By H_2O

Volume absorption coefficients for each laser frequency in the power spectrum for midlatitude summer conditions at sea level and at 5 km were obtained from the tabulation by Manning and Matisse [11]. These coefficients were converted to cross sections ($cm^2/molecule$), which are independent of water-vapor amount. The actual cross section at the altitude of each individual layer was found by logarithmic interpolation of the values at 0 and 5 km. The optical depth in any layer is the product of the absorption cross section, the number density of H_2O molecules in the layer, and the path length through the layer.

4.1.2.2 Line Absorption By Species Other Than H_2O

Volume absorption coefficients for species other than H_2O were obtained from the tabulations of Manning and Matisse [11] for a midlatitude summer standard atmosphere at altitudes of 0 and 5 km. The absorption coefficients tabulated by Manning and Matisse were based on line-by-line calculations which included a sub-Lorentz lineshape for CO_2 and far-wing effects for all major species.

The actual absorption coefficient in any level is found by logarithmic interpolation between the values at 0 and 5 km. The optical depth of the layer for non-H₂O line absorption is the product of the volume absorption coefficient and the path length through the layer.

4.1.2.3 Water-Vapor Continuum

The optical depth in a layer due to the water-vapor continuum is calculated using an algorithm based on the measurements of White, et al. [12] and Watkins, et al. [13]. The algorithm calculates absorption as a function of frequency, temperature, and H₂O concentration. It is described in the High Energy Laser Propagation Handbook [10].

4.1.2.4 Nitrogen Continuum

The optical depth through the N₂ continuum is calculated for each layer and for each laser frequency using an algorithm based on the data of Shapiro and Gush [14]. The algorithm calculates absorption by the N₂ continuum as a function of frequency, temperature, and atmospheric density. It is described in the High Energy Laser Propagation Handbook [10].

4.2 RESULTS OF TRANSMITTANCE CALCULATIONS

Computer program TRANS, described in Section 4.1, was used to calculate transmittances for each measured water vapor profile. The data did not extend to the surface. In order to do these calculations, the water vapor concentration at the lowest altitude in each profile was extended down to the surface, and the concentration in the highest altitude was extended up to 2 km. A more realistic method of extending the measured profiles in both directions could

certainly have been found; in fact, for these data, the first and last points in each profile are probably the least accurate. The laser transmittances were so high, however, that it was decided that such "fine tuning" of the model was not necessary.

The transmittance calculations were done for two-km ranges for vertical paths, paths at 30-degree and 60-degree zenith angles, and for horizontal paths. Since the same range was used for each path, it was possible for transmittance to actually be higher for the slant paths than for the vertical path. This would occur if there was a high concentration of water vapor in the upper layer; the vertical path would pass through that water vapor, but the slant paths would have ended before reaching the upper layers. This actually did occur several times.

The sea-level horizontal path transmittance calculations were generally not meaningful. An example is shown in Figure 32 for flight 5. These calculations were based on the data point for the lowest altitude in each profile; as just noted, this point is not expected to be very accurate. The strong, random fluctuations in Figure 32 indicate a high noise level in the data for the lowest altitude of each profile.

4.2.1 CW LASER TRANSMITTANCE FOR INDIVIDUAL PROFILES

The results of the cw laser transmittance calculations for flight 1 are shown in Figure 33 for the vertical path and the two slant paths. There are two curves on each plot because the aircraft changed directions during the course of flight 1. The directions are shown by arrows on the first plot of the figure. The transmittances are lower for the 30-degree and 60-degree zenith angle paths. This is

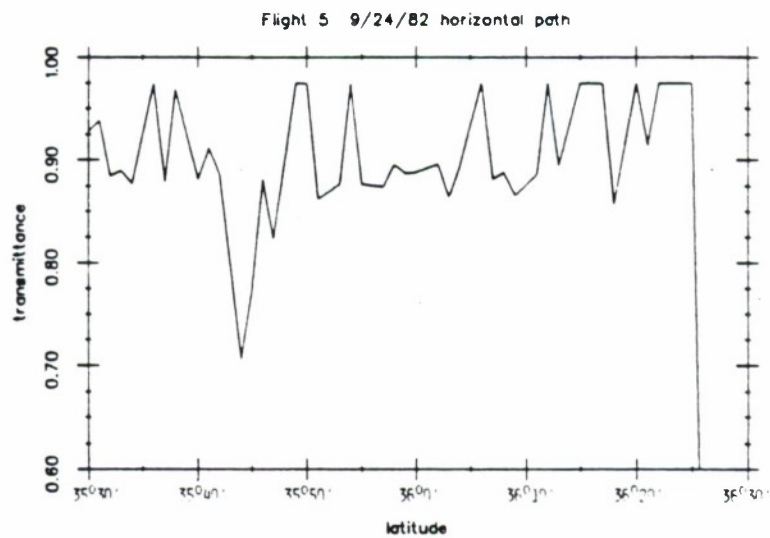


FIGURE 32. CW DF LASER TRANSMITTANCE FOR A HORIZONTAL PATH AT SEA LEVEL CALCULATED FROM THE DATA FOR FLIGHT 5.

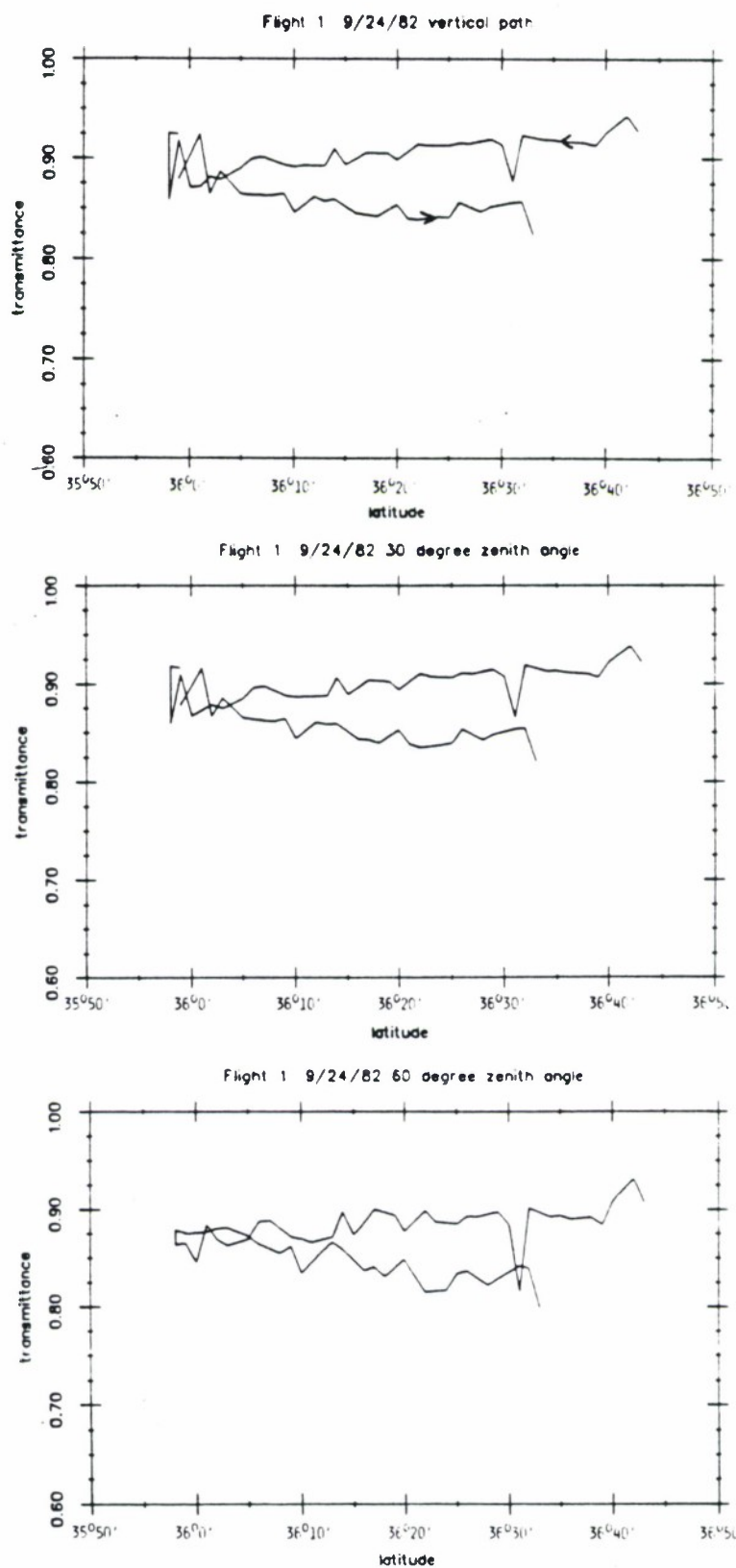


FIGURE 33. CW DF LASER TRANSMITTANCE CALCULATED FROM DATA FOR FLIGHT 1.

generally the expected result, despite the fact that all three paths have the same range; the water vapor concentration generally falls off with altitude, and the slant paths have longer paths through the lower layers where the concentration is high. The difference between the vertical transmittance and the transmittance for the 60-degree zenith angle ranges from zero to about 4% (transmittance units).

The calculation results for cw lasers for flight 2 are shown in Figure 34. In some regions the transmittances are nearly the same for the vertical and slant paths, while for other regions the transmittance for the 60-degree zenith angle is as much as 5% lower (transmittance units). Transmittance for 2-km paths is around 90%.

Cw results for flight 3 are shown in Figure 35 for the vertical path. The slant-path transmittances (not shown) were lower, but only by 0 to 2%. The same was true for flights 4 and 5 (Figures 36 and 37). The slant path transmittances for flights 6 and 7 (Figures 38 and 39) were nearly identical to the vertical transmittances. For flight 8 (Figure 40) the slant path transmittances were slightly lower in some places and about the same as the vertical transmittances in other places. Some of the slant path transmittances for flight 9 (Figure 41) were higher than the corresponding vertical path transmittances, indicating high water vapor concentrations in the upper layers. For flights 10 and 11 (Figures 42 and 43) the slant path transmittances were slightly lower than the vertical path values. The aircraft changed directions during flight 11, causing the loop in the transmittance-versus-longitude plots of Figure 43.

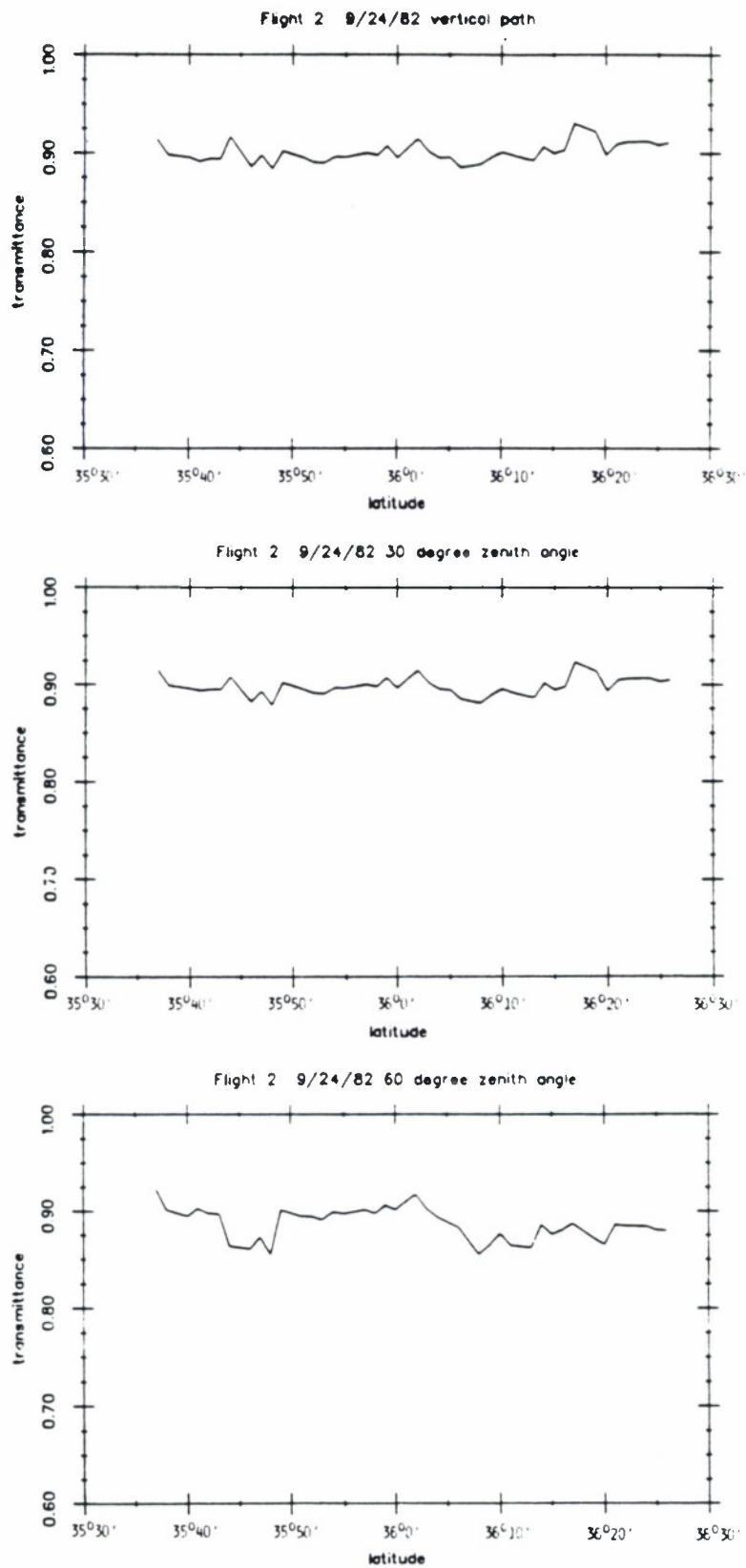


FIGURE 34. CW DF LASER TRANSMITTANCE CALCULATED FROM DATA FOR FLIGHT 2.

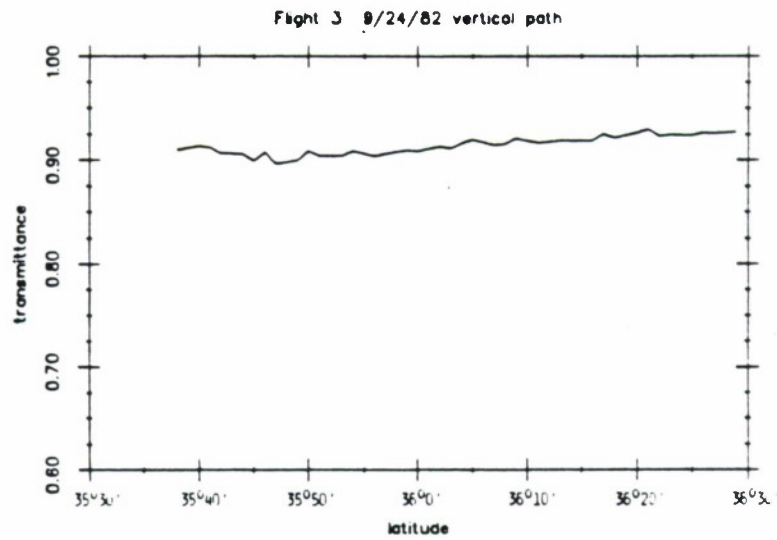


FIGURE 35. CW DF LASER TRANSMITTANCE CALCULATED FROM DATA FOR FLIGHT 3.

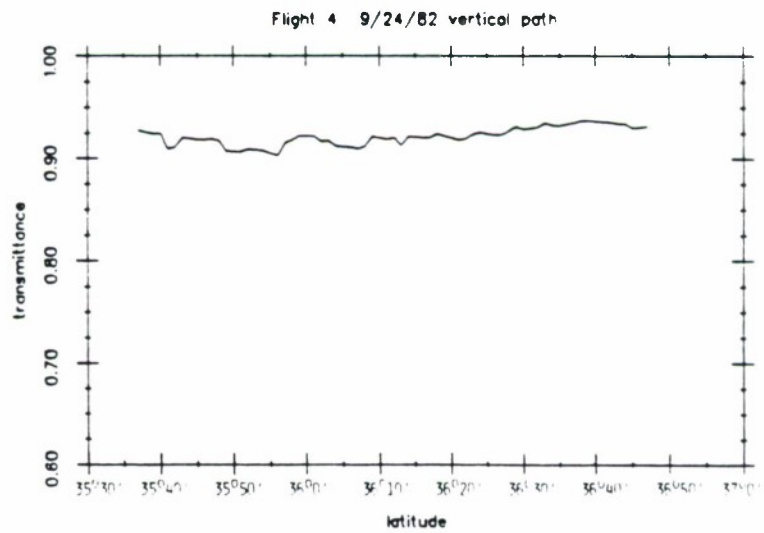


FIGURE 36. CW DF LASER TRANSMITTANCE CALCULATED FROM DATA FOR FLIGHT 4.

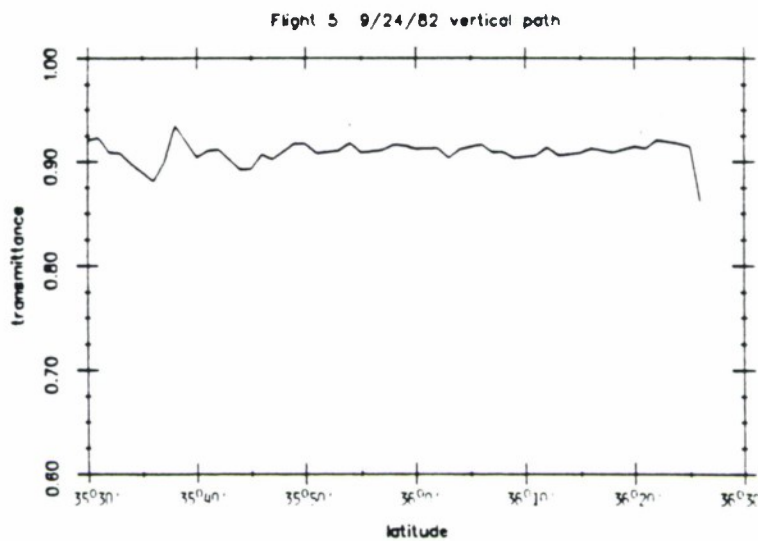


FIGURE 37. CW DF LASER TRANSMITTANCE CALCULATED FROM DATA FOR FLIGHT 5.

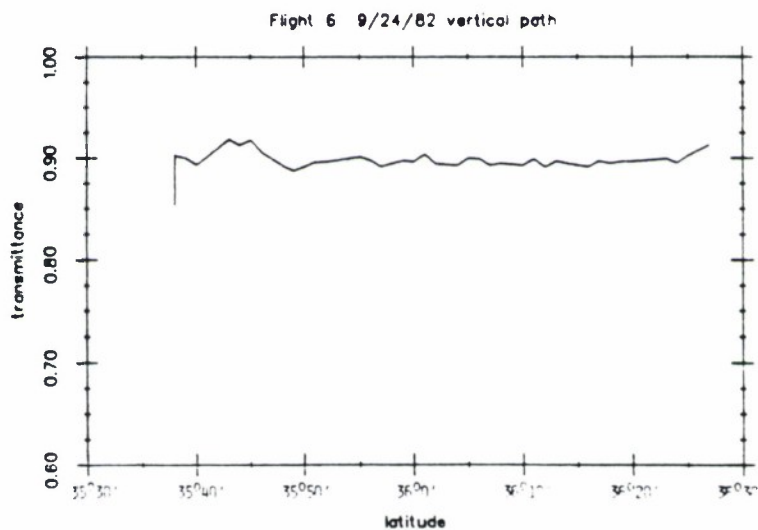


FIGURE 38. CW DF LASER TRANSMITTANCE CALCULATED FROM DATA FOR FLIGHT 6.

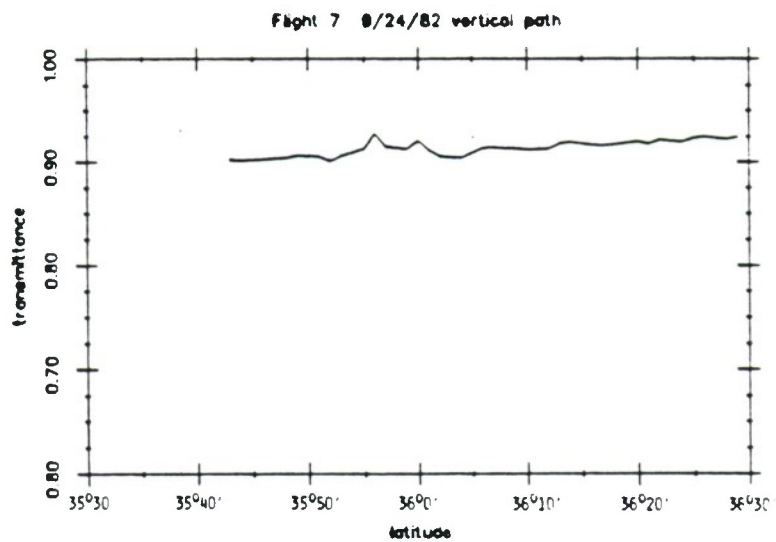


FIGURE 39. CW DF LASER TRANSMITTANCE CALCULATED FROM DATA FOR FLIGHT 7.

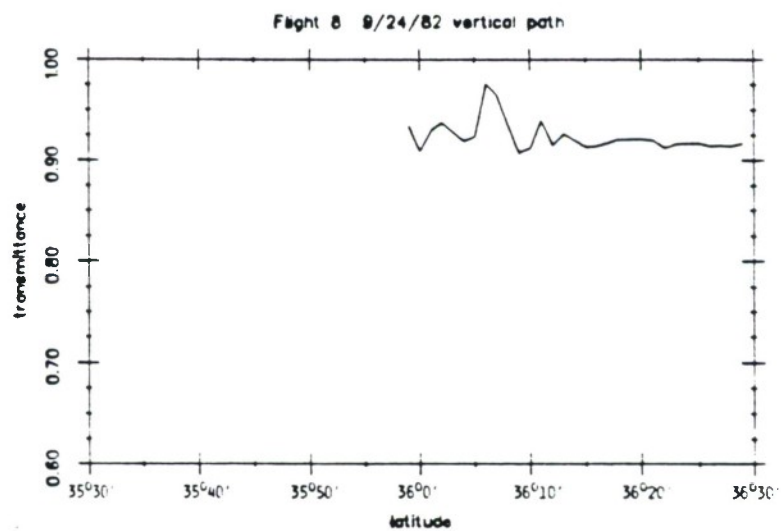


FIGURE 40. CW DF LASER TRANSMITTANCE CALCULATED FROM DATA FOR FLIGHT 8.

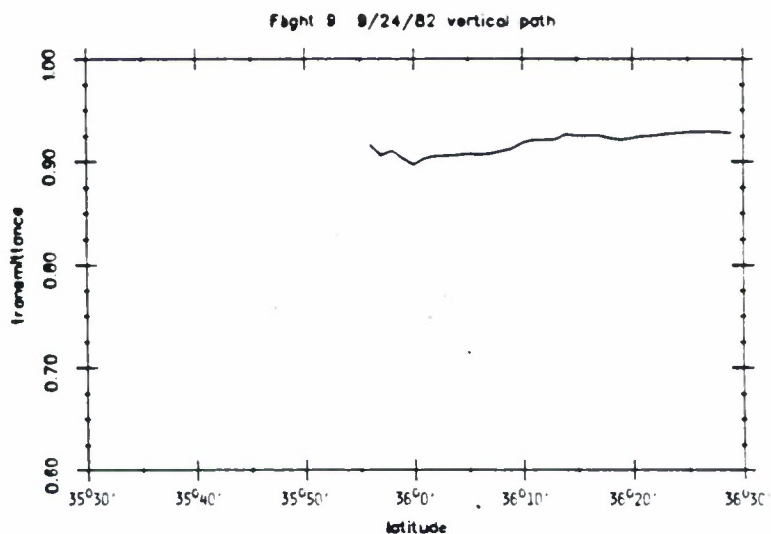


FIGURE 41. CW DF LASER TRANSMITTANCE CALCULATED FROM DATA FOR FLIGHT 9.

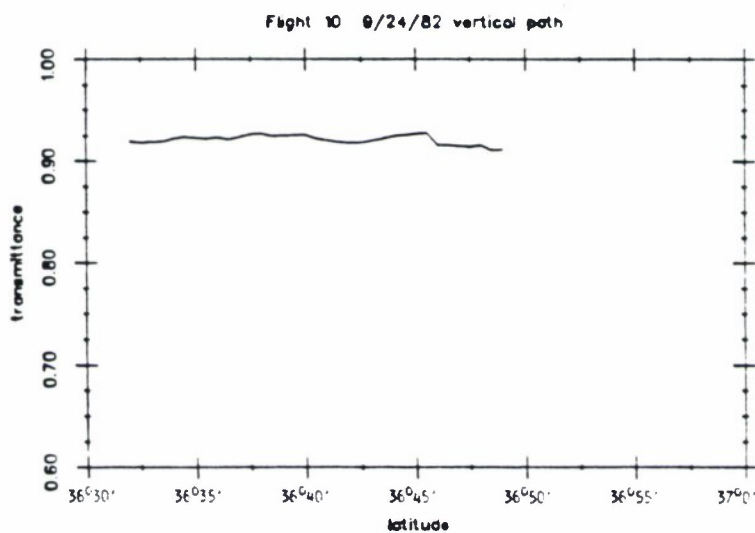


FIGURE 42. CW DF LASER TRANSMITTANCE CALCULATED FROM DATA FOR FLIGHT 10.

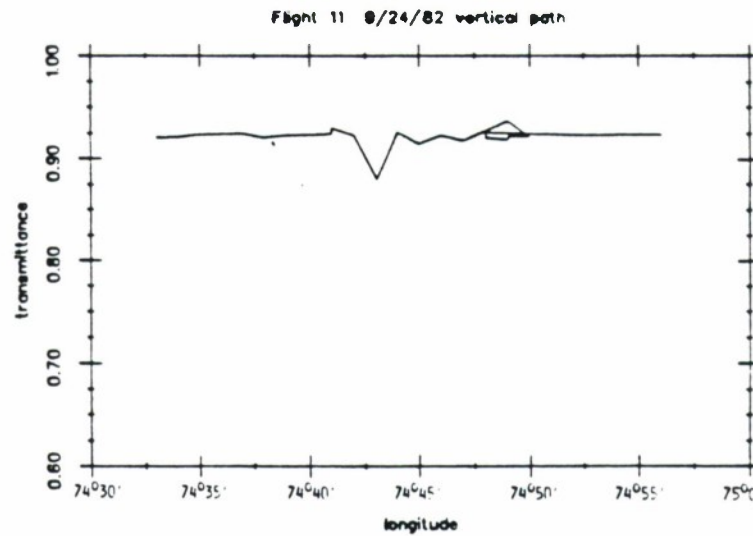


FIGURE 43. CW DF LASER TRANSMITTANCE
CALCULATED FROM DATA FOR
FLIGHT 11.

The transmittances plotted in Figures 33 through 43 are all around 90% for a two-km range. These calculations included line and continuum absorption by all atmospheric gases. Although there is some fluctuation in the transmittance, which must be caused by water vapor variation, the fluctuations are small, and no spatial pattern is seen in the results. The gulf stream boundary appears to have no influence on cw DF laser transmittance.

4.2.2 PULSED LASER TRANSMITTANCES FOR INDIVIDUAL PROFILES

Transmittance calculations were also done for a pulsed DF laser for each measured profile. The transmittances were somewhat lower than the cw transmittances. Part of the reason for this is that several laser lines on the long-wavelength side of the $4.3\text{ }\mu\text{m}$ CO_2 band are included in the pulsed laser power spectrum, and these lines are subject to fairly strong H_2O absorption. Whether these lines would be present in the power spectrum of an actual device would depend on how the device was configured, and in particular how the lines in the region of the CO_2 band were suppressed.

The results of the pulsed DF laser transmittance calculations for flight 1 are shown in Figure 44. As was noted earlier, the aircraft changed directions during flight 1, so that each latitude was covered twice. The slant-path transmittances are slightly lower than the vertical-path transmittances. The calculated transmittances for a pulsed DF laser for flights 2 through 10 are shown in Figures 45 through 53. In each of these figures, the transmittances for the vertical path and for the 30-degree and 60-degree zenith angles are shown on the same plot. For flight 2 (Figure 45) the slant-path transmittances are lower than the vertical-path transmittances for part of the flight and are

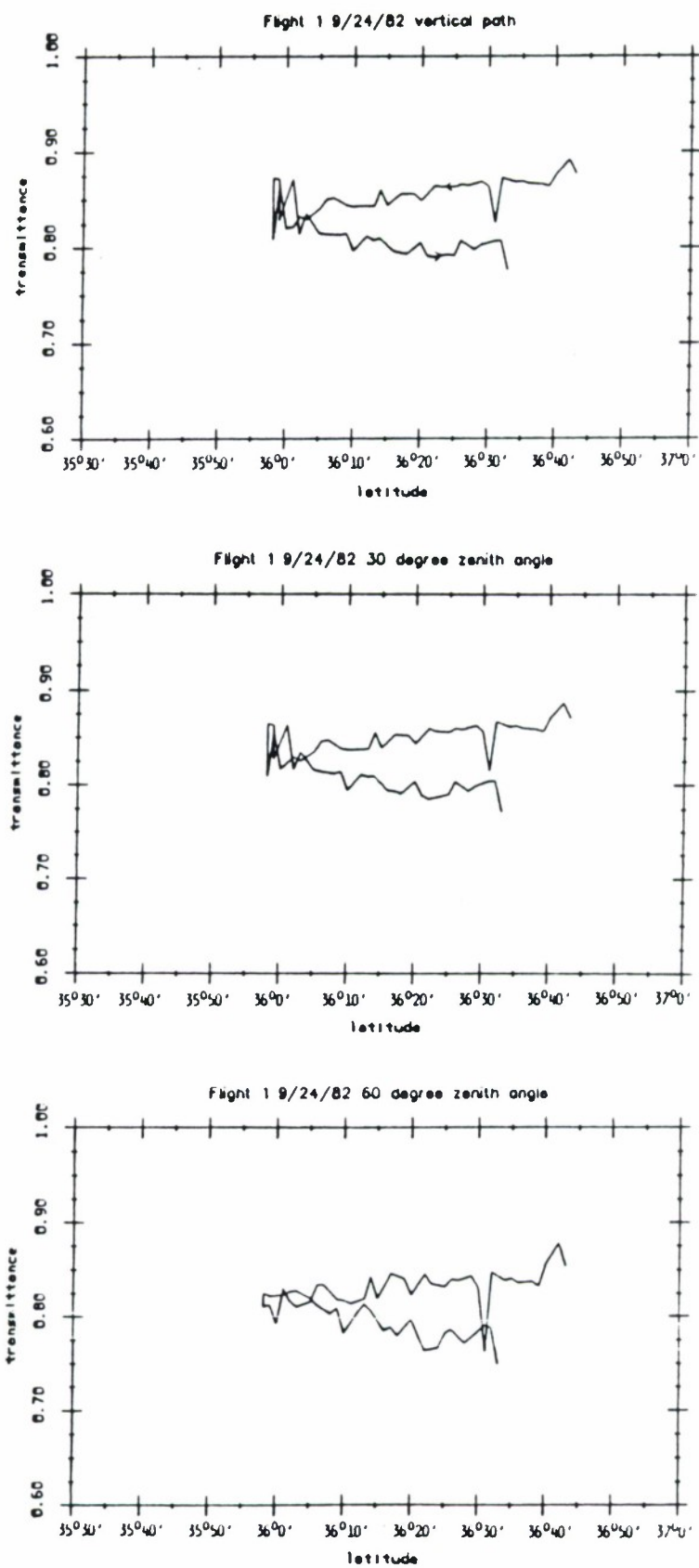


FIGURE 44. PULSED DF LASER TRANSMITTANCE
CALCULATED FROM DATA FOR FLIGHT 1.

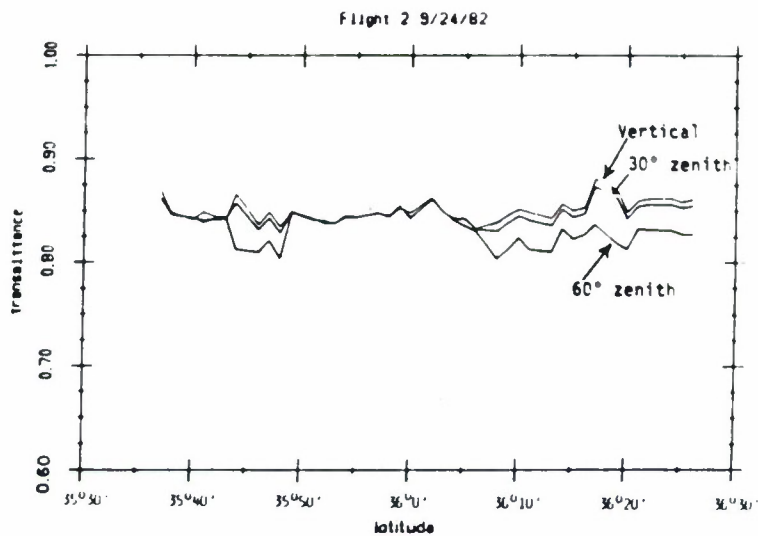


FIGURE 45. PULSED DF LASER TRANSMITTANCE
CALCULATED FROM DATA FOR FLIGHT 2.

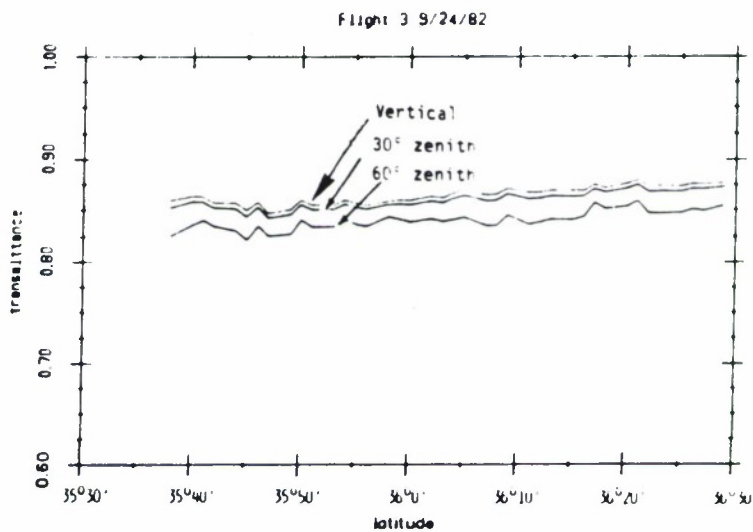


FIGURE 46. PULSED DF LASER TRANSMITTANCE
CALCULATED FROM DATA FOR FLIGHT 3.

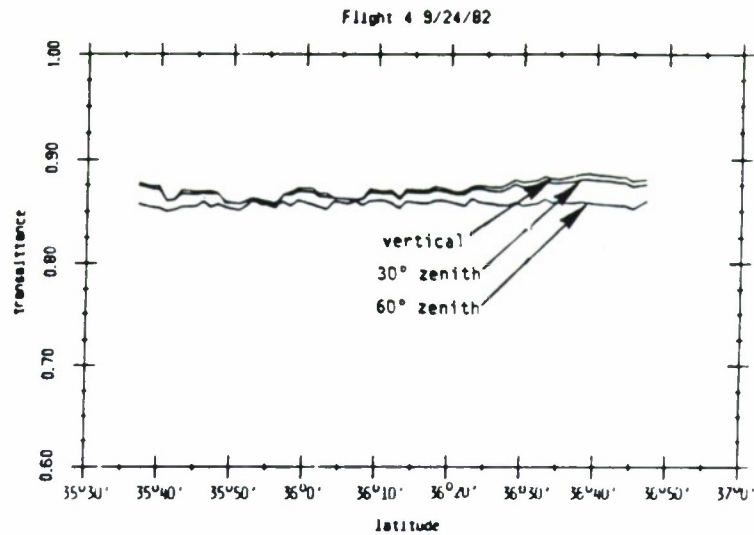


FIGURE 47. PULSED DF LASER TRANSMITTANCE
CALCULATED FROM DATA FOR FLIGHT 4.

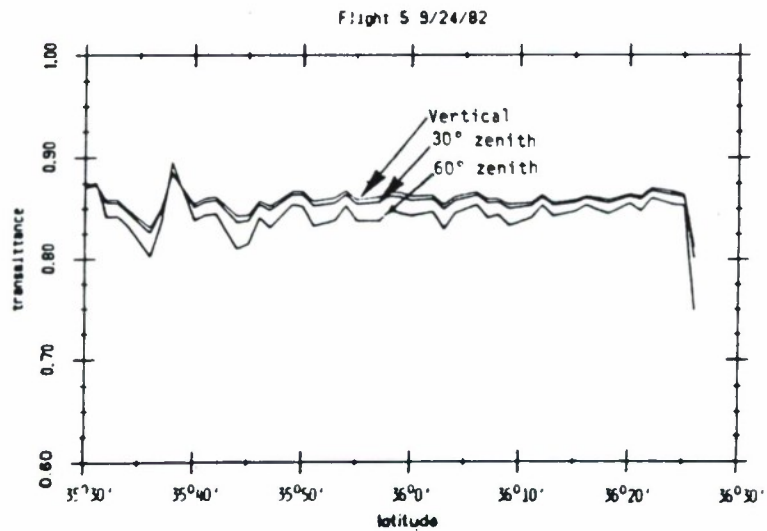


FIGURE 48. PULSED DF LASER TRANSMITTANCE
CALCULATED FROM DATA FOR FLIGHT 5.

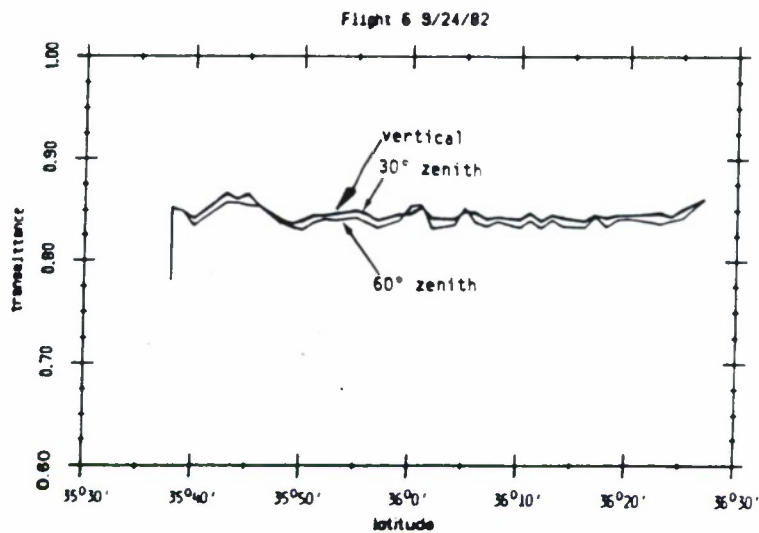


FIGURE 49. PULSED DF LASER TRANSMITTANCE
CALCULATED FROM DATA FOR FLIGHT 6.

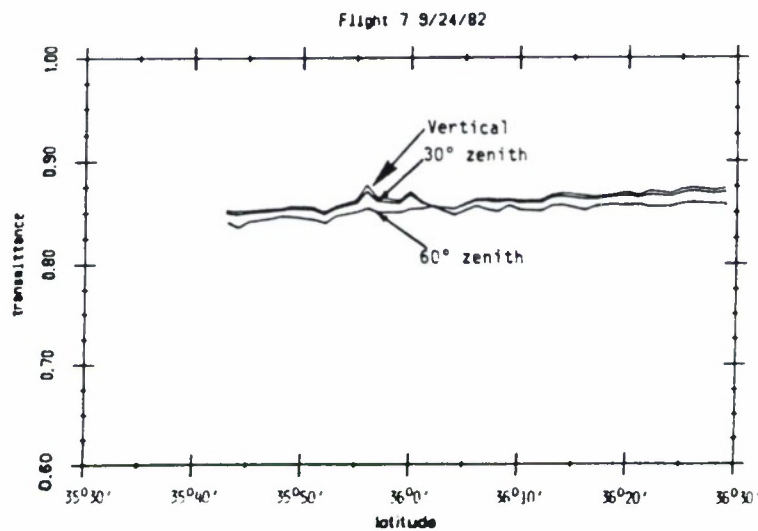


FIGURE 50. PULSED DF LASER TRANSMITTANCE
CALCULATED FROM DATA FOR FLIGHT 7.

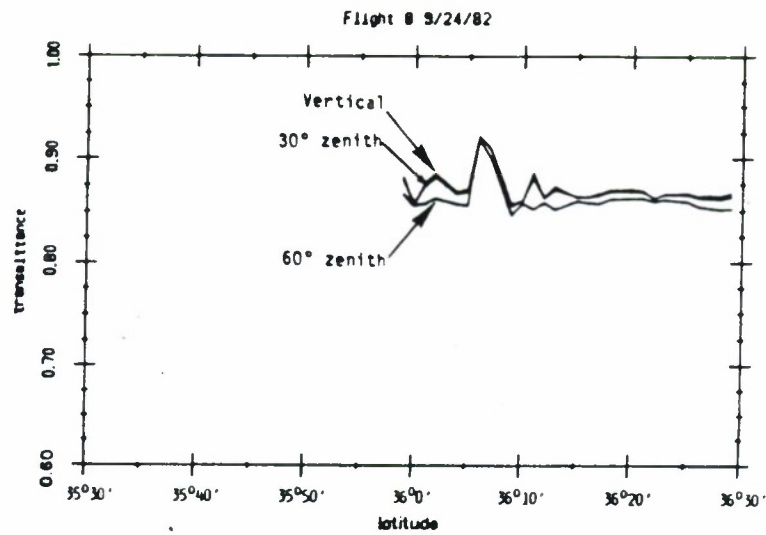


FIGURE 51. PULSED DF LASER TRANSMITTANCE
CALCULATED FROM DATA FOR FLIGHT 8.

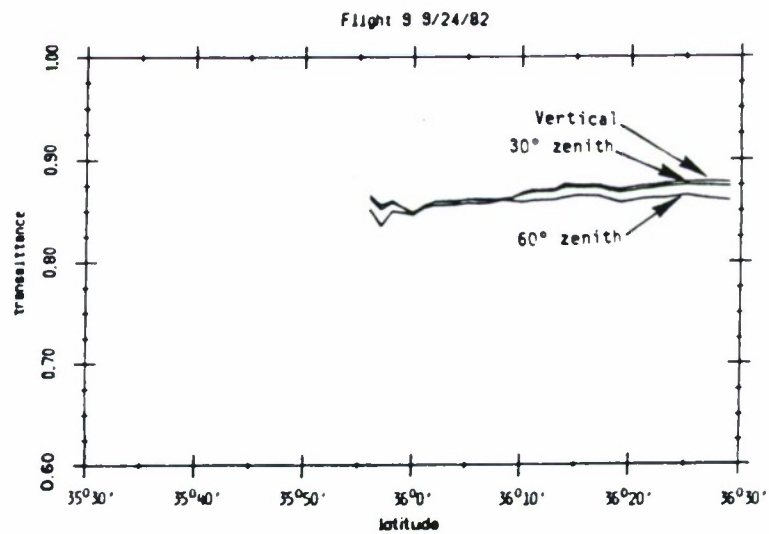


FIGURE 52. PULSED DF LASER TRANSMITTANCE
CALCULATED FROM DATA FOR FLIGHT 9.

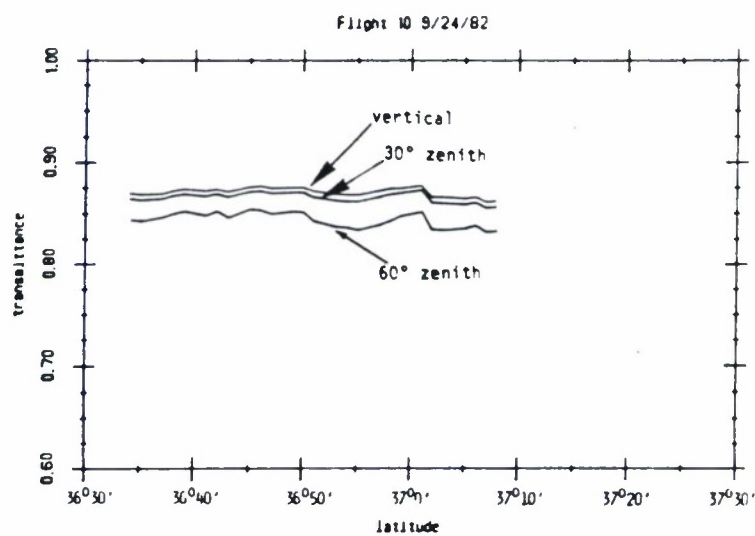


FIGURE 53. PULSED DF LASER TRANSMITTANCE
CALCULATED FROM DATA FOR FLIGHT
10.

about the same for other parts; at one point the slant-path transmittances are higher. As noted in the discussion of the cw laser transmittance calculations, this depends on the shape of the water vapor profile. For most of the remaining flights, the slant-path transmittances were lower than the vertical-path transmittances, although the curves do cross briefly for flights 5 and 6.

The transmittances calculated for a pulsed DF laser were generally in the range of 85% to 88% for a 2-km range. As with the cw transmittances, the pulsed laser transmittances contain small fluctuations which must be due to variations in the water vapor profile (because other parameters, such as CO₂ concentration, were taken from standard atmosphere models and did not vary from sounding to sounding). There was no significant spatial variation in the results which might correlate with the gulf stream boundary.

4.2.3 TRANSMITTANCES FOR AVERAGE AND EXTREME PROFILES

Transmittances were calculated using TRANS for the average profile discussed in Section 3. This profile was determined by taking the average of all of the data at each altitude. High and low humidity profiles were defined by adding and subtracting the standard deviation of the data at each altitude to the average at that altitude. Calculations were also done for these profiles. The calculations are the same as those done for the individual profiles: transmittances for vertical paths and 30-degree and 60-degree zenith angles, all with identical ranges of 2 km. The results of these calculations are shown in Table 21. The cw transmittances are about 5% higher (in transmittance units) than the pulsed transmittances. The difference between the high-humidity and low-humidity profile transmittances is only 4% or 5% transmittance.

TABLE 21. DF LASER TRANSMITTANCES CALCULATED FOR THE AVERAGE WATER VAPOR PROFILE DERIVED FROM THE DATA, AND FOR PROFILES DEFINED BY THE AVERAGE MINUS AND THE AVERAGE PLUS THE STANDARD DEVIATION σ OF THE DATA AT EACH ALTITUDE.

	PROFILE		
	AVE - σ	AVERAGE	AVE + σ
CW DF LASER			
Vertical	0.928	0.910	0.888
30° zenith	0.925	0.906	0.884
60° zenith	0.910	0.890	0.866
PULSED DF LASER			
Vertical	0.877	0.860	0.839
30° zenith	0.873	0.855	0.834
60° zenith	0.855	0.836	0.814

4.2.4 TRANSMITTANCE CALCULATIONS FOR A STANDARD ATMOSPHERE

TRANS was used to calculate cw and pulsed DF laser transmittances for 2-km paths through the midlatitude summer standard atmosphere and through the midlatitude summer atmosphere with water vapor shifted so that the surface humidity was 100%. The water vapor profile for this modified midlatitude summer atmosphere is almost identical to that of the tropical standard atmosphere.

The results of these calculations are given in Table 22. The transmittances are slightly lower than those calculated for the data, because the water vapor amounts are somewhat higher for the standard atmosphere than for the measured profiles. As was noted for the calculations for the data averages, a fairly substantial change in the water vapor amount produces only a small change in the transmittance.

4.3 DESCRIPTION OF THERMAL BLOOMING CALCULATIONS

A high energy laser beam which propagates through the atmosphere has an optimum power level at which the intensity at the target is maximized. If the laser power is increased above the optimum value, the resulting increase in thermal blooming will cause a decrease in the intensity at the target. The optimum power depends on the laser power spectrum, the amount of atmospheric absorption on each laser line, and the degree of focusing. Optimum power for a given laser system and scenario can be calculated using the BRLPRO code.

BRLPRO is a scaling-law nonlinear propagation code originally developed by H.J. Breaux of the Army Ballistic Research Laboratory [15]. It is in common use in the prop-

TABLE 22. DF LASER TRANSMITTANCES CALCULATED FOR A MIDLATITUDE SUMMER STANDARD ATMOSPHERE AND FOR A MIDLATITUDE SUMMER ATMOSPHERE WITH THE WATER VAPOR PROFILE SHIFTED TO RESULT IN 100% RELATIVE HUMIDITY AT THE SURFACE.

	PROFILE	
	MIDLATITUDE SUMMER	MIDLATITUDE SUMMER WITH 100% SURFACE HUMIDITY
CW DF LASER		
Vertical	0.898	0.854
30° zenith	0.892	0.848
60° zenith	0.876	0.829
PULSED DF LASER		
Vertical	0.849	0.806
30° zenith	0.842	0.799
60° zenith	0.822	0.778

agation community, and is now incorporated in the Army's EOSAEL library of propagation codes [16]. The code performs calculations for a beam which is assumed to have a Gaussian cross section. It steps along the beam path, calculating the beam size and intensity at each point along the path, considering atmospheric absorption, scattering, turbulence, jitter, and thermal blooming. The calculations are done for a beam consisting of a single laser line, so a power spectrum must be simulated using power-weighted absorption coefficients.

The calculations described here were done for a high energy laser system used in a ship defense scenario. It is important for such a system to operate near its optimum power, and ideally the concentrations of absorbing atmospheric species should be known at all altitudes so that the optimum power level can be determined. In the absence of such atmospheric profile measurements, standard atmosphere profiles would probably be used in conjunction with surface measurements to determine optimum power. The calculations were done to determine the difference between the "real optimum power" based on the measured water vapor profiles determined by the DIAL system and the "assumed optimum power" based on standard atmosphere information.

A schematic of the scenario is shown in Figure 54. A ship is the target of an incoming missile. A DF laser system is on an escort ship located 1 km from the targeted ship. The missile is currently located such that its range from the laser is 2 km and the beam path is elevated from horizontal by 30 degrees. Both cw and pulsed DF lasers were considered. The source aperture diameter is 1 m and the laser is capable of operating at powers in excess of 1 Mw. For the pulsed laser calculations, a pulse duration of 2 μ s and a repetition frequency of 50 hz were used. Turbulence

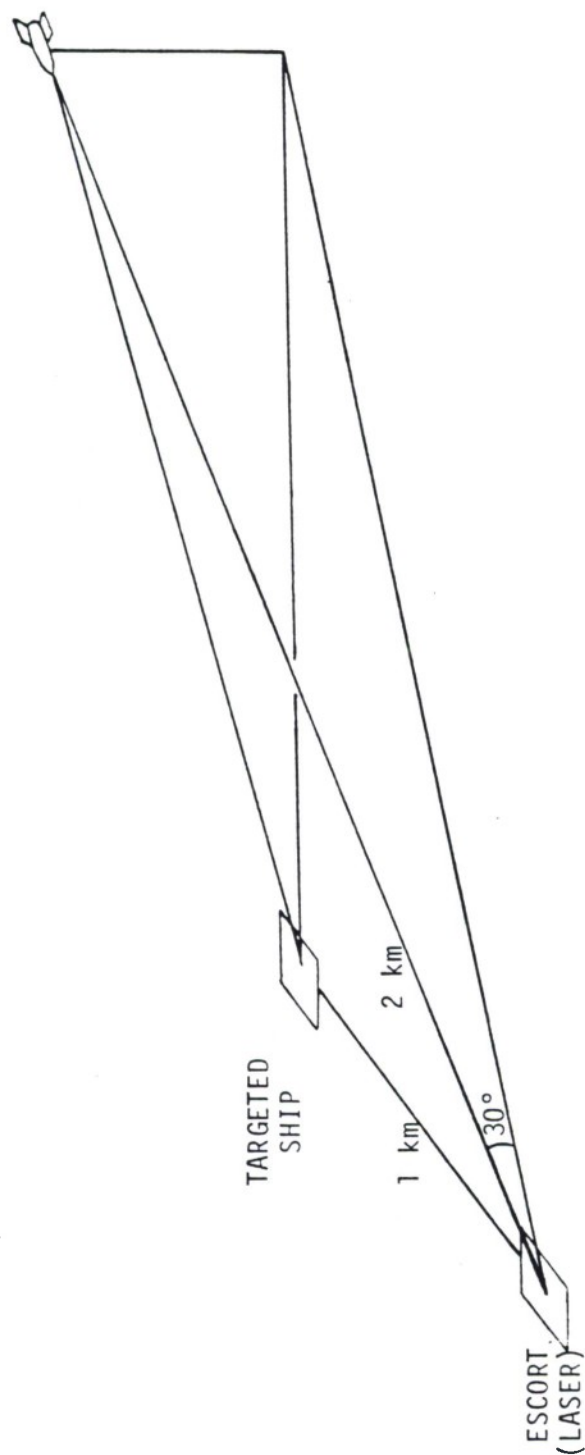


FIGURE 54. SHIP DEFENSE ESCORT SCENARIO.

was included in the calculations with C_n^2 of $1 \times 10^{-15} \text{ m}^{-2/3}$. A 5 m/s cross wind was assumed.

Absorption coefficients for both the measured profiles and the standard atmosphere profiles were determined from the transmittances for cw and pulsed systems described in Section 4.3 of this report. These absorption coefficients are power-weighted values averaged over the beam path.

4.4 RESULTS OF THERMAL BLOOMING CALCULATIONS

The results of the BRLPRO calculations are shown in Table 23 for both cw and pulsed systems operating over a 2-km range. The calculations were done for the average profile which was derived from the DIAL data by averaging all of the data at each altitude, and the "ave+ σ " and "ave- σ " profiles which represent the average value plus and minus the standard deviation of the data at each altitude. The results for the average profile show the typical error which might have been expected by using standard atmospheres rather than actual profiles to determine optimum laser power on the day the data were taken. The results for the "ave- σ " and "ave+ σ " profiles show the range of error. The "ave+ σ " profile was the closest of the three to the standard atmosphere.

The first column in Table 23 contains the absorption coefficients used for the calculations. As noted previously, these were obtained from the transmittances calculated earlier, and represent power-weighted coefficients averaged over the path for each power spectrum and each profile. The second column lists the "assumed optimum" power which was obtained through a BRLPRO calculation using the midlatitude summer standard atmosphere profiles for all species, including water vapor. The third column contains the "real

TABLE 23. INTENSITY LOSS CAUSED BY USING STANDARD ATMOSPHERE PROFILES RATHER THAN REAL PROFILES TO DETERMINE OPTIMUM LASER POWER.

	TARGET INTENSITIES					% LOSS	

	"REAL" PROFILE	ABSORPTION COEFFICIENT (km^{-1})	"ASSUMED OPTIMUM" POWER (kw)	"REAL OPTIMUM" POWER (kw)	USING		
"ASSUMED OPTIMUM" AND REAL PROFILE (kw/cm^2)					"REAL OPTIMUM" AND REAL PROFILE (kw/cm^2)		
<u>cw DF laser, 2-km range</u>							
ave- σ		0.0472	920	1271	273	284	4%
ave		0.0583	920	1038	226	227	<1%
ave+ σ		0.0719	920	851	181	181	<1%
<u>pulsed DF laser, 2-km range</u>							
ave- σ		0.0783	2618	3272	674	687	2%
ave		0.0896	2618	2862	586	587	<1%
ave+ σ		0.1029	2618	2494	498	499	<1%

optimum" power values obtained by using the actual water vapor profile. Note that the pulsed laser can operate at much higher powers, despite the slightly higher absorption coefficients.

Column four lists the target intensities which would be achieved if the laser operated at the "assumed optimum" power in an atmosphere with the appropriate "real" water vapor profile. This is the intensity which might be expected if no equipment were available to measure the water vapor profile and a standard atmosphere were assumed. Column five gives the target intensities obtained using the "real optimum" power; this is the maximum target intensity which could be achieved for those atmospheric conditions. The last column lists the percentage loss of intensity caused by using the standard atmosphere rather than the real profile to determine optimum power for the laser.

In the worst case, there is only a 4% loss of target intensity caused by using the standard atmosphere rather than the real water vapor profile to determine the optimum operating power for the laser. Similar calculations were done for a 6-km range, with similar results.

REDUCTION AND ANALYSIS OF THE LFLID SUPPORT AND RADIOSONDE TRANSMITTANCE DATA

Records of the radiosonde data collected during the times that the most reliable long-path transmittance measurements were made (the times are listed in Table 5, Section 2.2) were provided to OMI by John Toner of the Naval Air Development Center (NADC), the organization sponsoring the LFLID test series. Temperature and relative humidity values from the radiosonde data were extracted for 300 m intervals between sea level and the AMOS observatory altitude of 3.05 km. These data were used as the basis of slant-path transmittance calculations performed using the LOWTRAN 6 computer model [2].

Figures 55-72 present plots of the results of the LOWTRAN calculations together with the corresponding experimental measurements. The figures are divided into two groups corresponding to the two wavelength regions of interest. Figures 55-62 show the results for the spectral region between 3.0 and 6.0 μm . Figures 63-67 show the comparisons between the calculated and measured transmittances for the 7.0 to 14.0 μm region.*

In the comparisons shown in Figures 55-67 the identification code of the measured transmittance spectrum is indicated (see Table 5 in Section 2.2 for an explanation of this code). The LOWTRAN calculations shown in Figures 55-67 were performed omitting the contribution due to aerosol atten-

* A data reduction error was discovered after the plots were prepared. Corrected scale values for the 7.0 to 14.0 μm experimental spectra are given in the figure captions.

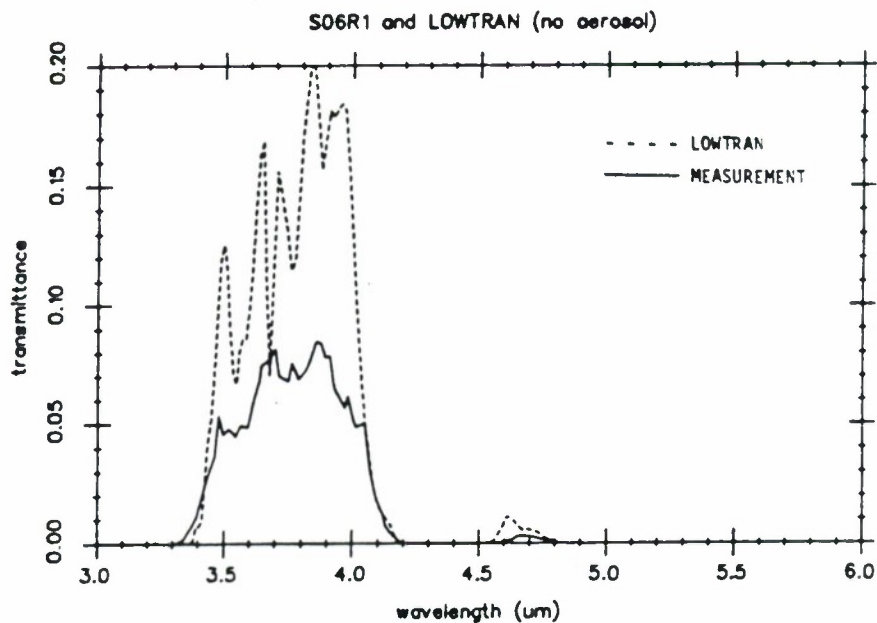


FIGURE 55. TRANSMITTANCE VERSUS WAVELENGTH FOR MEASURED SPECTRUM S06R1 COMPARED WITH LOWTRAN 6 CALCULATIONS PERFORMED USING NO AEROSOL ATTENUATION.

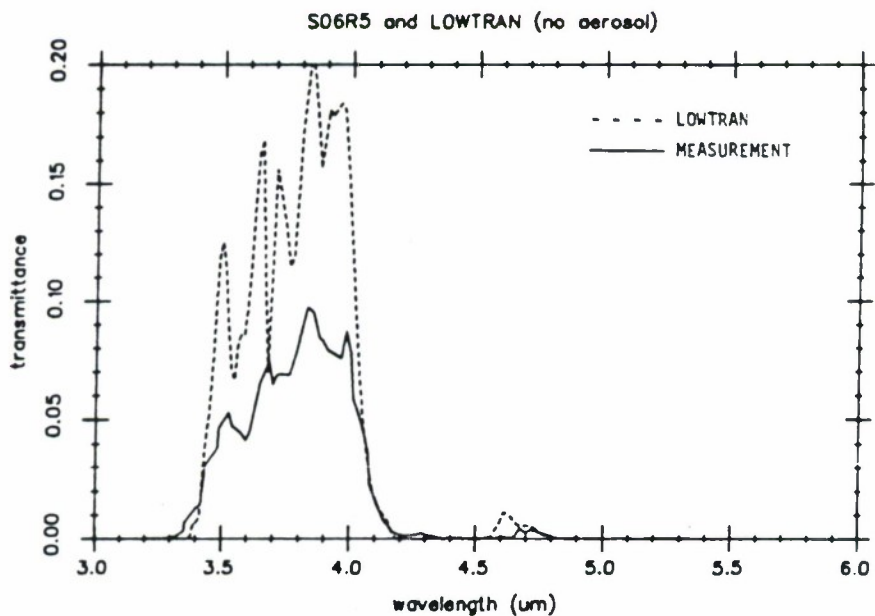


FIGURE 56. TRANSMITTANCE VERSUS WAVELENGTH FOR MEASURED SPECTRUM S06R5 COMPARED WITH LOWTRAN 6 CALCULATIONS PERFORMED USING NO AEROSOL ATTENUATION.

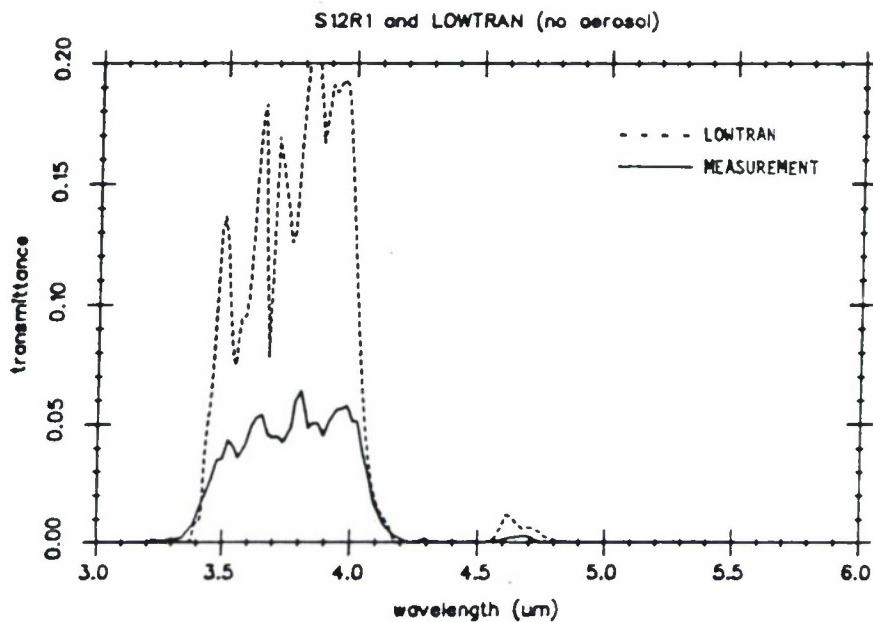


FIGURE 57. TRANSMITTANCE VERSUS WAVELENGTH FOR MEASURED SPECTRUM S12R1 COMPARED WITH LOWTRAN 6 CALCULATIONS PERFORMED USING NO AEROSOL ATTENUATION.

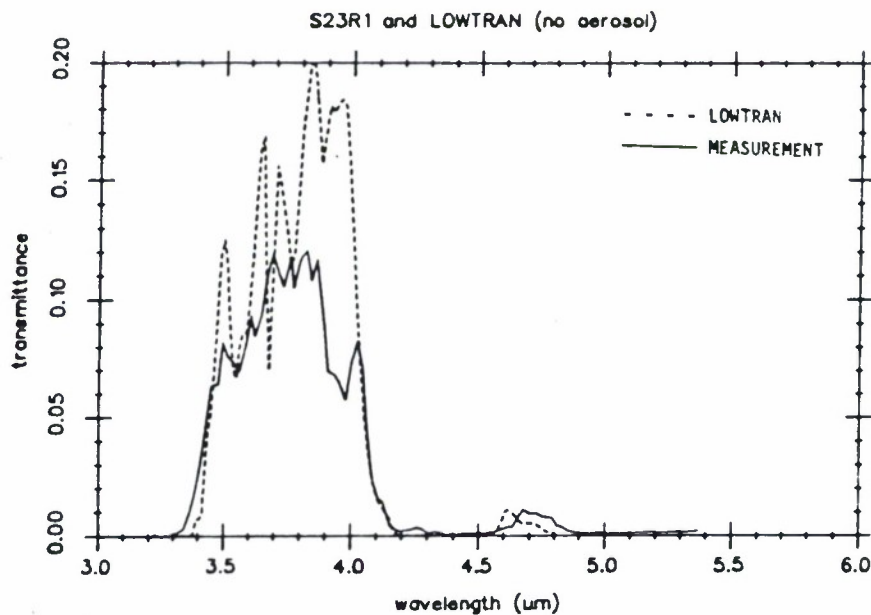


FIGURE 58. TRANSMITTANCE VERSUS WAVELENGTH FOR MEASURED SPECTRUM S23R1 COMPARED WITH LOWTRAN 6 CALCULATIONS PERFORMED USING NO AEROSOL ATTENUATION.

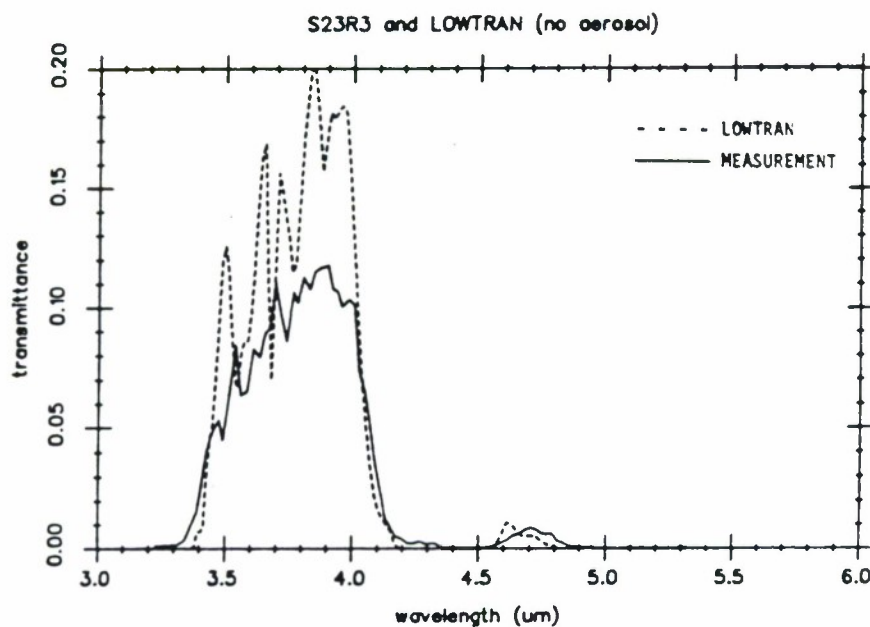


FIGURE 59. TRANSMITTANCE VERSUS WAVELENGTH FOR MEASURED SPECTRUM S23R3 COMPARED WITH LOWTRAN 6 CALCULATIONS PERFORMED USING NO AEROSOL ATTENUATION.

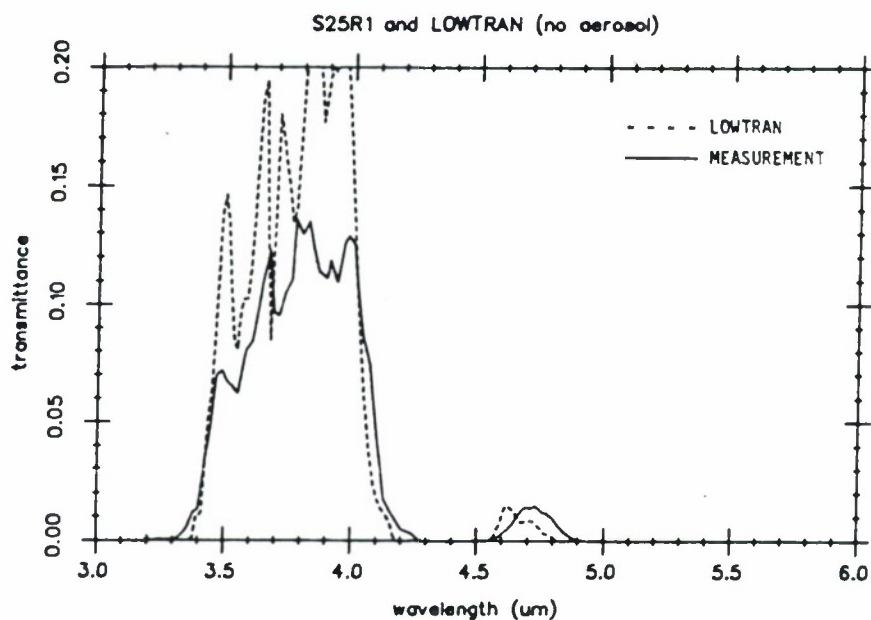


FIGURE 60. TRANSMITTANCE VERSUS WAVELENGTH FOR MEASURED SPECTRUM S25R1 COMPARED WITH LOWTRAN 6 CALCULATIONS PERFORMED USING NO AEROSOL ATTENUATION.

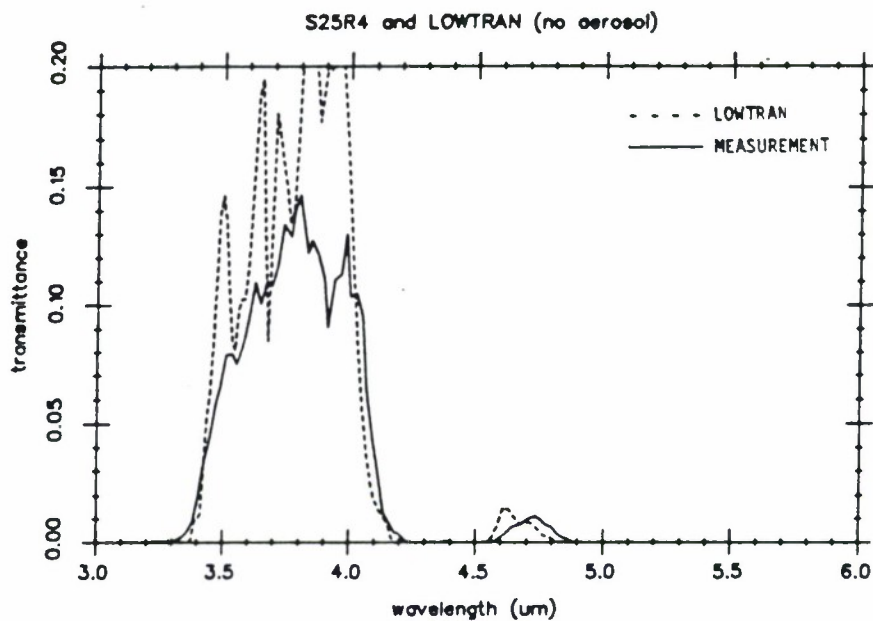


FIGURE 61. TRANSMITTANCE VERSUS WAVELENGTH FOR MEASURED SPECTRUM S25R4 COMPARED WITH LOWTRAN 6 CALCULATIONS PERFORMED USING NO AEROSOL ATTENUATION.

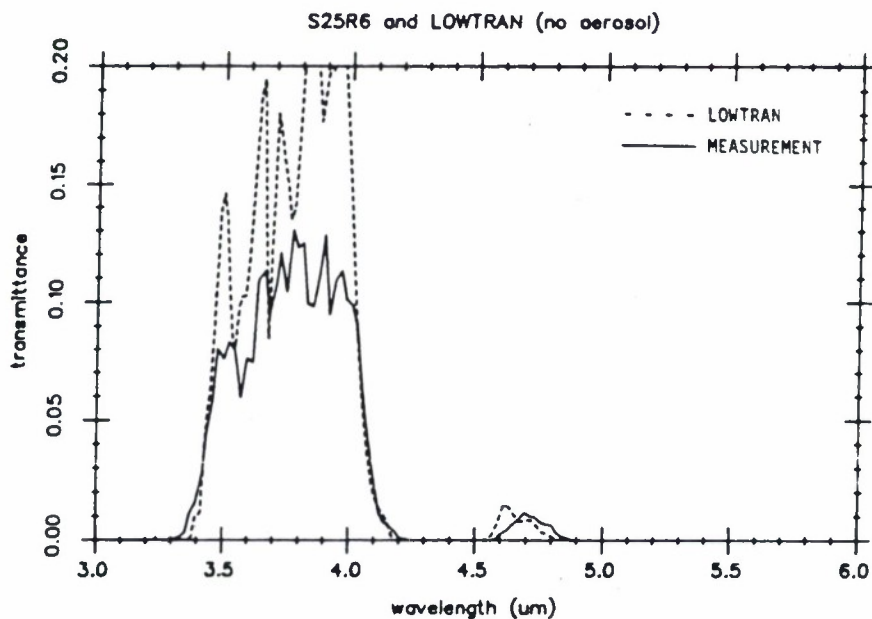


FIGURE 62. TRANSMITTANCE VERSUS WAVELENGTH FOR MEASURED SPECTRUM S25R6 COMPARED WITH LOWTRAN 6 CALCULATIONS PERFORMED USING NO AEROSOL ATTENUATION.

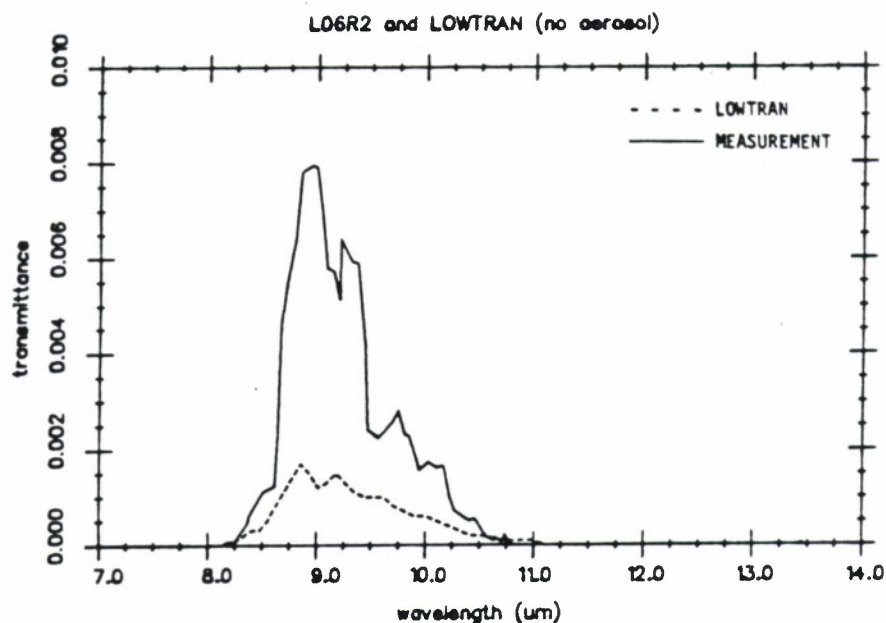


FIGURE 63. TRANSMITTANCE VERSUS WAVELENGTH FOR MEASURED SPECTRUM L06R2 COMPARED WITH LOWTRAN 6 CALCULATIONS PERFORMED USING NO AEROSOL ATTENUATION. Note: The plotted experimental data are in error and should be multiplied by a factor of 0.50, resulting in a peak transmittance of 0.0043 at 8.89 μm .

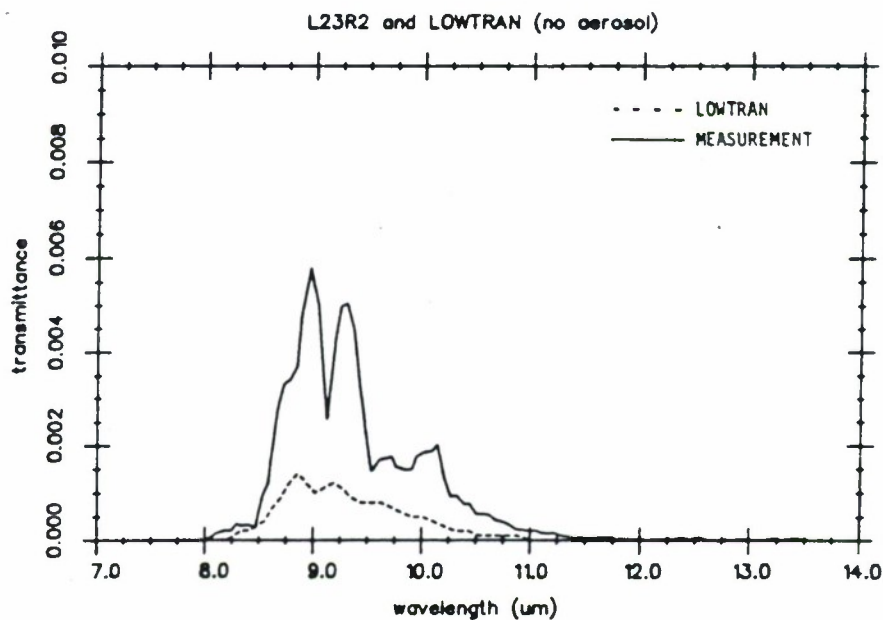


FIGURE 64. TRANSMITTANCE VERSUS WAVELENGTH FOR MEASURED SPECTRUM L23R2 COMPARED WITH LOWTRAN 6 CALCULATIONS PERFORMED USING NO AEROSOL ATTENUATION. Note: The plotted experimental data are in error and should be multiplied by a factor of 3.32, resulting in a peak transmittance of 0.0199 at 8.96 μm .

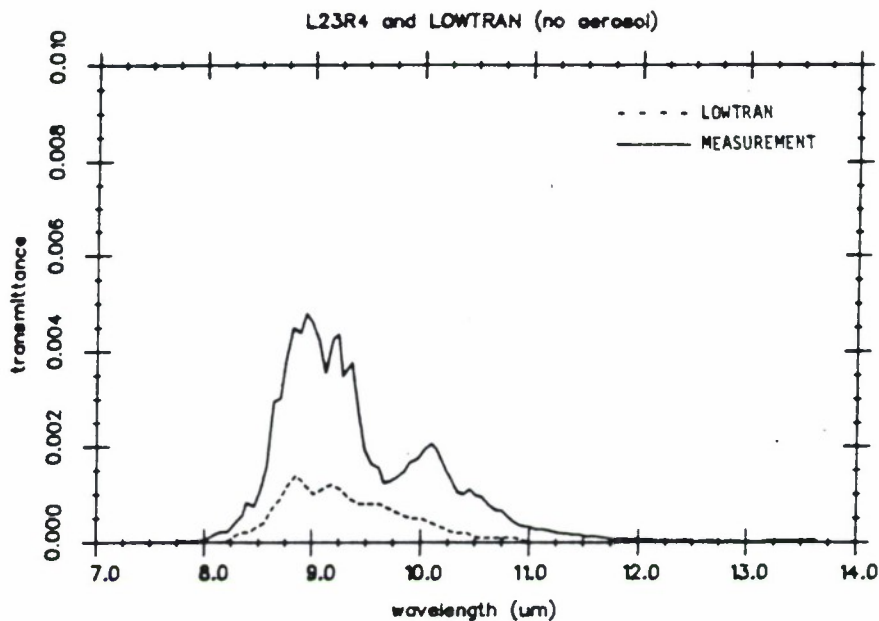


FIGURE 65. TRANSMITTANCE VERSUS WAVELENGTH FOR MEASURED SPECTRUM L23R4 COMPARED WITH LOWTRAN 6 CALCULATIONS PERFORMED USING NO AEROSOL ATTENUATION. Note: The plotted experimental data are in error and should be multiplied by a factor of 3.28, resulting in a peak transmittance of 0.0164 at 8.92 μm .

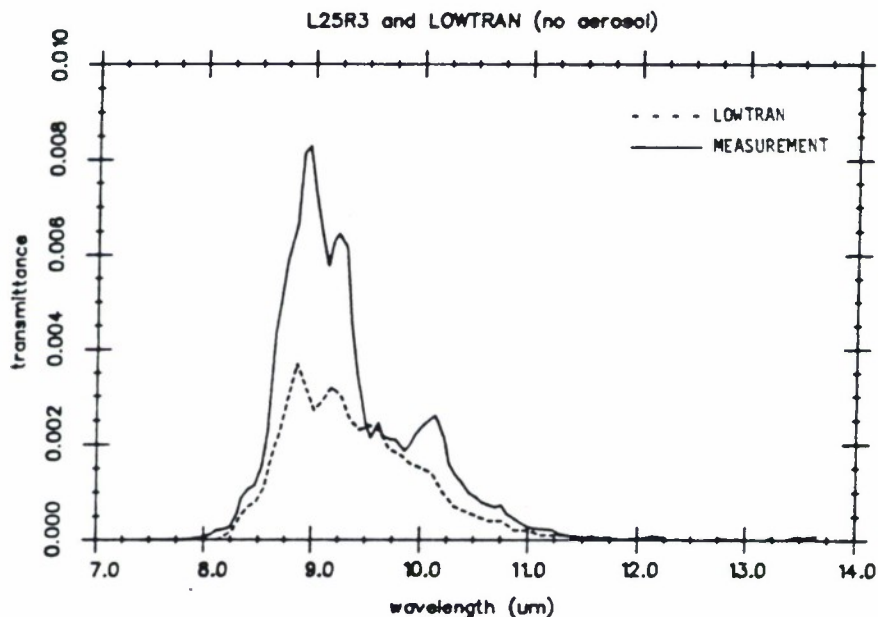


FIGURE 66. TRANSMITTANCE VERSUS WAVELENGTH FOR MEASURED SPECTRUM L25R3 COMPARED WITH LOWTRAN 6 CALCULATIONS PERFORMED USING NO AEROSOL ATTENUATION. Note: The plotted experimental data are in error and should be multiplied by a factor of 2.58, resulting in a peak transmittance of 0.0219 at 8.96 μm .

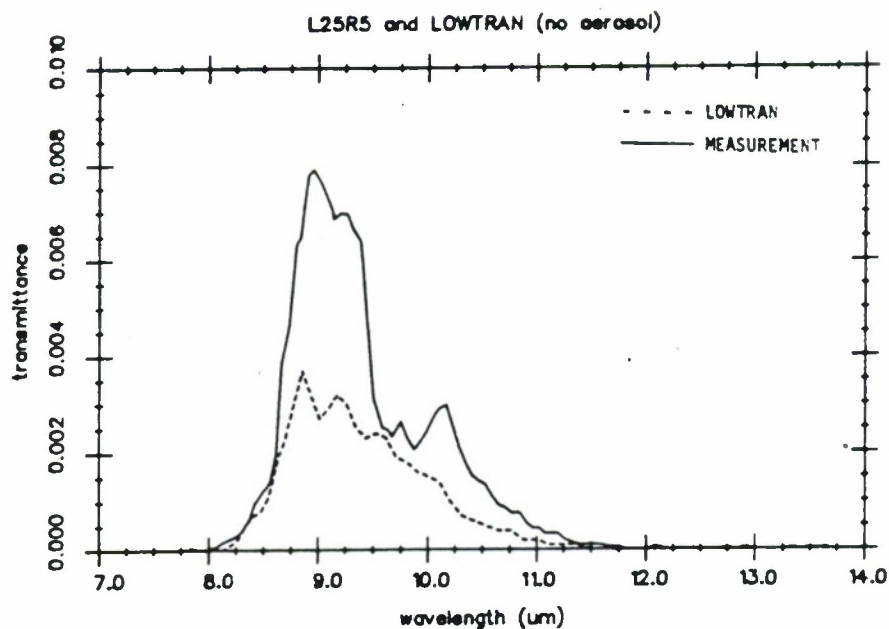


FIGURE 67. TRANSMITTANCE VERSUS WAVELENGTH FOR MEASURED SPECTRUM L25R5 COMPARED WITH LOWTRAN 6 CALCULATIONS PERFORMED USING NO AEROSOL ATTENUATION. Note: The plotted experimental data are in error and should be multiplied by a factor of 2.59, resulting in a peak transmittance of 0.0207 at 8.90 μm .

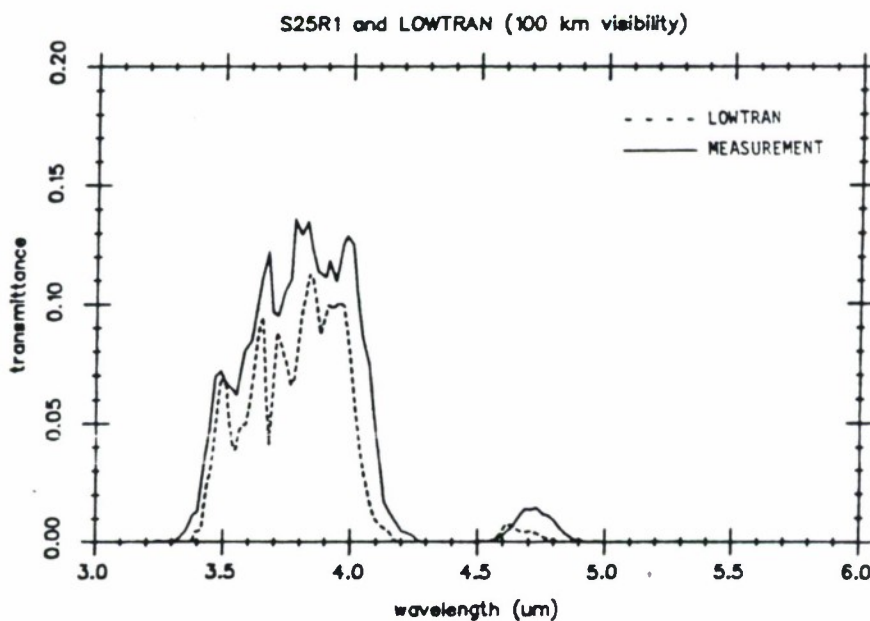


FIGURE 68. TRANSMITTANCE VERSUS WAVELENGTH FOR MEASURED SPECTRUM S25R1 COMPARED WITH LOWTRAN 6 CALCULATIONS PERFORMED USING A VISIBILITY OF 100 km.

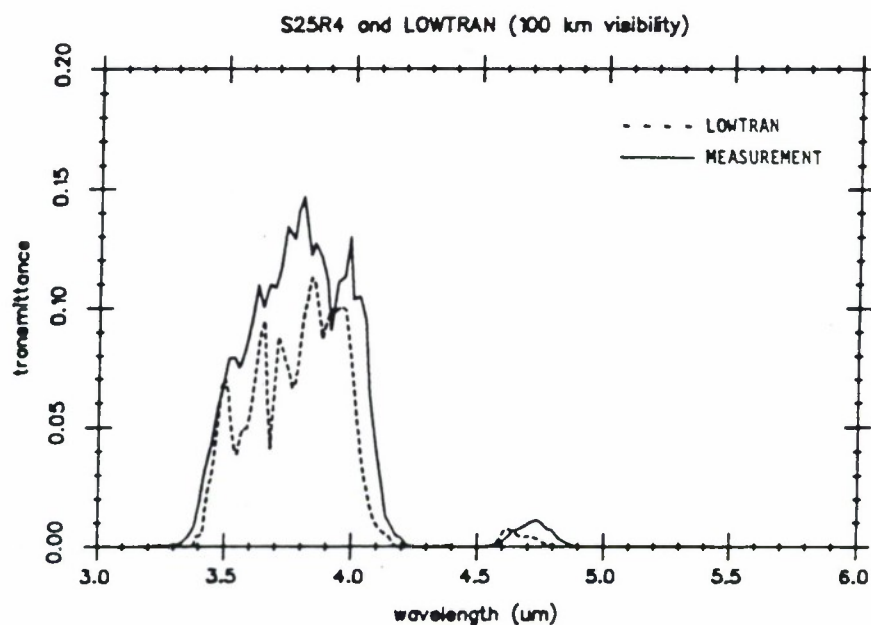


FIGURE 69. TRANSMITTANCE VERSUS WAVELENGTH FOR MEASURED SPECTRUM S25R4 COMPARED WITH LOWTRAN 6 CALCULATIONS PERFORMED USING A VISIBILITY OF 100 km.

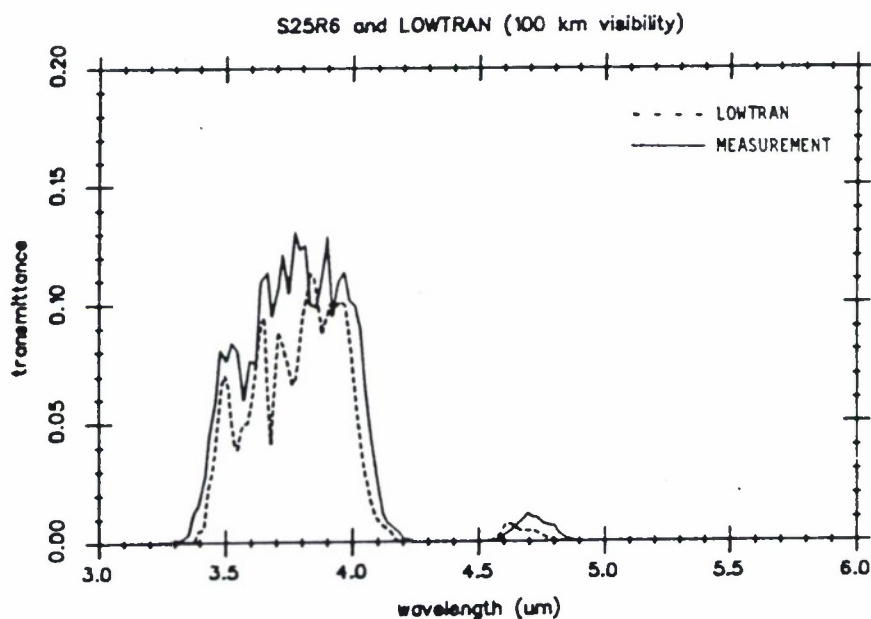


FIGURE 70. TRANSMITTANCE VERSUS WAVELENGTH FOR MEASURED SPECTRUM S25R6 COMPARED WITH LOWTRAN 6 CALCULATIONS PERFORMED USING A VISIBILITY OF 100 km.

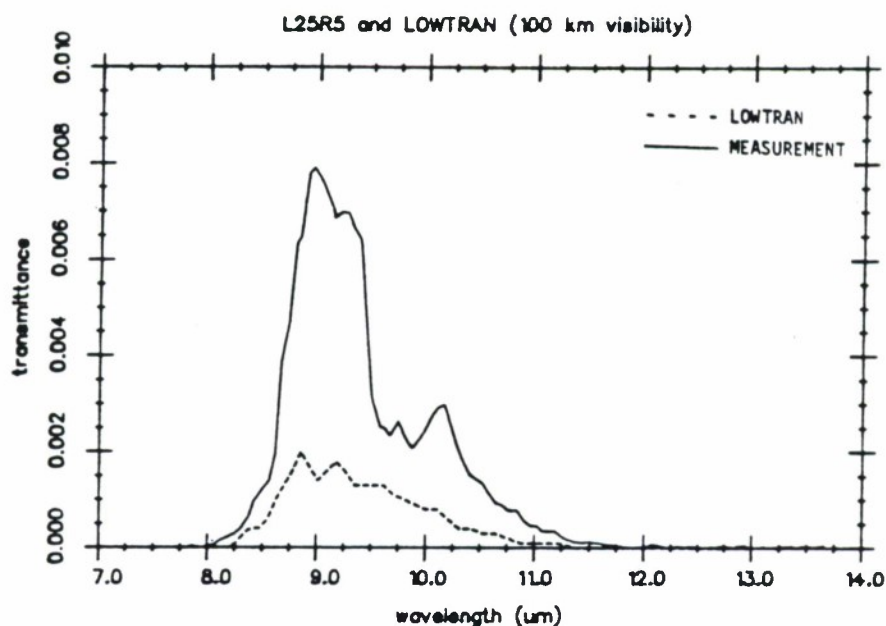


FIGURE 71. TRANSMITTANCE VERSUS WAVELENGTH FOR MEASURED SPECTRUM L25R5 COMPARED WITH LOWTRAN 6 CALCULATIONS PERFORMED USING A VISIBILITY OF 100 km. Note: The plotted experimental data are in error and should be multiplied by a factor of 2.59, resulting in a peak transmittance of 0.0207 at 8.90 μm .

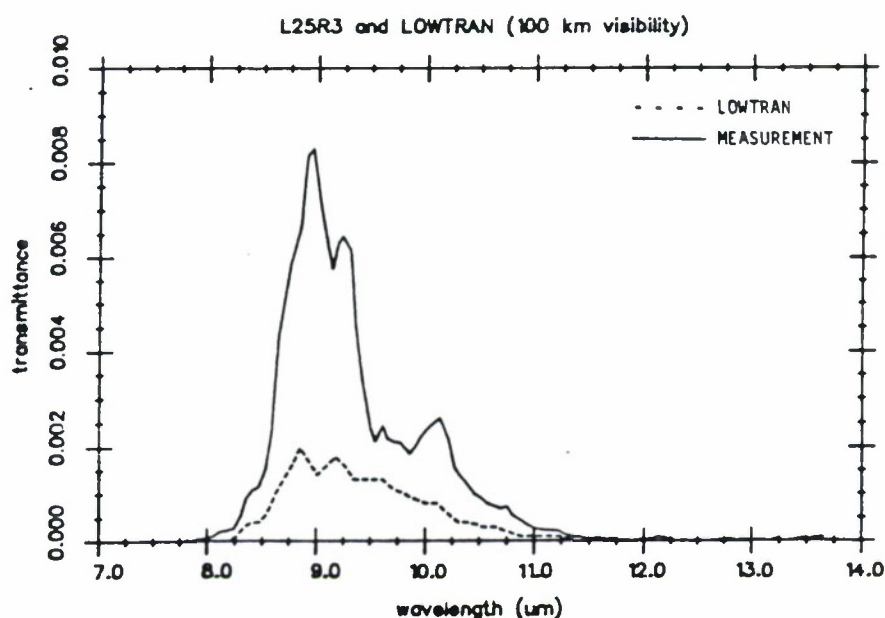


FIGURE 72. TRANSMITTANCE VERSUS WAVELENGTH FOR MEASURED SPECTRUM L25R3 COMPARED WITH LOWTRAN 6 CALCULATIONS PERFORMED USING A VISIBILITY OF 100 km. Note: The plotted experimental data are in error and should be multiplied by a factor of 2.58, resulting in a peak transmittance of 0.0219 at 8.96 μm .

uation along the measurement path. The rationale behind this omission is twofold: (1) The aerosol attenuation along the very long paths studied in this experiment is expected to be substantially smaller than the corresponding molecular absorption and the approach to modeling this aerosol attenuation is quite uncertain. Visibilities estimated at sea level during the experimental period were nominally in the range of 40 km [17]. However, outdoor lights in the vicinity of the AMOS observatory were clearly visible from the source locations on Lanai over a 66.2 km path using the unaided eye; and (2) In the event that transmittance spectra calculated without an aerosol extinction component exhibit lower transmittance values than the measured spectra, it can be clearly shown that the molecular absorption modeling is too pessimistic.

This is indeed the case for the comparisons shown in Figures 63-67 for the 7.0-14.0 μm spectral band.

The comparisons of the measured transmittance spectra collected on 25 July with the corresponding LOWTRAN calculations were repeated using a value of 100 km for the visibility in the LOWTRAN 6 Navy maritime aerosol model. The results of these comparisons are shown in Figures 68-72.

As can be seen from an examination of the comparisons shown in Figures 55-62 for the 3.0-5.0 μm band, the calculated peak transmittances, with no aerosol attenuation included, are typically about a factor of 2 to 3 greater than the measured values. The general shape of the band envelope is comparable for the measured and calculated spectra; however, the detailed structure of measured data is seen to vary for the different measurements. It is felt that the residual effects of low frequency refractive-index turbulence, incompletely averaged in the measurement, as

well as the intermittent presence of very thin clouds along the line of sight are responsible, at least part, for the high frequency structure seen in the experimental data.

The measured long-wavelength spectra shown in Figures 63-67 consistently show what appears to be an absorption feature occurring between 9.5 and 10.0 μm . A strong O_3 absorption band is centered at 9.6 μm and might possibly be responsible for this feature. No ozone absorption was included in the LOWTRAN calculation because of the uncertainty in assigning a concentration for this highly variable atmospheric constituent. One can see from an examination of Figures 63-67 that the calculated peak transmittance values near 9.0 μm are lower than the measured values by about a factor of 3 to 13. Again, no aerosol extinction component is included in the comparisons shown in Figures 63-67.

In the comparisons shown in Figures 68-72 a value of 100 km was used for the visibility in calculating the aerosol attenuation using the LOWTRAN 6 maritime aerosol model. The general agreement in trend and magnitude for the 3-5 μm comparisons shown in Figures 68-70 is quite good. The experimental transmittances are about 10-40% greater than the calculated values, a level of agreement which is within the range of uncertainty in the experimental data.

It is instructive to note in these same comparisons that the small region of measureable transmittance between 4.6 and 4.8 μm is peaked at a longer wavelength in the measured spectra than in the calculations. The relative discrepancies in maximum transmittance values in this region (4.6-4.8 μm) shown in Figures 68-70 are much larger (about a factor of 2) than in the region between 3.3 and 4.3 μm , in-

dicating that the LOWTRAN calculation is relatively more pessimistic in the long wavelength region of the 3-5 μm atmospheric window near 4.6 μm .

The 7.0-14.0 μm comparisons shown in Figures 71 and 72 are also based on a value of 100 km for the visibility in the LOWTRAN Navy maritime aerosol model. Whereas comparability in the magnitude of transmittance values is seen for the 3-5 μm data shown earlier in Figures 68-70, the 7-14 μm comparisons shown in Figures 71 and 72 show that measured transmittance values exceed the calculations by about a factor of 10.

SUMMARY AND CONCLUSIONS

6.1 THE NASA DIAL DATA

6.1.1 SUMMARY

Transmittances were calculated for each of the measured water vapor profiles for a cw DF laser with the MIRACL power spectrum, and for a pulsed DF laser power spectrum with a generic power spectrum. All atmospheric gases which absorb in the DF spectral region were included in the calculations. With the exception of water vapor, all gases were assumed to be in their midlatitude summer concentrations. The calculations included line absorption and continuum. Aerosols were not included. Transmittances were also calculated for average profiles based on the data and for standard atmosphere profiles.

Thermal blooming calculations were done to determine the importance of having a shipboard system to monitor water vapor profiles. These calculations were also done for both cw and pulsed DF laser systems.

These data and the calculations based on them represent one day at one particular location. They are useful in developing a perspective on the magnitudes of some of the problems involved in DF propagation in the real atmosphere, but sweeping generalizations should not be made.

6.1.2 CONCLUSIONS AND RECOMMENDATIONS

For the conditions represented by the water vapor profile data, transmittance for a cw DF laser over a 2-km path, either vertical or slant, was about 90%. For a pulsed DF

laser, the 2-km transmittance was around 85%. The pulsed transmittance would have been higher if the long-wavelength lines (4.6 to 4.8 μm) had not been included. There was only a small amount of fluctuation about these transmittance values, and they differed only slightly from transmittances calculated using the standard atmosphere water vapor profile.

No significant spatial patterns were observed in the transmittances. In particular, no effect of the gulf stream boundary on transmittance was observed.

In the thermal blooming calculations, the performance of a laser optimized using a standard atmosphere water vapor profile was compared to the performance of a laser optimized using the profile generated from the DIAL data. Both lasers were assumed to be operating in an atmosphere represented by the DIAL-generated profile. The difference in intensity delivered to the target was small, less than four percent for both pulsed and cw systems and a 2-km range. The conclusion is that on this particular day, for this particular scenario, a system to monitor the water vapor profile would not have been necessary.

The water vapor profile has only a minor effect on DF laser propagation, either cw or pulsed, both in terms of linear and of nonlinear degradation of the beam. Based on these data, precise knowledge of the water vapor profile does not appear to be critical.

Detailed treatment of the propagation of DF laser radiation can be quite complicated, as a high-energy beam in this spectral region can have some complex nonlinear interactions with atmospheric N_2 , N_2O , CO_2 , and aerosols. Of this group, only aerosols are highly variable. Aerosols were not considered at all in this study. Aerosol data were

not supplied, and aerosol models were not included in the transmittance modeling or the thermal blooming calculations. Future work on the effects of atmospheric variability on DF laser radiation should probably concentrate on aerosols rather than water vapor. Open ocean data are needed to verify existing aerosol models or for use in generation of better models. Nonlinear effects, especially aerosol enhancement of thermal blooming, may be important in DF propagation, and study of this subject requires reliable information about the aerosols encountered at sea. The importance of aerosol growth with humidity, and the resulting dependence of the aerosol profile on the water vapor profile, should be established; the DIAL system seems uniquely suited for measurements related to this subject.

6.2 THE LFLID SUPPORT DATA

The long-path atmospheric transmittance and radiosonde measurements performed in support of the LFLID tests were carried out during the month of July 1984. After editing the transmittance data to remove those measurements which were affected by cloud occurrences along the measurement line of sight, data collected during the early morning hours (HST) on four days were selected for further analysis. The measurement dates and times for these data are given in Table 5, Section 2.2. Figures 15 and 16 in Section 2.2 show the vertical temperature and water vapor profiles determined from radiosonde data which were collected during the four selected measurement periods.

The temperature profiles show the presence of inversions occurring at altitudes between 1.5 and 2.1 km during three of the four periods. Reduced water vapor densities above 1.8 km appear to be correlated with the temperature inversions.

The results of the long-path transmittance measurements and corresponding LOWTRAN calculations are shown in Figures 55-72 in Chapter 5. An examination of the measured and calculated 3-5 μm transmittance comparisons shown in these figures indicates that reasonably good agreement between the measured data and the LOWTRAN 6 model exists. Two variations of the LOWTRAN calculations were performed, one omitting any aerosol attenuation contribution whatsoever, and the other using a nominal visibility of 100 km. It can be seen from an examination of the plotted results shown in Figures 60-62, compared with those shown in Figures 68-70, that the two LOWTRAN calculations bracket the experimental data in the 3-5 μm region. The 100 km visibility calculation is seen to agree with the measured data to within the estimated range of experimental uncertainty.

Comparisons similar to those in the 3-5 μm region were carried out for the long-wavelength (7.0-14.0 μm) band and are shown in Figures 63-67 and Figures 71 and 72.* The calculations performed using a visibility of 100 km show that the LOWTRAN model underestimates the measured transmittance values by about a factor of ten (Figures 71 and 72) while the comparable comparisons in the 3-5 μm region (Figures 68-70) show good agreement.

The lack of conformance of the model to the measured transmittance in the 7-14 μm band can very likely be associated with an overestimate of the 8-14 μm water vapor continuum absorption component of the LOWTRAN model.

* Note the error in the plotted experimental results for the 7.0 to 14.0 μm spectra. The corrected peak transmittances are given in the figure captions.

This observation is consistent with results obtained in an analysis of atmospheric CO₂ laser transmittance measurements in the 9-11 μm region performed by NRL in previous experiments at Cape Canaveral, Florida [18].

The experimental data presented in Figures 68-70 show that the measured transmittance in the region between 4.6 and 4.9 μm is about a factor of two larger than the calculated value, indicating that the model is relatively pessimistic in this sub-region when compared with the good agreement evident in the 3.3-4.3 μm sub-region.

The measured transmittances in the 7-14 μm region consistently show the presence of an absorption feature between 9.5 and 10.2 μm . This feature is very likely due to the presence of ozone in the propagation path. The uncertainty associated with determination of an appropriate O₃ concentration for use in the LOWTRAN calculations precluded incorporation of the O₃ absorption features into the calculated transmittance spectra.

REFERENCES

1. D.H. Leslie, P.B. Ulrich, and G.L. Trusty Technical Analysis of a Proposed Ship-to-Ship Chemical Laser Transmission Experiment, NRL Memorandum Report 4745, Naval Research Laboratory, Washington, D.C., February 1982.
2. F.X. Kneizys, E.P. Shettle, W.O. Gallery, J.H. Chetwynd, Jr., L.W. Abreu, J.E.A. Selby, S.A. Clough, and R.W. Fenn, Atmospheric Transmittance/Radiance: Computer Code LOWTRAN 6, AFGL-TR-83-0187, Air Force Geophysics Laboratory, Hanscom AFB, Massachusetts, 1983.
3. E.V. Browell, A.F. Carter, S.T. Shipley, R.J. Allen, C.F. Butler, M.N. Mayo, J.H. Siviter, Jr., and W.M. Hall, NASA Multipurpose Airborne DIAL System and Measurements of Ozone and Aerosol Profiles, Appl. Opt. 22, 522-534, 1983.
4. J.M. Meserve, U.S. Navy Marine Climatic Atlas of the World, Volume I, North Atlantic Ocean, Superintendent of Documents, U.S. Government Printing Office, Washington, D.C., NAVAIR 50-1C-528, December 1974.
5. V.P. Starr, J.P. Peixoto and R.G. McKean, "Pole-to-Pole Moisture Conditions for the IGY", Pure and Appl. Geophys., 73, 85-116, 1969.
6. AMOS Users Manual, Revision 5, AVCO Everett Research Laboratory, Omaopio & Hansen Roads, P.O. Box 261, Puunene, Maui, Hawaii 96784, Report Number AERL M1176, 30 September 1982.
7. G. Dahlquist and A. Bjorck, Numerical Methods, Prentice-Hall, Inc., Englewood Cliffs, New Jersey, 227-233, 1974.
8. S. Manabe and R.T. Wetherald, Thermal Equilibrium of the Atmosphere with a Given Distribution of Relative Humidity, J. Atmos. Sci., 24, 241-259, 1967.
9. A. Rosenberg and D.B. Hogan, Lidar Technique of Simultaneous Temperature and Humidity Measurements: Analysis of Mason's Method, Appl. Optics., 20, 3286-3288, 1981.

10. J.A. Dowling and J.L. Manning, editors, High Energy Laser Propagation Handbook, Vol. I: Phenomenological Basis, OMI-83-001, OptiMetrics, Inc., Ann Arbor, Michigan, July 1983; ASL-TR-0148, US Army Electronics Research and Development Command, Atmospheric Sciences Laboratory, White Sands Missile Range, New Mexico, February 1984.
11. J.L. Manning and B.K. Matise, Chemical Laser Modeling, Vol. I: Propagation of DF Laser Radiation, OMI-82-010 (I), OptiMetrics, Inc., Ann Arbor, Michigan, August 1982.
12. K.O. White, W.R. Watkins, C.W. Bruce, R.E. Meredith, and F.G. Smith, Water Vapor Continuum Absorption in the 3.5 to 4.0 μm Region, Appl. Opt. 17, 2711-2720, 1978.
13. W.R. Watkins, K.O. White, L.R. Bower, and B.Z. Sojka, Pressure Dependence of the Water Vapor Continuum Absorption in the 3.5 to 4.0 μm Region, Appl. Opt. 18, 1149-1159, 1979.
14. M.M. Shapiro and H.P. Gush, The Collision-Induced Fundamental and First Overtone Bands of Oxygen and Nitrogen, Canad. J. Phys. 44, 949-963, 1966.
15. H.J. Breaux, Simplified Predictive Methodology for Nonlinear Repetitive Pulse and CW High Energy Laser Propagation, SPIE Vol. 195, Atmospheric Effects on Radiative Transfer, pp. 192-202, 1979.
16. R.C. Shirkey, editor, EOSAEL 82 Volume IV: Radiative Transfer and Turbulence Effects, ASL-TR-0122, US Army Electronics Research and Development Command, Atmospheric Sciences Laboratory, White Sands Missile Range, New Mexico, November 1982.
17. Michael Hess, Naval Air Development Center, private communication.
18. J.A. Dowling, Analysis of 1977 Cape Canaveral Air Force Station Laser and High Resolution Atmospheric Transmission Data Base, NRL Report to be published (1985).

ACKNOWLEDGEMENTS

The authors wish to thank Andreas Goroch (NEPRF) and Ed Browell (NASA) for providing the NASA DIAL and associated meteorological data. The reduction and calibrations for the LFLID transmittance data were provided by Richard Horton (AVCO Corporation) who also supplied these data to OMI. John Toner (NADC) supplied the radiosonde data from the LFLID support tests which were used as a basis for the LOWTRAN calculations.

Andreas Goroch, Robert Fett, and Julie Haggerty (NEPRF) provided assistance in the administration of this contract during the modifications and extensions required to complete the work.

The authors would also like to acknowledge the excellent work performed by Sharon Wolters and Fae Mallery in the preparation of the text and numerous figures contained in this report.

DISTRIBUTION

CHIEF OF NAVAL RESEARCH (2)
LIBRARY SERVICES, CODE 784
BALLSTON TOWER #1
800 QUINCY ST.
ARLINGTON, VA 22217-5000

OFFICE OF NAVAL RESEARCH
CODE 422AT
ARLINGTON, VA 22217-5000

CHIEF OF NAVAL OPERATIONS
U.S. NAVAL OBSERVATORY
DR. RECHNITZER, OP-952F
34TH & MASS AVE.
WASHINGTON, DC 20390

COMMANDING OFFICER
NAVAL RESEARCH LAB
ATTN: LIBRARY, CODE 2620
WASHINGTON, DC 20390

COMMANDING OFFICER
NAVEASTOCEANCEN
MCADIE BLDG. (U-117)
NAVAL AIR STATION
NORFOLK, VA 23511

DIRECTOR OF RESEARCH
U.S. NAVAL ACADEMY
ANNAPOLIS, MD 21402

NAVAL POSTGRADUATE SCHOOL
METEOROLOGY DEPT.
MONTEREY, CA 93943

NAVAL POSTGRADUATE SCHOOL
PHYSICS & CHEMISTRY DEPT.
MONTEREY, CA 93943-5100

LIBRARY
NAVAL POSTGRADUATE SCHOOL
MONTEREY, CA 93943-5100

COMMANDER (2)
NAVAIRSYSCOM
ATTN: LIBRARY (AIR-723D)
WASHINGTON, DC 20361-0001

COMMANDER
NAVAIRSYSCOM (AIR-330)
WASHINGTON, DC 20361-0001

COMMANDER
NAVAL SEA SYSTEMS COMMAND
ATTN: LT S. PAINTER
PMS-405/PM-24
WASHINGTON, DC 20362-5101

COMMANDER
NAVOCEANSYSCEN
DR. J. RICHTER, CODE 54
SAN DIEGO, CA 92152-5000

COMMANDER
NAVAL WEAPONS CENTER
DR. A. SHLANTA, CODE 3918
CHINA LAKE, CA 93555-6001

COMMANDER
NAVSURFWEACEN, CODE R42
DR. B. KATZ, WHITE OAKS LAB
SILVER SPRING, MD 20910

DIRECTOR
NAVSURFWEACEN, WHITE OAKS
NAVY SCIENCE ASSIST. PROGRAM
SILVER SPRING, MD 20910

COMMANDER
NAVAL SURFACE WEAPONS CENTER
ATTN: CODE 44
DAHLGREN, VA 22448-5000

USAFETAC/TS
SCOTT AFB, IL 62225

AFGL/OPI
HANSCOM AFB, MA 01731

COMMANDER & DIRECTOR
ATTN: DELAS-D
U.S. ARMY ATMOS. SCI. LAB
WHITE SAND MISSILE RANGE
WHITE SANDS, NM 88002

COMMANDER & DIRECTOR
ATTN: DELAS-AS
U.S. ARMY ATMOS. SCI. LAB
WHITE SANDS MISSILE RANGE,
NEW MEXICO 88002

COMMANDER/DIRECTOR
US ARMY ATMOS. SCIENCE LAB.
ATTN: DELAS-AT-0
WHITE SANDS MISSILE RANGE, NM
88002

DIRECTOR (12)
DEFENSE TECH. INFORMATION
CENTER, CAMERON STATION
ALEXANDRIA, VA 22314

DIRECTOR, ENV. & LIFE SCI.
OFFICE OF UNDERSECRETARY OF
DEFENSE FOR RSCH & ENG E&LS
RM. 3D129, THE PENTAGON
WASHINGTON, DC 20505

NATIONAL CENTER FOR ATMO. RSCH
P.O. BOX 3000
BOULDER, CO 80307

DR. F. BROWELL
NASA-LANGLEY RSCH CENTER
LANGLEY, VA 23665

AMERICAN METEORO. SOCIETY
METEOR. & GEOASTRO. ABSTRACTS
P.O. BOX 1736
WASHINGTON, DC 20013